DESIGN OF HIGH PERFORMANCE AND POWER EFFICIENT ELECTROCARDIOGRAM DETECTORS FOR IMPLANTABLE CARDIAC PACEMAKER SYSTEMS

A Thesis

Submitted in Partial Fulfilment of the

Requirements for Award of the Degree of

Doctor of Philosophy

by

ASHISH KUMAR

Enrolment No: E16SOE800

under the supervision of

Dr. Rama Komaragiri

Dr. Manjeet Kumar

DEPARTMENT OF ELECTRONICS AND COMMUNICATION ENGINEERING

SCHOOL OF ENGINEERING AND APPLIED SCIENCES

BENNETT UNIVERSITY

GREATER NOIDA, UTTAR PRADESH, INDIA

September 2019

Thesis Evaluation

This is to certify that **ASHISH KUMAR** (Enrolment Number: E16SOE800) has successfully defended the Thesis entitled **Design of High Performance and Power Efficient Electrocardiogram Detectors for Implantable Cardiac Pacemaker Systems** on --/-- /20--.

The committee recommends the candidate for the award of the degree of Doctor of Philosophy.

Signature of External Examiner Signature of Internal Examiner

Declaration

I hereby declare that except where specific reference is made to the work of others, the contents of this thesis are original and have not been submitted in whole or in part for consideration for any other degree or qualification in this, or any other university. This thesis is my work and does not contain any outcome of work done in collaboration with others, except as specified in the text and Acknowledgements.

(Signature)

ASHISH KUMAR

Enrolment No: E16SOE800

Bennett University,

Greater Noida

11/09/2019

Certificate

This is to certify that the thesis entitled ***Design of High Performance and Power Efficient Electrocardiogram Detectors for Implantable Cardiac Pacemaker Systems*** submitted by **ASHISH KUMAR** to Bennett University for the award of the degree of Doctor of Philosophy is a bonafide record of the research work carried out by him under my/our supervision and guidance. The content of the thesis, in full or parts, has not been submitted to any other institute or university for the award of any degree.

Dr. Rama Komaragiri
Professor
Department of ECE
SEAS
Bennett University

Dr. Manjeet Kumar
Assistant Professor
Department of ECE
SEAS
Bennett University

Place: Bennett University

(Head of the Department)

Date: 11 /09 /2019

(*Office Seal*)

I would like to dedicate this thesis to my loving parents

Acknowledgements

My research work has been made possible through many blessings I received in my life. First of all, I would like to praise and thank God, the Almighty, for bestowing, Blessings: without which I am nothing.

I would like to express my profound gratitude to my advisors Dr. Rama Komaragiri and Dr. Manjeet Kumar for their invaluable guidance, continuous encouragement, and support in every stage of the work. Their technical acumen, precise suggestions and guidance has been an invaluable source of inspiration and moral support.

I am deeply indebted to Prof. Sudhir Chandra and Prof. Suneet Tuli whose encouragement helped me in all the time of the research.

I would like to acknowledge Dr. Sanjay Kataria, Dr. Samayveer Singh, Dr. Nidhi Sinha, for their support.

I gratefully acknowledge the support provided by my fellow Research Scholars at Bennett University to get through the high pressure stage of this work. My special thanks are due to Mr. Ramana Ranganatham, Mr. Virender Kumar Mehla for providing valuable suggestion and support whenever required. I am also grateful to all the members of ECE Research Lab for creating a joyful environment. I also thank all the staff members of Department of ECE, Bennett University for their help whenever needed.

Most importantly, my heartfelt gratitude to my family for their love and support throughout my life. With their blessings this work could has been accomplished. I am indebted to my father, Shri Kuldeep Singh and mother, Smt. Krishna Devi for their love and care. I would like to thank my sister Anu Singroha for all support during these years.

I regret for any inadvertent omissions because enlisting all the individuals whose contributions went into the making of the thesis is a very difficult task.

Abstract

The new-age advancements in biomedical signal processing are due to circuits and systems which can process complex data, which made the healthcare facilities more compact and affordable. Among healthcare devices, cardiac pacemakers have become a recurrent biomedical device which is engrafted in the human body to monitor and detect a subject's heart rate. Cardiovascular diseases (CVDs) or diseases related to the heart are due to abnormalities or disorders of the heart and blood vessels. Till date, limited literature is available, which focuses on a single technique that can perform ECG signal denoising, ECG signal detection, and lossless data compression. Current circuitry can be interpreted as a cardiac electrical signal compression algorithm representing the time signal information into a single event description of the cardiac activity. ECG signal detection techniques like an artificial neural network, genetic algorithm, Hilbert transform, hidden Markov model are some sophisticated algorithms which provide suitable results, but their realization using IC technologies is very complicated. Due to less complexity and high performance, wavelet transform based approaches are widely used. In this thesis, after a thorough analysis of various wavelet transforms, it is found that biorthogonal wavelet transform is best suitable to detect ECG signal. The main steps involved in the ECG detection process consist of de-noising and locating different ECG waves using adaptive slope prediction thresholding.

The significant challenges involved in the wireless transmission of ECG data are data conversion and power consumption. As medical regulatory boards demand a lossless compression technique, lossless compression technique with a high bit compression ratio is highly required. In this thesis, biorthogonal wavelet transform based ECG signal compression technique is proposed. The proposed methodology achieves the lowest signal to noise ratio, and the lowest root mean square error. Also, the proposed ECG detection technique is capable of distinguishing accurately between healthy, myocardial infarction, congestive heart failure and coronary artery disease patients with a detection accuracy, sensitivity, specificity, and error of *99.92%*, *99.94%*, *99.92%* and *0.0013*, respectively. The use of biorthogonal wavelet transform based data compression of ECG signal achieves a high compression ratio of *22.61*. The advantages and effectiveness of the proposed algorithm are verified by comparing with the existing methods. System Verilog hardware description language and Xilinx® Vivado® design suite are used for coding and functional verification of the proposed scheme. Area, power, and

delay requirements of the proposed scheme are calculated by implementing the proposed detector on the Xilinx® Virtex®-7 FPGA. Lowest power consumption, area, delay, and switching energy, respectively, of *99 nW*, *1.1* mm^2, *10 ns,* and *0.990 µJ* has been achieved using the proposed scheme.

Keywords: ECD, CVD, Discrete wavelet transform, lossless compression, QRS complex, heart rate monitoring

Table of Contents

List of Figures

List of Tables

List of Abbreviations

ACS : Acute Coronary Syndrome

AHA : American Heart Association

APC : Atrial Premature Contraction

ASIC : Application Specific Integrated Circuit

AV : Atrioventricular

AZTEC : Amplitude Zone Time Epoch Coding

BSN : Body Sensor Networks

BSP : Biosignal Processor

BWN : Baseline Wandering Noise

CAD : Coronary Artery Disease

CBCTA : Chopper Based Continuous Time Amplifier

CEEMD : Modified Ensemble Empirical Mode Decomposition

CHF : Congestive Heart Failure

CSE : Common Standards for Electrocardiography

CVD : Cardiovascular Diseases

CWT : Continuous Wavelet Transform

DCT : Discrete Cosine Transform

DWT : Discrete Wavelet Transform

ECG : Electrocardiogram

FPGA : Field Programmable Gate Array

GLRT : Generalized Likelihood Ratio Test

GMBO : Gases Brownian Motion Optimization

HMM : Hidden Markov Model

HPSDM : Highpass Sigma Delta Modulator

IMPROVE : Improving Control of Patient Status in Critical Care

LMS : Least Mean Square

LTST : Long Term ST

LZMA : Lempel Ziv Markov Chain Algorithm

LZO : Lempel Ziv Oberhumer

LZW : Lempel Ziv Welch

MI : Myocardial Infarction

MIMIC : Medical Information Mart for Intensive Care

MIT-BIH : Massachusetts Institute of Technology- Boston's Beth Israel Hospital

OOK : On-Off Kaying

PLI : Power Line Interference

PSO : Particle Swarm Optimization

PVC : Premature Ventricular Contraction

RLE : Run Length Encoding

RTL : Register Transfer Level

SA : Sino-Atrial

SAR-ADC : Successive Approximation Register - Analog to Digital Converter

SDM : Sigma Delta Modulator

SoC : System on Chip

SRAM : Static Random Access Memory

SSLMS : Sign Sign Lease Mean Square

SVM : Support Vector Machine

TERMA : Two-Evenet Related Moving Averages

WDF : Wave Digital Filter

WFB : Wavelet Filter Bank

WHO : World Health Organization

List of Symbols

ACC : Overall accuracy

C_g : Compression gain

CR : Compression ratio

DER : Detection error rate

E_{energy} : Energy content

$E_{entropy}s(t)$: Shannon entropy

$E_{relative}$: Relative entropy

HR : Heartrate

MAE : Maximum absolute error

MDL: Minimum description length

I_{mutual} : Mutual information

PSNR : Peak signal to noise ratio

PRD : Percentage root-mean-square difference

Q_s : Quality score

R : Cross correlation

RMSE : Root mean square error

Se : Sensitivity

SNR : Signal-to-noise ratio

S_S : Space-saving

Sp : Specificity

CHAPTER 1

INTRODUCTION

1.1 DEVELOPMENT OF IMPLANTABLE CARDIAC PACEMAKER SYSTEM

A cardiac pacemaker is a device that can treat cardiac dysrhythmia by rapidly tracking human’s heartrate and rhythm. Cardiac pacemakers deliver rhythmic electric stimulus in a controlled manner to the heart to maintain the heartbeat. In 1950 John Hopps and Wilfred Bigelow presented the first cardiac pacemaker. Ability to deliver a periodic and administrated electric stimulus made the implantable and wearable cardiac pacemakers a reality in today’s globally emerging world of healthcare devices. Different researchers have not only made the heavy pacemakers undergo a physical change in terms of reduction in size and weight but also economical and within reach to many, thus being a lifesaver. Evolution of a cardiac pacemaker system is shown in Fig. 1.1 [1].

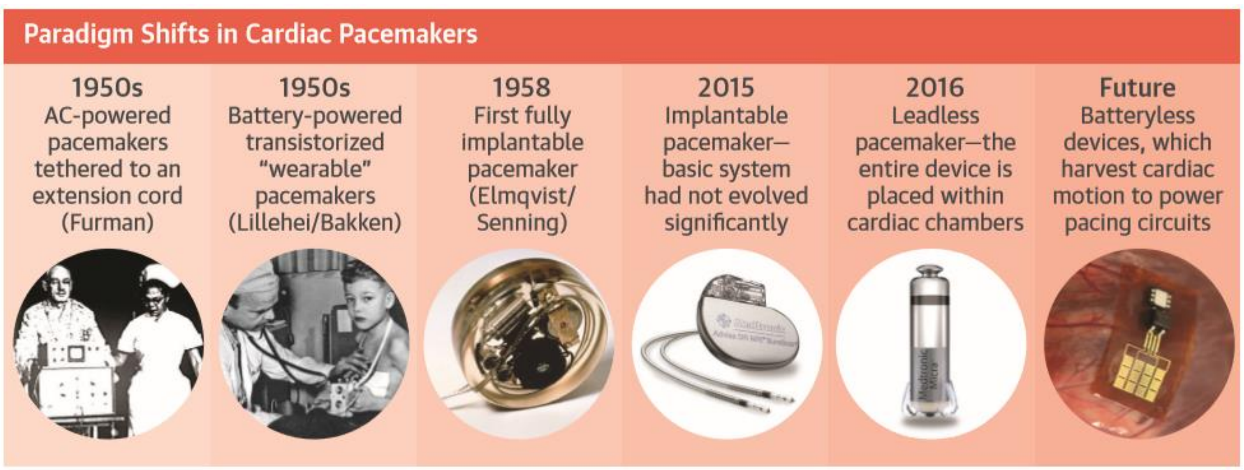

Fig. 1. 1 Evolution of cardiac pacemaker system

The market share of pacemaker products is increasing rapidly in the biomedical device domain, as shown in Fig. 1.2 [2]. The requirements of modern-day pacemakers are small in size, lightweight, programmable, extended lifetime of the pacemaker device, and more efficient. The advent of modern technological breakthroughs and inventions have left behind all the lacunas like single-chamber, asynchronous, non-programmable pacing. Pacemakers are versatile and can be implanted in a physician's office to make the therapy unique to human needs.

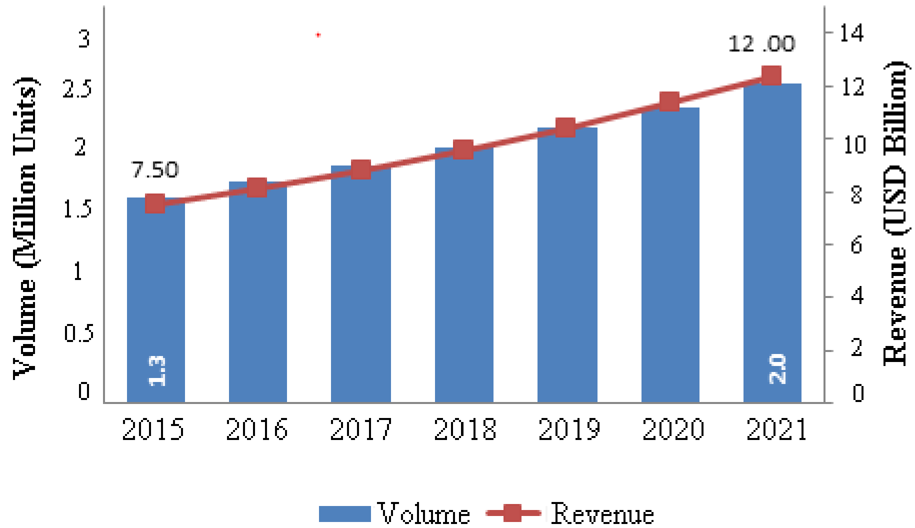

Fig. 1. 2 Market share of pacemaker products

1.2 NEED AND MOTIVATION

The heart is a vital organ in the human body and is an undeniable fact that one needs a healthy heart. The structure and working of a human heart are very complicated. Millions of patients use personal medical devices which can analyze health condition. Personal medical devices collect medical data, which is then transmitted to medical personnel to provide necessary medical care. One of such personal medical device is cardiac pacemaker. Pacemaker device usually detects and monitors the subject’s heartbeat. The essential care is provided to the subject after receiving abnormal signals from the heart. In this way, pacemaker helps to maintain the heart beat rate of a person in a safe range. Once the pacemaker is implanted into a human body, the pacemaker is expected to operate for several years without any intervention [3]. The big challenge here is to develop a self-effacing, reliable, and patient-friendly device for reading and monitoring electrocardiogram (ECG) data continually and uninterruptedly. The next level of challenge for such devices is to be light in weight with extended battery life, which requires a substantial integration and simulation of signals and complex data.

1.3 IDENTIFYING THE RESEARCH PROBLEM

Medical expenditures are on the all-time surge and high with the fast growth in world population. In Europe, one-third of the population will be aged over 65 years by the year 2035. China and India are also facing the fastest-growing aging problem. Over one-third of the world's elderly population lives in China and India, and this proportion is envisaged to increase up to 40% by 2020 [4]. Healthcare became an important agenda for both individuals and governments. The latest reports from the World Health Organization (WHO) purport that dealing with the aging population is a vital healthcare aspect [5, 6]. The present healthcare structures and approaches are facing more significant challenges in dealing with the healthcare problems of the aging population. Accordingly, identifying human diseases in a cost-effective and timely manner with precision has taken center stage [7-10]. ECG monitoring became ubiquitous because of its supremacy in the diagnosis of heart-related diseases and is also making its way both in hospitals and research areas [11].

The present medical fraternities are dependent on the usage of bulky conventional ECG equipment with multiple electrodes for ECG signal acquisition. ECG equipment having twelve electrodes is the norm of the day but suffers from the limitations of efficient data handling even on a short-term basis. As the twelve electrode ECG equipment has portability limitations, the activities of the subject are measured only during data collection, thus making continuous patient monitoring a tedious task. Modern ECG data acquisition devices are not only expensive but also need the training to handle the equipment. Thus, even for regular health monitoring, a subject needs frequent and regular hospital visits. The frequent visits to the hospital have severe limitations like irregular health monitoring, increase in hospital’s burden, and most importantly causing physical and monetary hardship to the subject. Hence, the need of the day is a cheap, simple, portable, reliable, and long-term ECG signal monitoring system [12]. Many long-term ECG signal monitoring approaches are proposed during the last few decades. First ECG signal monitoring system based on system-on-chip (SoC) was introduced in 2012 [13], but this system consumed significant amounts of energy as it transmitted raw data. Hence, a combined technique for ECG signal denoising, ECG detection, and data compression is highly required.

1.4 OBJECTIVE OF THE WORK

Based on the above-mentioned brief overview, the following were identified as objectives of the work.

- Designing an efficient ECG signal denoising technique. The metric under consideration is Signal-to-noise-ratio.
- Designing an efficient ECG signal detection algorithm with a high detection accuracy and low overall system complexity.
- Finding a suitable process for ECG signal denoising and detection.
- Developing an algorithm which is useful for both ECG detection and data compression.
- Performance comparison of the proposed algorithm with existing algorithms on different standard ECG databases.
- Hardware implementation of a combined ECG signal denoising and ECG detection technique.

1.5 OUTLINE OF THE THESIS

The proposed thesis comprises seven chapters. In Chapter 1, a basic introduction to the development of implantable cardiac pacemaker systems, need, motivation, and identification of research problem are discussed. Then, the objectives and scope of the proposed work and organization of the thesis are presented.

Chapter 2 provides a discussion on the functionality and electrical activity of the human heart. Characteristics and parameters of a typical ECG signal and various noises which corrupt an ECG signal are discussed. Implantable cardiac pacemaker systems are also discussed.

In Chapter 3, a detailed survey of various ECG signal detection and data compression techniques are presented. A detailed description of various benchmark databases and statistical metrics used to evaluate the performance of the combine ECG denoising, ECG signal detection, and lossless data compression Technique is also presented.

In Chapter 4, ECG signal denoising, wave detection, and lossless data compression Techniques for cardiac pacemaker systems are studied. ECG signal denoising, ECG signal detection, and lossless data compression are discussed further. A detailed discussion of the proposed approaches and their theoretical backgrounds are presented.

In Chapter 5, various performance evaluation metrics, experiment results of the proposed combine ECG signal denoising, ECG signal detection, and lossless data compression are discussed.

In Chapter 6, FPGA implementation of combine ECG signal denoising, and ECG signal detection Technique for cardiac pacemaker systems are carried out, and the thesis is concluded in Chapter 7.

CHAPTER 2

BASIC THEORY OF ELECTROCARDIOGRAPHY

Human life and behavior are changing very rapidly due to fast industrial and economic growth. The most common effect of change in lifestyle is increasing the risk of cardiac diseases, which is one of the major causes of human causalities. The human heart is a vital organ as it circulates blood through the body. Many diseases related to heart have various causes, and most of them can be diagnosed by observing and conjecturing ECG. In this chapter, important information about the structure of human heart, and its electrical behavior, a cardiac pacemaker with its structure and the characteristics of ECG are discussed to understand the functionality of the heart and heartbeat.

2.1 BASIC INTRODUCTION TO CARDIOVASCULAR SYSTEM

Human cardiovascular system generally consists of three interrelated components, namely, heart, blood, and blood vessels. The cardiovascular system, also known as the circulatory system, is the blood transportation system of a human body. The heart pumps the blood to move nutrients through the blood vessels to nourish and remove the metabolic wastes from the body. The heart has two circuits within the circulatory pathway, which work together as a closed circulatory system. These two pathways are called as pulmonary pathway and systemic pathway. In a human body, the right side of the heart pushes the blood into the pulmonary pathway so that it can be oxygenated in the lungs. The left side of the heart pumps oxygenated blood to the entire body. The blood is then returned to the heart via the systemic pathway. The heart is an involuntary muscle that works somewhat independently from the nervous system. The heart is a muscular organ with four hollow chambers, as shown in Fig. 2.1. The heart consists of two upper chambers called atria, and two lower chambers called ventricles. The left and right side of the heart is divided by the septum. The heart is made up of three layers of tissues, namely, endocardium, myocardium, and pericardium. The conductive pathway within the heart has four main stations through which it senses electrical impulses and directs the heart beating. The four components of the conductive pathway are the sino-atrial (SA) node, atrioventricular (AV) node, a bundle of HIS, and the Purkinje fibers. SA node, also known as the pacemaker, is located in the right atria. SA node starts a spark and passes it onto the next relay station, the AV node. The AV node is located between the right atria and the ventricle on the back wall of the heart. The bundle of HIS located in the heart's septum passes the spark received by the AV node. The Purkinje fibers then spread the electrical charge throughout the myocardium, which is referred as the cardiac muscle. The spread of electric charge causes the heart to contract through the atria and the ventricles.

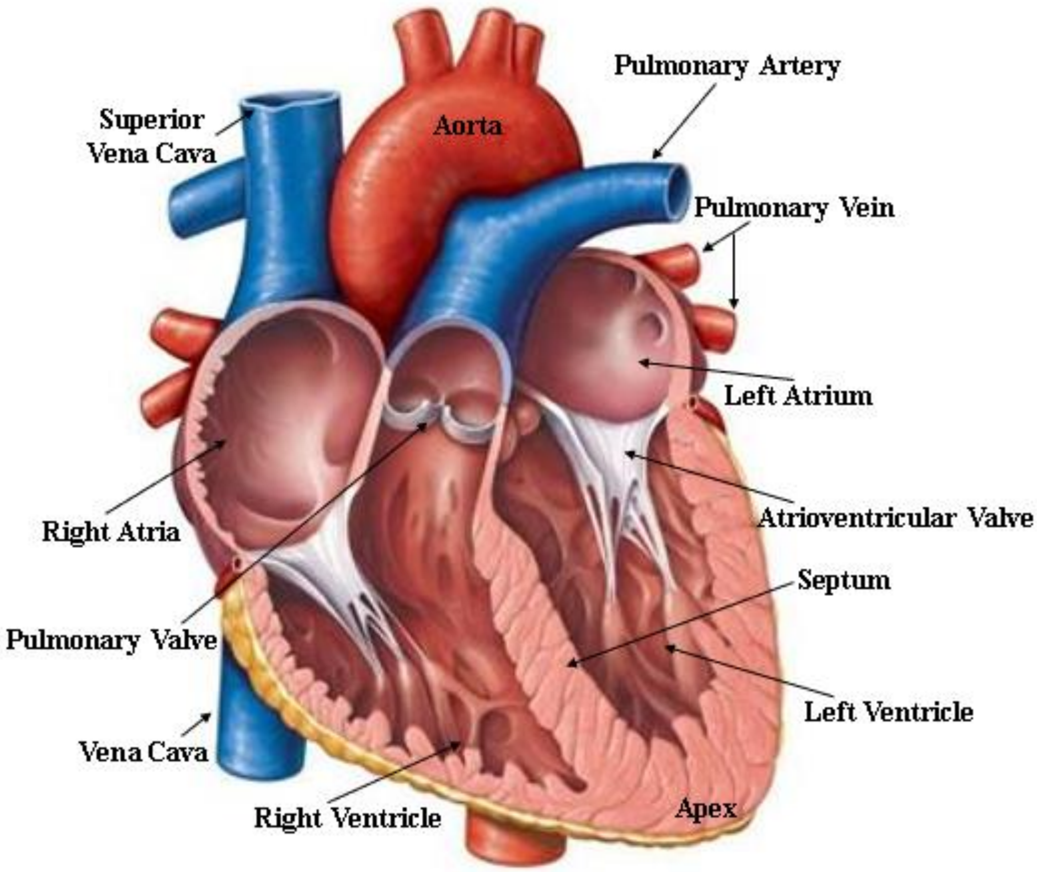

Fig. 2. 1 Internal structure of human heart

2.2 FUNCTIONING OF HUMAN HEART

The contraction and rarefication of atria and ventricles in a steady rhythm are known as the heartbeat. During a normal heartbeat, blood from tissues and lungs flows into the atria and then into the ventricles. There are two valves inside the heart called interatrial septum and interventricular septum. These two valves function like doors between the atria and ventricles and prevent the blood flowing from backward into the atria and keep the blood on the left and right side from mixing. The tricuspid valve opens into the right ventricle, and the bicuspid valve opens into the left ventricle. Muscular thin tissues called chordae tendineae hold the valves in place during the forceful contraction of the ventricles. Blood leaving the ventricles passes through another set of valves known as the pulmonary valve and the aortic valve.

In order to efficiently pump blood, heart muscles called myocardium are arranged in a unique pattern. Three layers of myocardium wrap around the lower part of the heart, which is twisted and tightened in different directions to push blood through the heart. When the pacemaker cells generate electrical signals inside the heart, the heart muscles called a myocytes contract as a group. The right and left half of the heart works together as a dual pump. On the right side of the heart, deoxygenated blood from the body’s tissues flows through large veins called the superior and inferior vena cava into the right atrium. Next, the blood moves into the right ventricle, which contracts and sends blood out of the heart to the lungs to get oxygen and get rid of carbon-di-oxide. On the left side of the heart, oxygen-rich blood from the lungs flows through the pulmonary veins into the left atrium. The blood then moves into the left ventricle, which contracts and sends blood out of the heart through the aorta to feed the cells and tissues. The first branches of the aorta are the coronary arteries which supply the heart muscle with oxygen and nutrients. Arteries branching from the middle and lower parts of the aorta supply blood to the rest of the body.

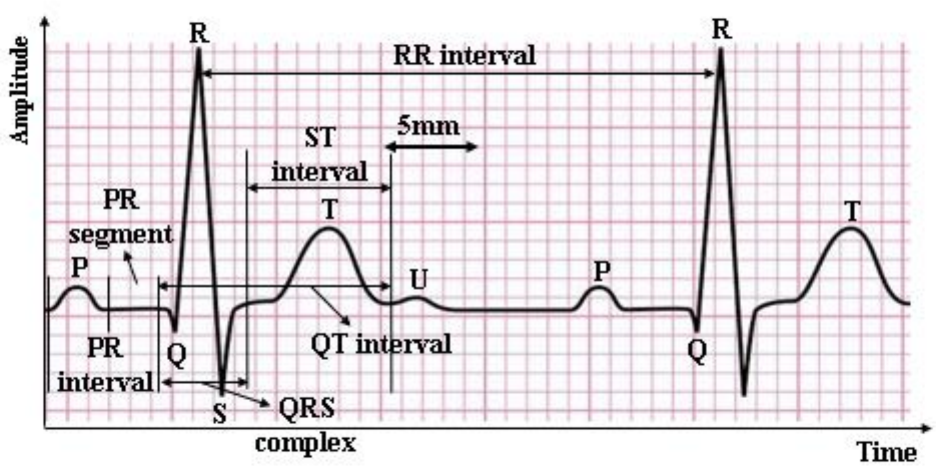

Fig. 2. 2 Graphical representation of a typical ECG signal

2.3 CHARACTERISTICS OF AN ELECTROCARDIOGRAM SIGNAL

The electrical conduction system of the heart controls the generation and propagation of electrical signals or action potentials that cause the heart's muscles to contract and pump blood. This electrical activity can be measured by electrodes placed at specific locations on the body from which a recording is produced in the form of a graph. The graph or recording showing the electrical activity of the heart as a function of time, famously known as an electrocardiogram or ECG. Thus, ECG contains tracing of the overall electrical activity of the heart resulting from the propagation of different action potentials. Each ECG representation of the cardiac cycle consists of waves, segments, and intervals, as shown in Fig. 2.2 [17]. An ECG signal normally consists of five waves, namely, P-wave, Q-wave, R-wave, S-wave, T-wave. Sometimes a sixth wave called U-wave is also observed. All these six waves either have a positive or negative deflection.

The flat isoelectric lines between the waves are called segments. The time duration of wave and segment collectively contribute to the duration of an interval. The cardiac cycle refers to the electrical and mechanical events generated during every heartbeat. It is a standard to display ECG signal on a screen or a paper, in which the vertical axis of an ECG signal indicates the amplitude of the electrical activity of the heart and the horizontal axis indicates the time. The ECG signal display is normally divided into large squares with a *5 mm* side length. These large squares are further sub-divided into smaller squares with a side length of *1 mm*. A standard ECG signal is recorded at a speed of *25 mm* per second. Thus, each large square measures a time interval of *0.20 seconds,* and small square measures a time interval of *0.04 seconds*.

P-wave in an ECG signal represents atrial depolarization and is best observed by using ECG recording lead II and lead V1. The duration of P-wave ranges from *0.06 - 0.10* seconds and the amplitude is less than *0.25 mV*. The Q-wave indicates depolarization of the interventricular septum. Q-wave is the first negative deflection after P-wave. R-wave is the first positive deflection after P-wave and Q-wave. The duration of a Q-wave is less than *0.04* seconds, and the amplitude of the Q-wave is less than *20%* of the corresponding R-wave amplitude in ECG recording leads III, AVF, V5, and V6. Q-wave is ordinarily absent in ECG recording leads V1 to V4. R-wave represents depolarization of the apex and lateral walls of the ventricles. S-wave

represents the depolarization of the base of the ventricle. Q-wave, R-wave, S-wave are collectively called a QRS-complex. The QRS-complex represents ventricular contraction.
S-wave is the second negative deflection in the QRS-complex or the first negative deflection after R-wave. The duration of R-wave ranges from *0.08 - 0.12* seconds, and the amplitude ranges from *1 - 1.5 mV*. In ECG recording leads V1 and V2, the amplitude of R-wave is smaller than the amplitude of S-wave. In ECG recording leads V3 and V4, the amplitude of R-wave and S-wave are almost equal. In ECG recording leads V5 and V6; the amplitude of R-wave is greater than the amplitude of S-wave. T-wave corresponds to ventricular repolarization. T-wave is an asymmetric wave. The duration of T-wave ranges from *0.13 - 0.30* seconds and the amplitude is less than one-third of the corresponding QRS-complex. U-wave is observed in a standard ECG signal which represents the repolarization of the papillary muscle and repolarization of the Purkinje fibers. The amplitude of the U-wave is less than one-fourth of the corresponding T-wave. U-wave is best observed when the heartrate decreases in hypokalemia using the ECG recording leads V1 and V2. The two segments that can be seen on an ECG are PQ-segment and ST-segment. The duration of the PQ-segment ranges from *0.06 - 0.10* seconds, and the duration of ST-segment ranges from *0.05 - 0.15* seconds. PR-interval, ST-interval, QT-interval, and RR-interval are four important intervals in an ECG signal. PR-interval corresponds to atrioventricular conduction and extends from the beginning of the P-wave until the beginning of the QRS-complex. PR-interval usually ranges between *0.12 - 0.20* seconds.

A prolonged PR-interval indicates atrioventricular block, and a shortened PR-interval indicates Wolff-Parkinson-White syndrome. ST-interval extends from the beginning of the ST-wave till the end of T-wave. Characteristic patterns of ST-interval indicate ischemic heart disease. QT-interval extending from the beginning of QRS-complex till the end of the T-wave denotes the time required for ventricular depolarization and repolarization. The duration of QRS-complex ranges typically between *0.35 - 0.45* seconds. The time duration between successive R-waves of QRS-complexes is called as RR-interval. RR-interval determines the heartrate [18]. Amplitude and time interval of various waves and intervals present in an ECG signal are summarized in Table 2.1.

In a healthy heart, each beat begins in the right atrium with an action potential signal from the SA node, also known as natural pacemaking signal. The signal then spreads across both atria,

Table 2. 1: Parameters of normal ECG signal

ECG Parameter	Normal Time Interval (seconds)	Normal Amplitude (mV)	Remarks
P wave	0.11 ± 0.02	0.25 ± 0.05	Increment and decrement in amplitude indicate hypokalemia and hyperkalemia, respectively.
QRS-complex	0.10 ± 0.02	1.60 ± 0.5	Increment in amplitude indicates cardiac hypertrophy
R wave	-----	1.60 ± 0.5	---
Q wave	-----	0.25 times that of the corresponding R-wave	---
T wave	-----	0.5	Indicates the possibility of a myocardial infraction
PR interval	0.12 – 0.20	------	Time is taken by the electrical signal to travel from atria to ventricle.

causing the muscle to depolarize and contract. In the ECG signal, the atrial depolarization is represented by P-wave.

The period of conduction that follows atrial systole and proceeds the contraction of the ventricle is depicted on the ECG by PR-segment (a flat line following the P-wave). The signal leaves atria and enters ventricle via the atrial-ventricular node located in the interatrial septum. As the signal spreads through the ventricles, including ventricle systole, the contractile fibers depolarize and contract very rapidly. The QRS-complex in an ECG signal represents rapid ventricular depolarization. Atrial repolarization also occurs at the same time but is hidden in the QRS-complex of ECG signal. Finally, as the electrical signal passes out of the ventricles, the ventricular wall starts to relax and recovers to a state described as ventricular diastole. The dome shape T-wave on the ECG marks the ventricular repolarization. In an ECG signal, the ST-segment depicts the period when the ventricles are depolarized. The QT-interval determines the time taken by the heart to depolarize and repolarize the ventricles. The sequence of events described above associated with an ECG signal are repeated during every normal heartbeat.

2.4 OVERVIEW OF IMPLANTABLE CARDIAC PACEMAKER SYSTEM

A cardiac pacemaker is a device used to treat cardiac dysrhythmia by rapidly tracking heartrate and rhythm of a heart. Cardiac pacemakers deliver rhythmic electric stimulus in a controlled manner to the heart to maintain the heartbeat. Pacemaker system mainly consists of two components [14]; pacing lead and pacemaker device, as shown in Fig. 2.3. The pacing lead is a flexible insulated wire which connects the human heart to the pacemaker device. The pacing lead, as shown in Fig. 2.4, is made up of four components: electrode tip, conductor, insulation, and electrode. The electrode tip is inserted into the heart through a vein that carries impulses between the pacemaker device and heart to stimulate the heartbeat. The same electrode tip is used to exchange information between heart and pacemaker device, which accesses the condition of the heart. A conductor coil delivers the pacing pulses to the heart, and an insulator isolates the conductor from the heart walls. Pacemaker device is a decision-making device in a cardiac pacemaker. Single chamber pacemaker, dual-chamber pacemaker, and Biventricular pacemaker are different types of pacemakers [15]. Single chamber pacemaker has one lead either positioned into the atria or ventricle, most commonly used by patients with sinus node disease.

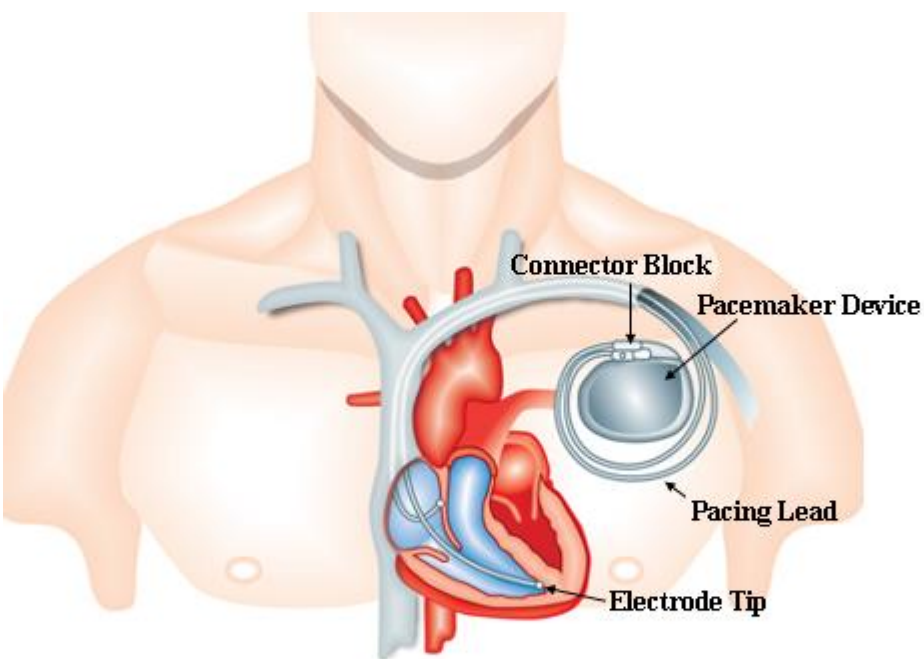

Fig. 2. 3 Cardiac pacemaker system

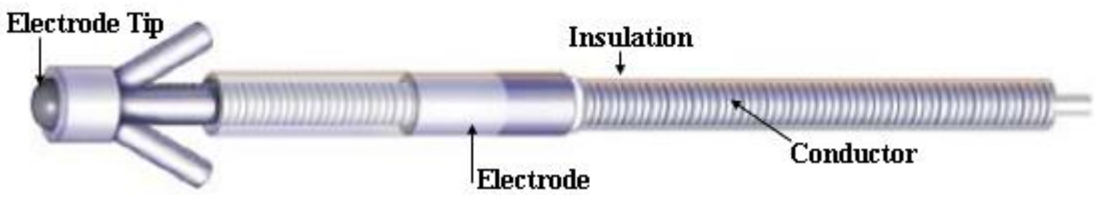

Fig. 2. 4 Basic components of a pacemaker's pacing lead

Dual-chamber pacemaker has two leads, each positioned in the right atria and right ventricle. Patients with a heart block most commonly use dual-chamber pacemakers. Biventricular pacemakers have three leads, each positioned into the right ventricle, left ventricle and left atria. Biventricular pacemakers are most commonly found in patients with heart failure.

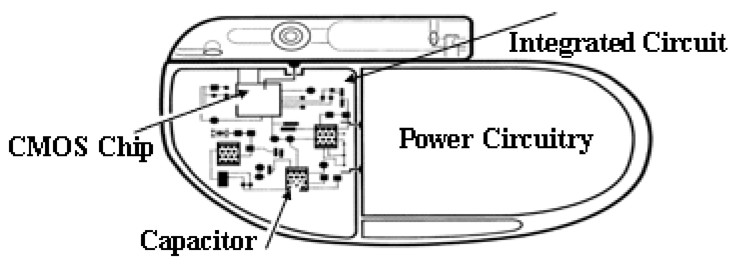

Fig. 2. 5 Main components in a pacemaker device

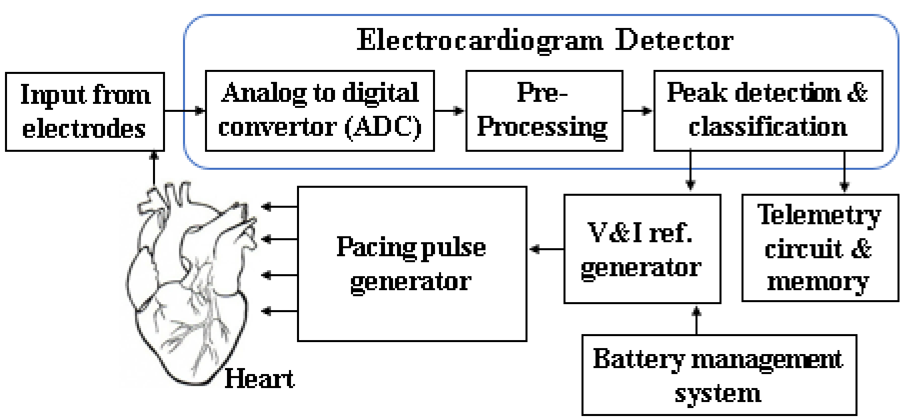

Fig. 2. 6 Block diagram of a cardiac pacemaker

Pacemaker device has two main components, as shown in Fig. 2.5, electronic circuitry and a power managing system. The electronic circuitry contains all the necessary circuits needed to operate the device, detect the heart activity, estimate the heartrate, and deliver the necessary rhythmic electric stimulus [16]. The electronic circuitry mainly consists of following subcircuits: ECG detector, wave counter, reference comparator, and pulse generator. Block diagram of a typical cardiac pacemaker circuit is as shown in Fig. 2.6.

2.6 NOISE EFFECTS IN ECG

The ECG signal, like any other electric signal, is prone to noises. Before processing an ECG signal, all noises need to be filtered using denoising techniques. The ECG signals shown in Fig. 2.7 (a-f) are sampled at 360 Hz. The most significant noises that corrupt an ECG signal are [19] as follows.

1) Powerline Interference: the noise component due to the interference between the powerline and the ECG signal is called as powerline interference. Power line interference introduces a signal with a constant amplitude at the frequency of powerline. The frequency of powerline is country-specific, which is 50 *Hz* or 60 *Hz*. The effect of power line interference on an ECG signal is shown in Fig. 2.7 (a). The power spectral density of the powerline interference corrupted ECG signal is shown in Fig. 2.7 (b).

2) Electrode Contact Noise: The noise component introduced into an ECG signal due to the lack of proper electrical contact between the electrode and skin is known as electrode contact noise. As shown in Fig. 2.7 (c) electrode contact noise is characterized by a baseline shift in the ECG signal. The power spectral density of the Electrode contact noise corrupted ECG signal is shown in Fig. 2.7 (d).

3) Motion Artefact: Motion artifact is a type of noise caused by the physical movement of the patient during the process of ECG recording. Motion artifact introduces a baseline shift in the ECG signal and can be as large as *500%* of the peak-to-peak amplitude of an ECG signal. The effect of motion artifact on the ECG signal is shown in Figure 2.7 (e). The power spectral density of the motion artefact corrupted ECG signal is shown in Fig. 2.7 (f).

4) Muscle Contraction: The contraction and expansion of muscles introduce noise in the frequency range of *10 kHz* in the ECG signal. As shown in Fig. 2.7 (g), muscle contraction introduces frequency distortion to an ECG signal. The power spectral density of the muscle contraction corrupted ECG signal is shown in Fig. 2.7 (h).

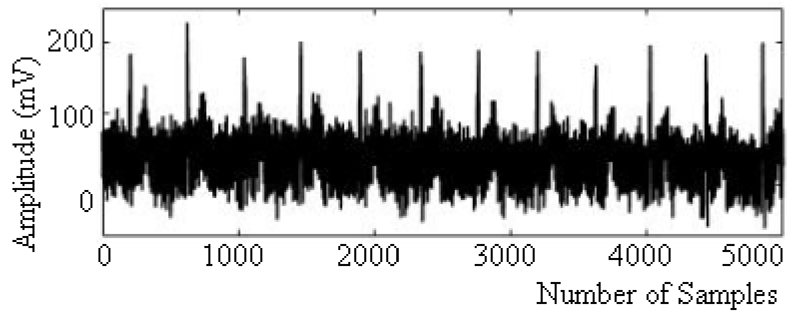
Amplitude (mV)
Number of Samples

(a)

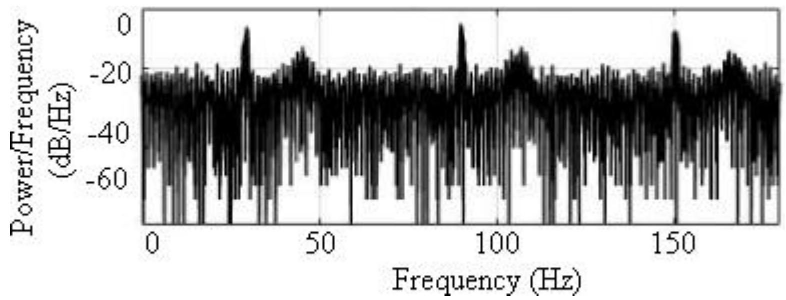
Power/Frequency (dB/Hz)
Frequency (Hz)

(b)

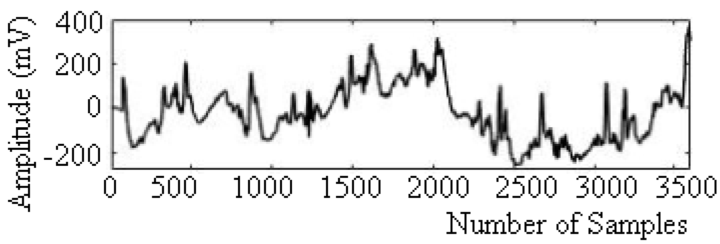
Amplitude (mV)
Number of Samples

(c)

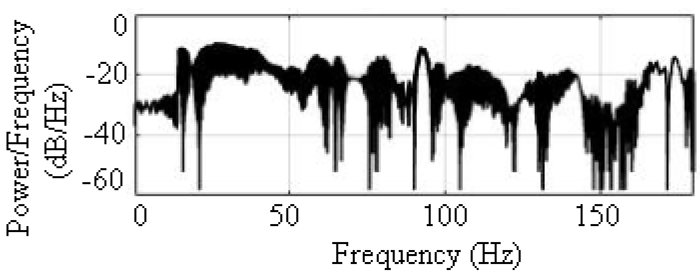
Power/Frequency (dB/Hz)
Frequency (Hz)

(d)

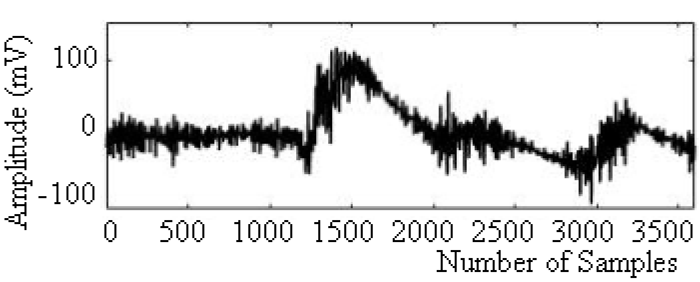
Amplitude (mV)
Number of Samples

(e)

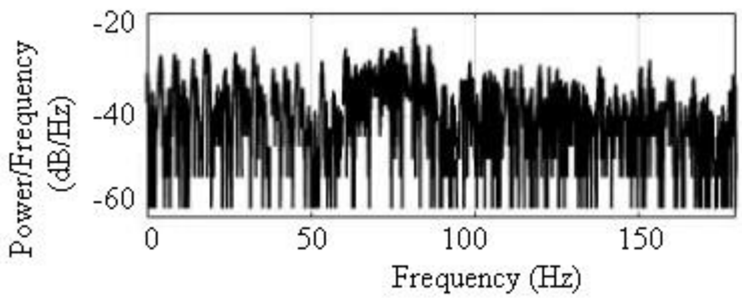

-20
-40
-60
Power/Frequency (dB/Hz)
0
50
100
150
Frequency (Hz)

(f)

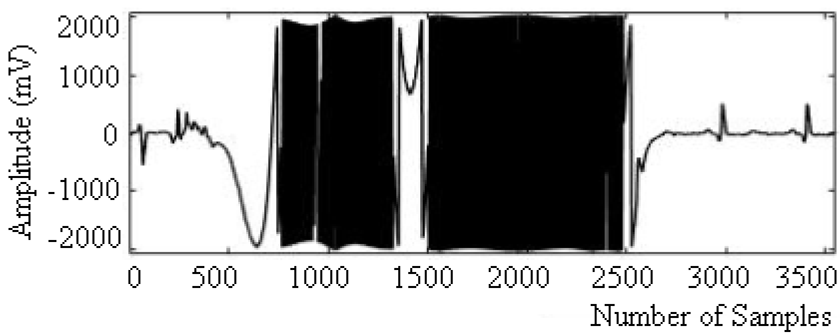

2000
1000
0
-1000
-2000
Amplitude (mV)
0
500
1000
1500
2000
2500
3000
3500
Number of Samples

(g)

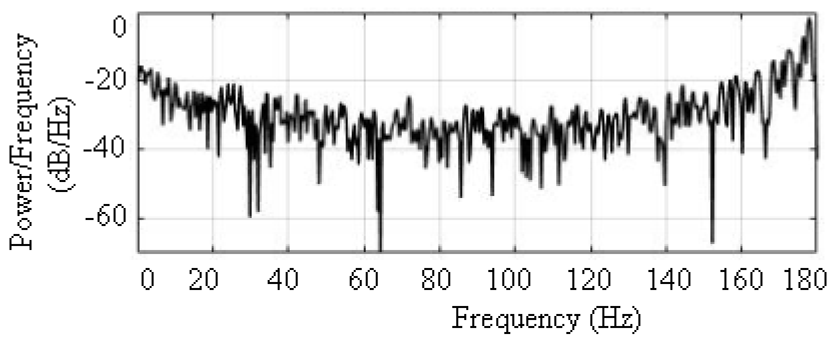

0
-20
-40
-60
Power/Frequency (dB/Hz)
0
20
40
60
80
100
120
140
160
180
Frequency (Hz)

(h)

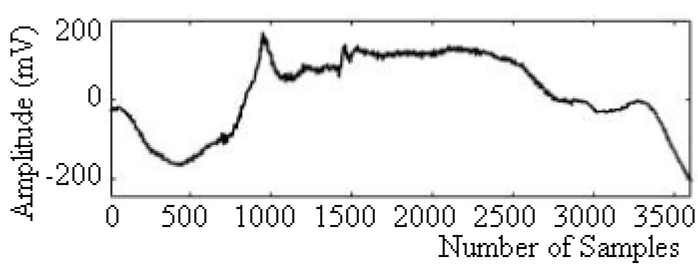

200
0
-200
Amplitude (mV)
0
500
1000
1500
2000
2500
3000
3500
Number of Samples

(i)

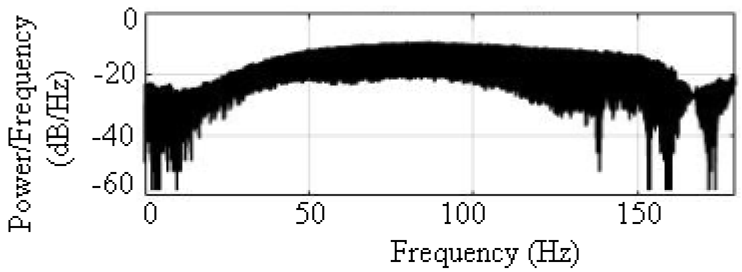

(j)

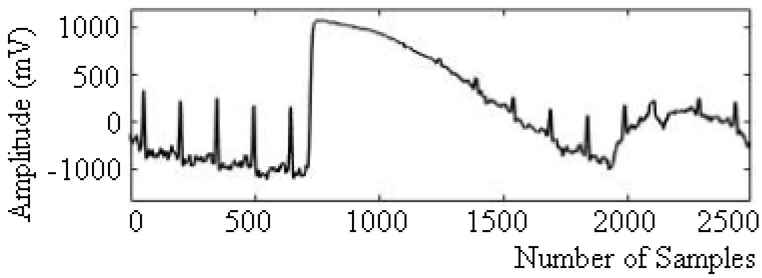

(k)

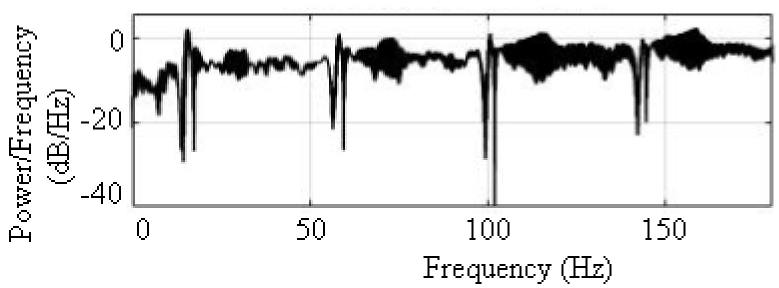

(l)

Fig. 2. 7 Effect of various noises on ECG signal, (a) powerline interference, (b) Power spectral density of powerline interference corrupted ECG signal, (c) electrode contact noise, (d) Power spectral density of electrode contact noise corrupted ECG signal (e) motion artefacts, (f) Power spectral density of motion artefact corrupted ECG signal (g) muscle contraction, (h) Power spectral density of muscle contraction corrupted ECG signal (i) baseline drift, (j) Power spectral density of baseline drift corrupted ECG signal, (k) instrumentation noise, and (l) Power spectral density of instrumentation corrupted ECG signal

5) Baseline Drift: Baseline drift is a form of noise that occurs mostly due to the respiration of the subject, resulting in noise in the frequency range of *0.15 - 0.3 Hz* in the ECG signal. The effect of baseline drift on an ECG signal is shown in Fig. 2.7 (i). The power spectral density of the baseline drift corrupted ECG signal is shown in Fig. 2.7 (j).

6) Instrumentation Noise: Instrumentation noise is due to the electrical nature of the ECG signal. An ECG signal is prone to noise due to interference from other electronic equipment due to

improper shielding. An ECG signal corrupted with instrumentation noise is shown in Fig. 2.7 (k). The power spectral density of the muscle contraction corrupted ECG signal is shown in Fig. 2.7 (l).

CHAPTER 3

LITERATURE SURVEY

Recent developments in health monitoring and assisting technologies like cardiac pacemakers have paved paths for less complex and cost-effective implantation practices and procedures. The protracted battery durability, enhanced device care, and security, better and reliable clinical results and conclusions have made these devices much dependable. The present study is a review of such enriching contributions and innovative studies done recently and in the past.

3.1 ALGORITHMIC STRUCTURES OF DIFFERENT ECG DETECTION AND DATA COMPRESSION TECHNIQUES

In the last few decades, rapid growth in the field of cardiac pacemakers can be attributed to biomedical signal processing algorithms and CMOS IC design. The circuit design efforts of biomedical CMOS ICs paved the path to implement complex signal analytical algorithms which can more accurately detect ECG signal features. Various approaches in the literature presented methods to increase the accuracy of wave detection, methods to increase the efficiency of the wave detection algorithms, and to reduce the effect of various noises present in an ECG signal. Pan et al. [20] developed the first real-time QRS-complex detection algorithm based on time-domain analysis by using ECG signal as input from Massachusetts Institute of Technology-Boston's Beth Israel Hospital (MIT-BIH) arrhythmia database [21]. ECG signals are de-noised using bandpass filters, realized by using cascade combinations of lowpass and highpass filters. The fiducial points; P-wave, QRS-complex, and T-wave are detected by finding the maximum value of the square of the slope of the denoised signal. The primary issue concerned with the time domain-based algorithm is that, extracting ECG signals by removing noises using a bandpass filter is not efficient and degrades the detection accuracy. Approaches based on ECG morphology [22–26], time domain [27], time-frequency domain [28-45] and genetic algorithm [46-50] are some ECG signal detection techniques which provide high detection accuracy. Morphology-based method for ECG signal detection uses approaches based on artificial neural networks. Time-frequency domain-based ECG signal detection methods use approaches based on wavelet transform, filter banks, and nonlinear transform.

Table 3. 1: Comparison of different published ECG detection algorithms

Method	Algorithm	Technique	Hardware Complexity	Detection Performance
Time-domain	Filtering	Bandpass filtering	Simple	96% - 98%
		Digital filtering		
		Adaptive filtering		
Derivative based	-	First derivative	Medium	95%-97%
		The first and second derivative		
ECG morphology	Artificial neural network	Artificial neural network	Complex	99%
Time-frequency Domain	Hilbert transform	Hilbert transform	Complex	95%
	Empirical mode decomposition	Empirical mode decomposition	Complex	95% - 98%
	Wavelet transform	Haar	Medium	< 99%
		Symlet		
		Biorthogonal		
		Reverse-Biorthogonal		
Combined Algorithm	Wavelet transform + genetic algorithm	-	Complex	~99.99%

Further, a combination of techniques like wavelet transform and genetic algorithm are also used to improve ECG signal detection accuracy [51-52]. A significant amount of work is published in the fields related to ECG signal detection uses techniques based on ECG signal enhancement [53–56] and pattern classification [57–62]. An overview of some of these approaches is presented in [63-65]. Various ECG detection algorithms are summarized in Table 3.1 [29]. As shown in Table 3.1, wavelet-based ECG signal detection algorithms provide a detection accuracy higher than 99% with a medium hardware complexity when compared to other techniques. Thus, wavelet transform based ECG signal detection technique is considered as one of the most efficient techniques [29] and further developed in this work.

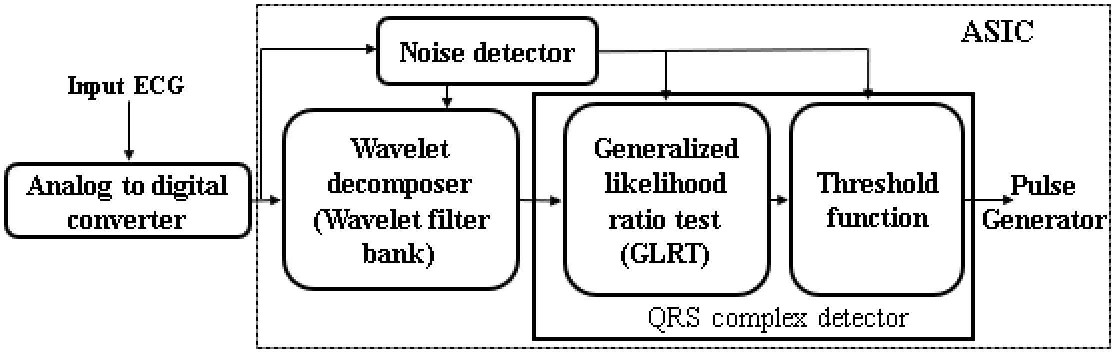

(a)

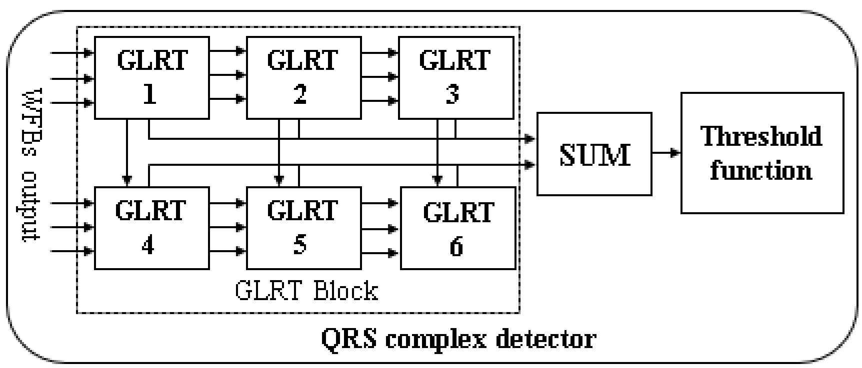

(b)

Fig. 3. 1 (a) Block diagram of generalized likelihood ratio test (GLRT) based ECG detector, (b) Block diagram of QRS-complex detector

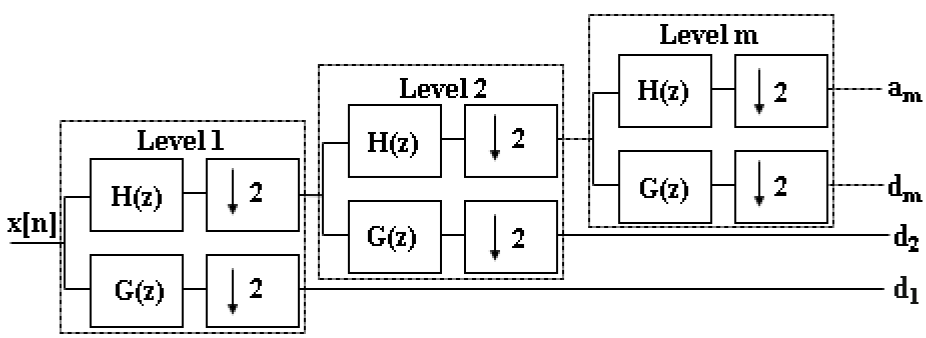

Fig. 3. 2 The dyadic wavelet transform based filter bank

Rodrigues et al. [66] introduced the digital implementation of a wavelet-based QRS-complex detector suitable for cardiac pacemakers. The proposed cardiac pacemaker in [66] uses a wavelet decomposer and a QRS-complex detector, as shown in Fig. 3.1 (a) [66]. QRS-complex detection block which includes a generalized likelihood ratio test (GLRT) [67] and threshold function is shown in Fig. 3.1 (b).

Dyadic wavelet transform based filter bank decomposes the input ECG signal into two sub-bands output, namely monophasic and biphasic. The advantage of dyadic wavelet transform is due to its low complexity as it uses undecimated lowpass and highpass filter [68, 69]. Wavelet decomposer consists of a dyadic wavelet transform based filter bank, as shown in Fig. 3.2 [68], and QRS detection block that includes a GLRT [67] and threshold function. Dyadic wavelet transform based filter bank decomposes the ECG signal into sub-bands with two outputs, namely monophasic and biphasic. The advantage of dyadic wavelet transform is due to its low complexity as it uses undecimated lowpass and highpass filter pairs [68, 69].

Symmetric and asymmetric wavelet filter banks used in a dyadic wavelet transform are mathematically expressed using Eq. (3.1), and Eq. (3.2).

$$H(z)=1+3z^{-1}+3z^{-2}+z^{-3} \tag{3.1}$$

$$G(z)=1+z^{-1} \tag{3.2}$$

Here, *H(z)* and *G(z)* are transfer functions of lowpass and highpass filter, respectively.

The noise level in the first filter output is determined by using a noise detector. The output of the wavelet filter bank is fed to QRS-complex detector, which in turn estimates the heartbeat rate. GLRT determines the presence of a QRS-complex based on the test computations using Eq. (3.3)

$$T(a)=x(a)^{T}\left(M^{T}M\right)^{-1}M^{T}x(a) \tag{3.3}$$

Here, *x(a)* is input to the wavelet filter bank, **M** is a linear combination matrix of representative functions. The major drawback of the GLRT based approach is that the QRS-complex detector requires more power compared to other existing techniques and results in low detection accuracy. The drawbacks in [66] have been overcome by Min et al. [70]. In [70], multiscale product-based wavelet transforms using soft threshold is used to develop decimator architecture-based ECG signal detector for low-power implantable cardiac pacemaker. The use of multiscaled product algorithm leads to considerable power reduction in hardware implementation, but QRS-complex detection accuracy is reduced when compared to [66]. Dyadic wavelet transform has low computational complexity, thus considered as most suitable to implement in an ECG signal detector [71].

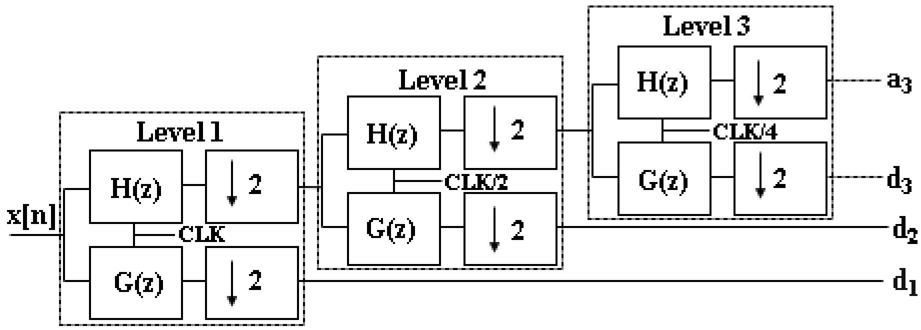

(a)

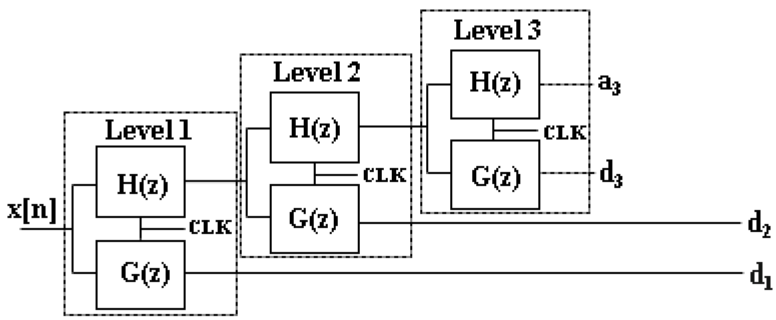

(b)

Fig. 3. 3 (a) Decimator based wavelet filter bank. (b) Undecimator based wavelet filter bank

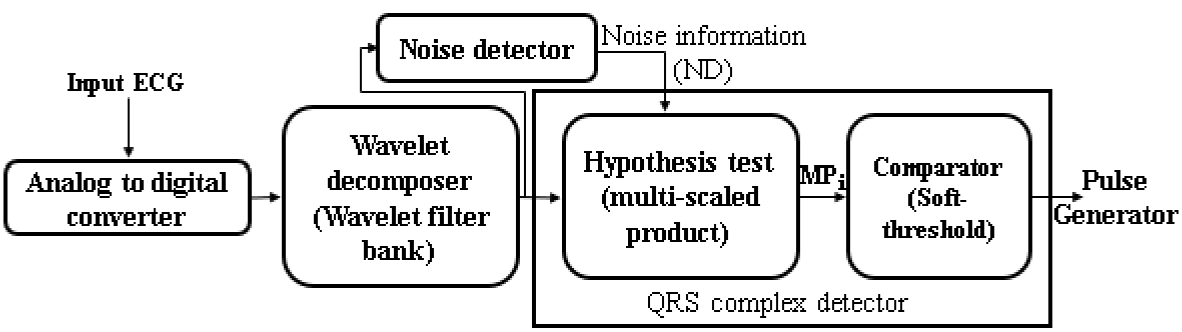

Fig. 3. 4 Multi-scaled product algorithm-based ECG detector

Wavelet filter bank architectures are of two types: undecimator and decimator based. Undecimator architecture has the advantage of translation invariance. Translation invariance is achieved by keeping same sampling rate (frequency) in all decomposition levels. The main disadvantage of undecimator-based architecture is that they require a constant clock and a large number of registers. The register count in an undecimator architecture is reduced by using a decimator based wavelet filter bank architecture. However, decimator based architecture can only be implemented by using a limited set of wavelet functions [72]. The architectures of decimator and un-decimator-based wavelet filter bank are shown in Fig. 3.3 [70].

Soft threshold algorithms [73] are used to boost the detection accuracy of the QRS-complex. Block diagram of a wavelet transform based ECG signal detector is shown in Fig. 3.4 [70]. Wavelet transform based QRS-complex detection approach requires one multiplier and two multiplexers while GLRT based QRS-complex detection requires forty-five adders and six multipliers. Eq. (3.4) expresses multiscaled product of wavelet filter bank output shown in Fig. 3.5 (a) [70]. Here, i is a subset of wavelet filter bank output [74, 75].

$$MP_i = \prod_i |WF_i| \tag{3.4}$$

Here, MP_i and WF_i, respectively, are the output of multi-scaled product algorithm and wavelet coefficients. The soft-threshold algorithm, as shown in Fig. 3.5 (b) [70], requires a smaller number of multiplication operations when compared to the hard threshold, thus resulting in a significant reduction in hardware complexity and power consumption. Unlike the fixed threshold value in the hard threshold algorithm, a soft threshold algorithm uses a variable threshold, which increases the probability to detect QRS-complex [73].

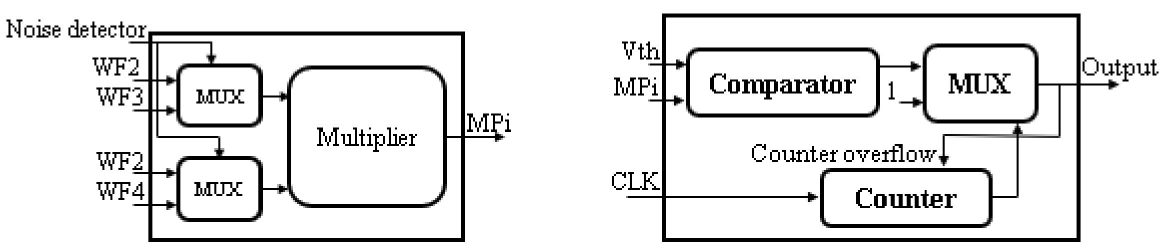

(a) (b)

Fig. 3. 5 (a) Multi-Scaled product algorithm. (b) Soft-threshold algorithm

The major concern with a soft threshold algorithm is the requirement of add and shift multiplier for signal multiplication, which requires more hardware and processing time. As shown in Fig.

3.6, Bhavtosh et al. [76] replaced add and shift multiplier in [73] with booth multiplier to reduce the ECG processing time. Use of booth multiplier reduces the complexity and overall delay.

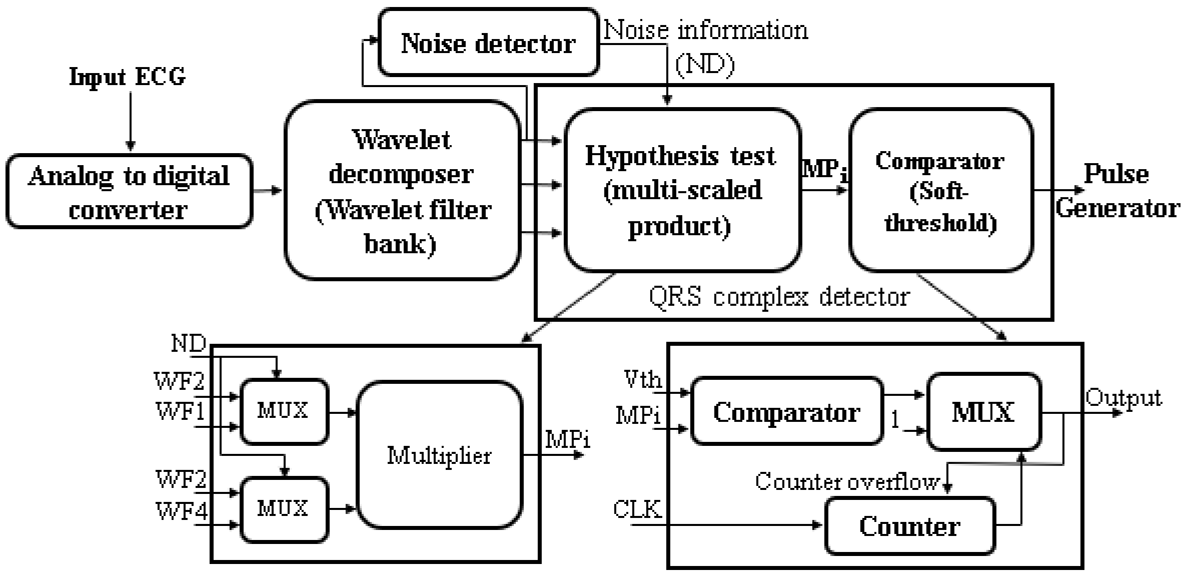

Fig. 3. 6 Booth multiplier-based ECG detector

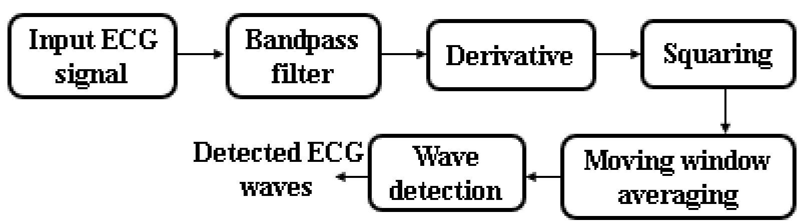

Fig. 3. 7 Block diagram representation of ECG detection flow

Using a booth multiplier instead of a conventional add shift multiplier for multiplication operation increases the complexity of multi-scaled product block. Wang et al. [77] proposed a low-cost application-specific integrated circuit (ASIC) ECG signal detector for real-time analysis. Different ASIC designs are presented in [78–82], and one of them is embedded in a biomedical system for ECG signal detection [82]. The basic ECG signal detection algorithm contains six steps. The signal processing flow of an ECG signal detection is shown in Fig. 3.7 [83]. Basic array structure used for filter design and processing unit of an ECG signal detector using ASIC is shown in Fig. 3.8 [77] and Fig. 3.9 [77], respectively. A bandpass filter is used to reduce the effect of various noises [84]. Eq. (3.5) and Eq.(3.6) gives the differential equations of a lowpass filter and a highpass filter, respectively.

$$y(aT) = 2y(aT-T) - y(aT-2T) + x(aT) - 2x(aT-6T) + x(aT-12T) \tag{3.5}$$

$$y(aT) = x(aT-16T) - (1/32)\left[y(aT-T) + x(aT) - x(aT-32T) \right] \tag{3.6}$$

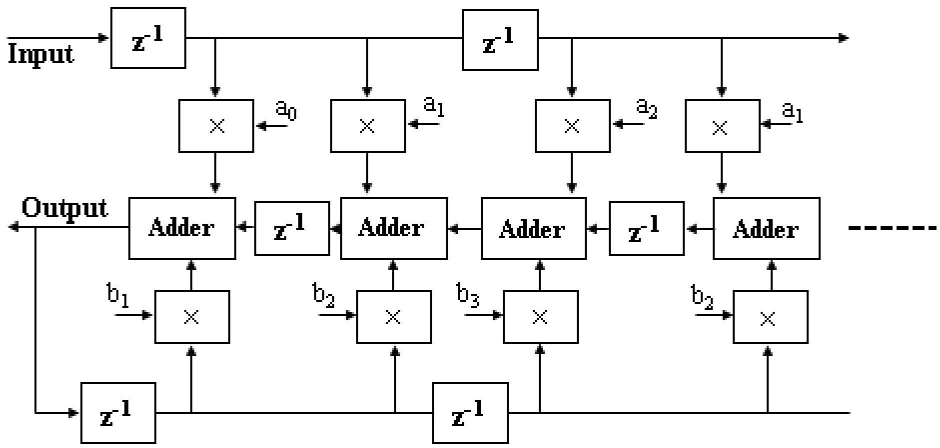

Fig. 3. 8 Basic array structure used for filter design

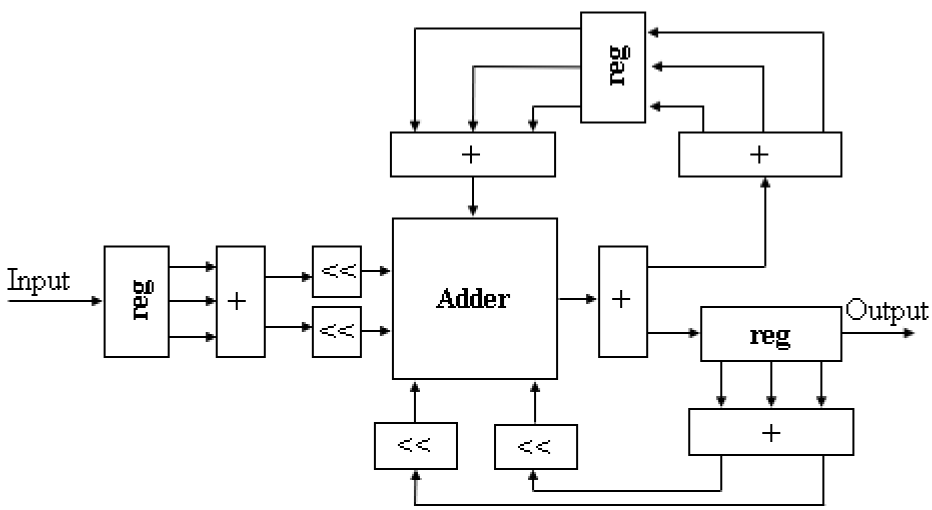

(* reg: register, +: adder, <<: Comparator)

Fig. 3. 9 Schematic representation of processing unit for ECG detection in ASIC

ECG signal is differentiated by passing it through a bandpass filter. After the differentiation stage, the slope information of an ECG signal is not appropriate hence, the output is squared at each point. Furthermore, a moving window average produces a signal containing the information of the slope as well as the width of the QRS-complex.

Difference equations of derivative, squaring, and moving window average are as given by Eq. (3.7), Eq. (3.8), and Eq. (3.9), respectively.

$$y(aT)=\left(\frac{1}{8}\right)\left[2x(aT)+x(aT\text{-}T)\text{-}x(aT\text{-}3T)\text{-}2x(aT\text{-}4T)\right] \tag{3.7}$$

$$y(aT)=\left[x(aT)\right]^2 \tag{3.8}$$

$$y(aT)=\left(\frac{1}{A}\right)\left[x\left(aT\text{-}(A\text{-}1)T\right)+x\left(aT\text{-}(A\text{-}2)T\right)+.....+x(aT)\right] \tag{3.9}$$

Here, *A* is the number of samples of the moving window, and *a* is a constant.

Filters circuits shown in Fig. 3.7 are represented using Eq. (3.10).

$$H\left(z^{-1}\right)=\frac{\sum_{i=0}^{N} p_i z^{-1}}{1-\sum_{i=1}^{N} q_i z^{-1}} \tag{3.10}$$

Here, $H(z^{-1})$ is the transfer function, and p_i and q_i are real coefficients. To reduce hardware cost, systolic array based digital filters, which also reduce noise, are used [85]. The systolic array based approach is not preferred because systolic architectures degrade the QRS-complex detection performance.

Many body sensor networks (BSN) based approaches are developed for wearable systems. A physiological measurement device is a fundamental component in a telemonitoring and remote healthcare system. Baek et al. [86] proposed a healthcare chair which provides noninvasive measurement of various biosignals, including ECG. The proposed healthcare chair uses capacitively coupled electrodes to continuously measure the ECG signal. Vuorela et al. [87] proposed a device that can continuously measure the ECG signal in a BSN environment. Vuorela et al. introduced a portable long-term physiological signal recorder to measure bioimpedance, electrocardiography, and user activity. The main drawback of the physiological signal recorder is the inability to store any recorded signals due to lack of memory. As demonstrated by Yang et al. [88], a low-power biopatch based design with flexible electrodes suits portable health monitoring systems. However, the system in [88] lacks a wireless communication feature. A complete BSN system for ECG signal measurement has been proposed by Tsai et al. [89]. High power consumption and constrained energy supply (battery) limits the long-term usage of the proposed portable ECG signal measurement system. A 25-electrode wearable cardiac monitoring system featuring a complete SoC system with wireless transmission capability of ECG signals is demonstrated by Yan et al. [90].

A fully integrated SoC based three lead ECG for wireless BSN applications is proposed by Khayatzadeh et al. [91]. The SoC consists of two-channel ECG frontend with successive approximation register analog-to-digital converter (SAR-ADC), microcontroller, static random-access memory (SRAM), and a medical implantation communication service band RF-transceiver. The ultra-low-power feature is achieved with the help of a low leakage sub-threshold SRAM and an energy-efficient microcontroller. Lee et al. [92] proposed a biological ECG acquisition and classification system for BSN. Block diagram of a low power wireless biosignal acquisition and classification system is shown in Fig. 3.10 [92].

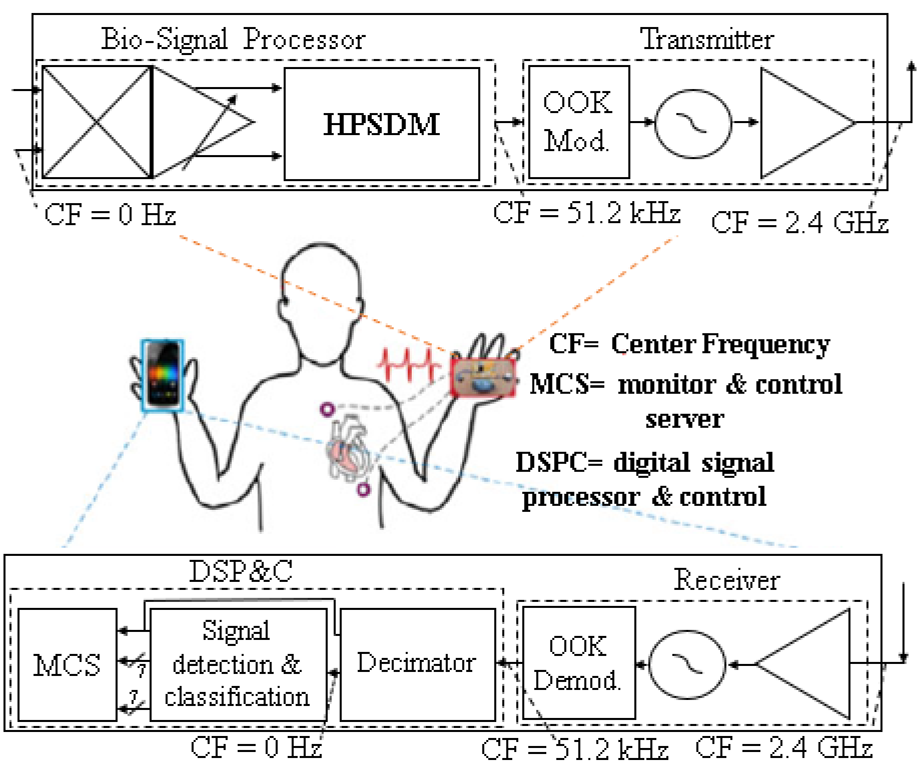

Fig. 3. 10 Block diagram of a low power wireless biosignal acquisition and classification system

A low-power wireless biosignal acquisition and classification system requires a biosignal processor (BSP), a low power super-regenerative on-off keying (OOK) transceiver, and a digital signal processor. The BSP circuit consists of a chopper-based continuous-time amplifier (CBCTA) shown in Fig. 3.11 [92], and a highpass sigma-delta modulator (HPSDM) shown in Fig. 3.12 [92]. If the resolution of the transceiver is greater than twelve bits, the resultant circuit provides low system complexity thus reducing the power consumption. In biosignal processing, noise reduction is a big challenge. CBCTA removes commonly present thermal noise and Flicker noise in biosignals.

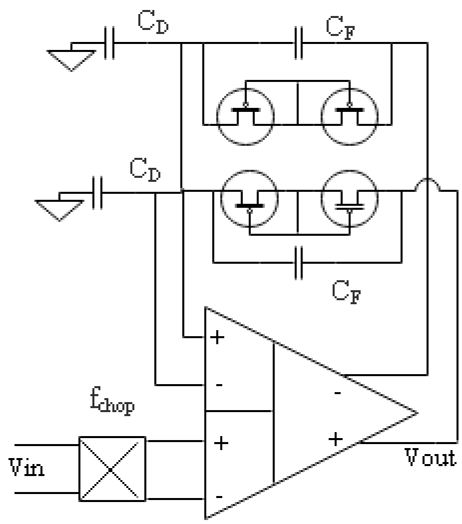

Fig. 3. 11 Chopper-based continuous-time amplifier

CBCTA can be used either as an amplifier and a band-pass filter [93]. Transfer function and characteristics of CBCTA are given by Eq. (3.11) through Eq. (3.15).

$$H(s) \approx \frac{P_{m1}\left[s+\dfrac{1}{R_F\left(C_F+C_D\right)}\right]}{C_C s^2+\dfrac{P_{m2}C_F}{C_F+C_D}s+\dfrac{P_{m2}}{R_F\left(C_F+C_D\right)}} \tag{3.11}$$

$$A_M = \frac{P_{m1}\left(C_F+C_D\right)}{P_{m2}C_F} \tag{3.12}$$

$$f_0 = \frac{1}{R_F\left(C_F+C_D\right)} \tag{3.13}$$

$$f_{high-3dB} = \frac{P_{m2}C_f}{\left(C_f+C_d\right)C_c} \tag{3.14}$$

$$f_{low-3dB} = \frac{P_{m2} C_F}{(C_F + C_D) C_C} \tag{3.15}$$

Here R_F is a feedback resistor. A_M is mid-band gain. P_{m1} and P_{m2} are the transconductances of the input stage, and C_F is the feedback capacitor.

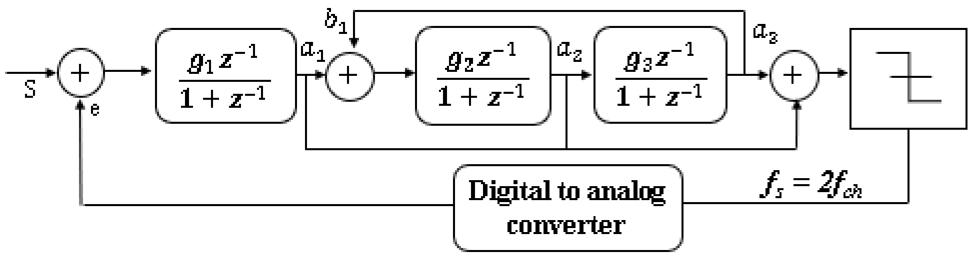

Fig. 3. 12 Highpass sigma-delta modulator

By using different sets of capacitances C_D, the CBCTA can be used in gain tunable applications. Due to the high resolution of sigma-delta modulator (SDM), it is broadly used in low-frequency applications. Fig. 3.12 shows system architecture of a highpass SDM(HPSDM) which is chosen as an ADC in the BSP circuit. A highpass filter is obtained by replacing z with $-z$ and by shifting central frequency from 0 to $\frac{fs}{2}$ in a lowpass filter. Stability of HPSDM is the same as that of a lowpass SDM [94]. Transfer function at the summation points a_1, a_2, and a_3 are given by Eq. (3.16) to Eq. (3.18):

$$H_{a1}(z) = (g - p)\frac{g_1 z^{-1}}{1 + z^{-1}} \tag{3.16}$$

$$H_{a2}(z) = (g - p)\frac{g_1 g_2 \left(1 + z^{-1}\right) z^{-2}}{\left(1 + z^{-1}\right)^3 + b_1 g_2 g_3 \left(1 + z^{-1}\right) z^{-1}} \tag{3.17}$$

$$H_{a3}(z) = (g - p)\frac{g_1 g_2 g_3 z^{-3}}{\left(1 + z^{-1}\right)^3 + b_1 g_2 g_3 \left(1 + z^{-1}\right) z^{-2}} \tag{3.18}$$

Here, g is input, p is error and g_1, g_2, g_3 are the constants. The switched-capacitor circuit shown in Fig. 3.13 [93], can be used to realize a first-order highpass integrator and Eq. (3.19) gives its transfer function.

$$H(z)=\frac{C_S}{C_I}\frac{z^{-1}}{1+\left(\frac{C_H}{C_I}-1\right)z^{-1}} \tag{3.19}$$

Here $C_H = 2C_I$.

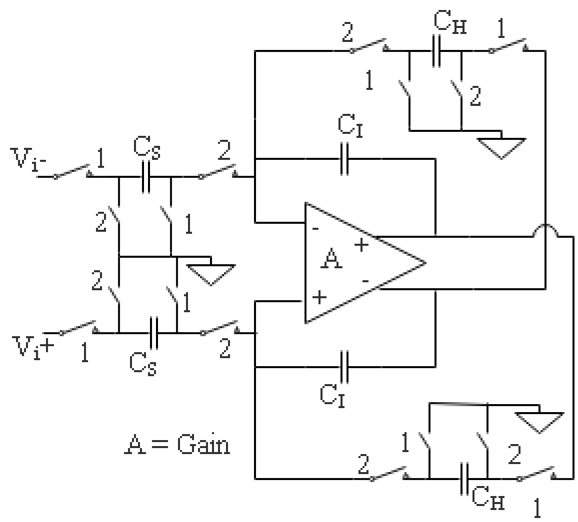

Fig. 3. 13 Schematic of the first-order highpass integrator

Block diagram of a wavelet transform processor and three stages of a Haar wavelet transform realization are shown in Fig. 3.14 (a) and Fig. 3.14 (b), respectively [92]. The DWT function defined in [95-97] is given by Eq. (3.20) and Eq. (3.21):

$$W_{\phi_{j0,r}}(n)=\frac{1}{\sqrt{M}}\sum_r \phi_{j0,r}(r)S(n-r) \tag{3.20}$$

$$W_{\psi_{j,r}}(n)=\frac{1}{\sqrt{M}}\sum_r \psi_{j,r}(r)S(n-r) \tag{3.21}$$

Here, $S(n)$ is input signal, $\phi_{j0,r}(r)$ and $\psi_{j,r}(r)$ are the impulse responses of scaling function and wavelet function, j_0 and j are the *scale-0* of the wavelet decomposition and *scale-1* of wavelet transform, M is dilation equal to one in this work and r is the number of sample points.

Considering the tradeoff between hardware cost and power consumption, the Haar wavelet transform is found suitable to implement the wavelet transform processor circuit. The transfer function of scales is given by Eq. (3.22) and Eq. (3.23).

$$W_i = M_{\phi i}(z) = 1 + z^{-2^{i-1}} \tag{3.22}$$

$$S_i = M_{\psi i}(z) = 1 - z^{-2^{i-1}} \tag{3.23}$$

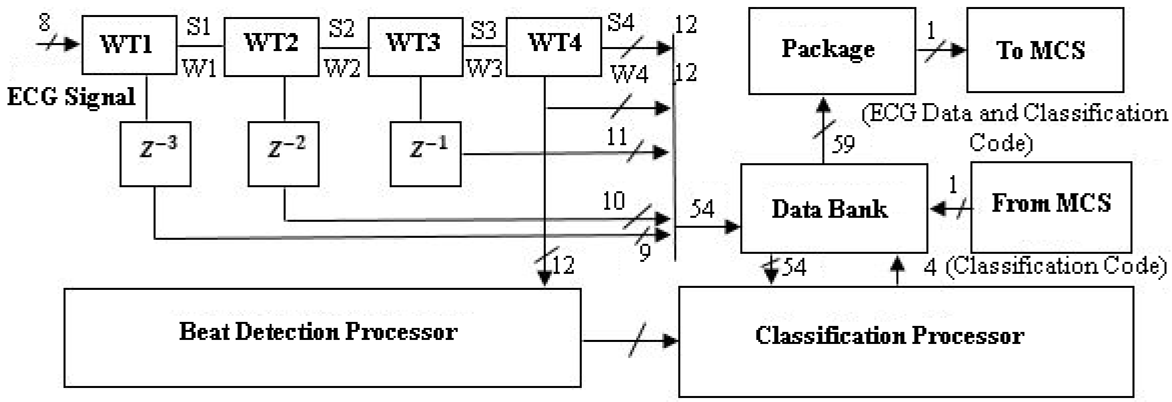

(a)

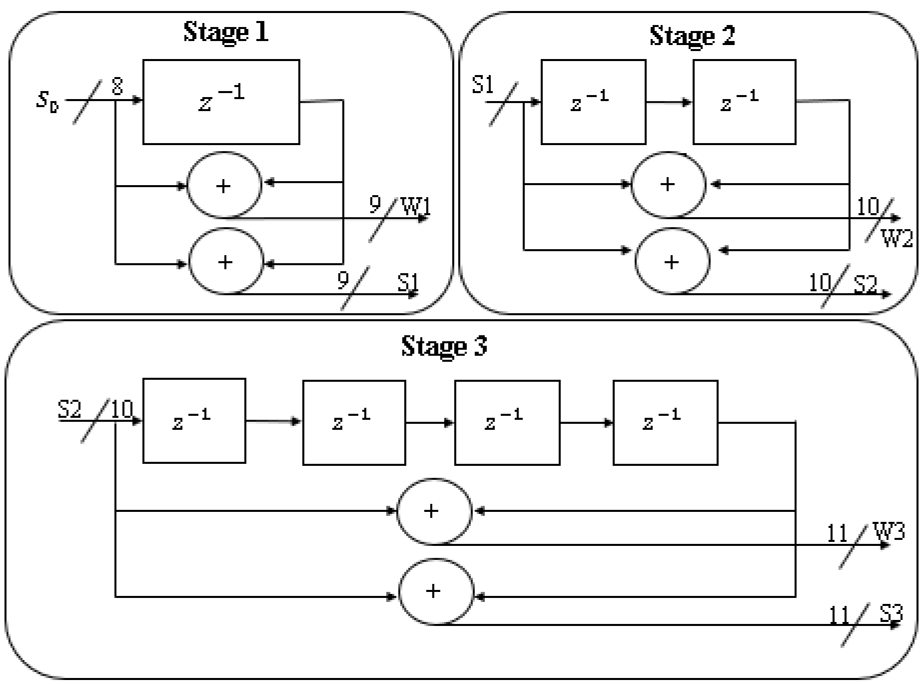

(b)

Fig. 3. 14 (a) Block diagram of the wavelet transform processor, (b) Block diagram of three stages of Haar wavelet

Here, i is the scale number. Compared to the previously designed beat-detection algorithms discussed in [64] and [65], this algorithm uses a sixth-order DWT [98]. A typical wearable ECG monitoring system that can process and enable wireless transmission of ECG signals is shown in Fig. 3.15 [104]. The main challenge with the development of these devices is their multi-functional ability and ease of usage. During the last few years, many ECG signal detection algorithms with low power consumption are proposed [99-102].

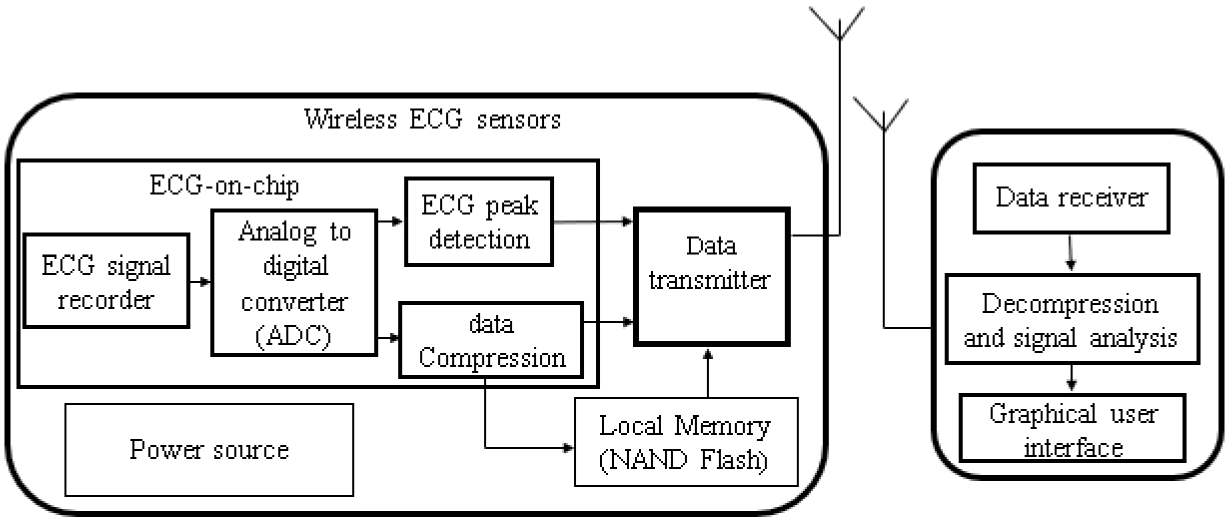

Fig. 3. 15 Block diagram of a wearable ECG monitoring system

Several integrated lossy and lossless ECG compression techniques are presented in [103, 104]. Using different approaches for ECG signal detection and data compression may increase the overall system complexity. An approach that combines ECG signal detection and lossless data compression used in wearable ECG detector are proposed by Deepu et al. [104]. The central idea behind this approach is to use a single algorithm for ECG signal detection and data compression instead of using two different algorithms. Average computational complexity per task is lowered by sharing the computational load between two different operations. Reports on many forward prediction based algorithms used for ECG signal detection are discussed in [105-107] in which a forward predictor is used to estimate current sample *x(a)* of an ECG signal which is given by Eq. (3.24).

$$\hat{x}(a) = \sum_{k=1}^{m} h^k x(a-k) \tag{3.24}$$

Here, $\hat{x}\,(a)$ is the estimation of ECG signal *x(a)* and h^k is the predictor coefficient. The prediction error *e(a)*, the difference between the actual ECG signal *x(a)* and its estimation $\hat{x}\,(a)$ is given by Eq. (3.25).

$$e(a)=x(a)-\hat{x}(a) \tag{3.25}$$

Combined ECG signal detection and lossless compression technique proposed in [104] is shown in Fig. 3.16.

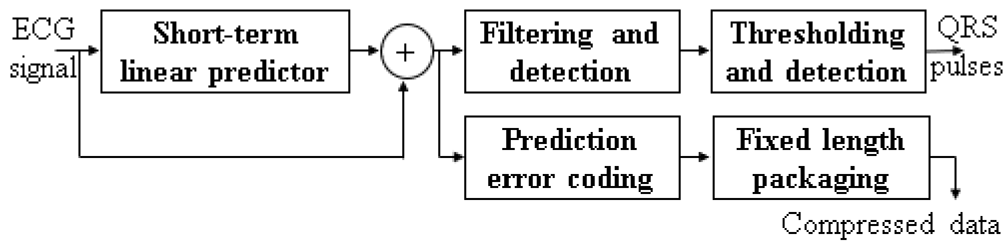

Fig. 3. 16 Block diagram of combine ECG detection and lossless compression Technique

A linear predictor is used for the estimation of current samples of ECG signal *x(a)* based on previous *m* samples. By subtracting the estimated value from the actual value, instantaneous prediction error *e(a)* is calculated and used to identify the QRS-complex location. *e(a)* is encoded and packaged to get a compressed lossless representation of original data for wireless transmission. The adaptive linear predictor which self-adjusts the output based on the statistics of the incoming signal is shown in Fig. 3.17 [104].

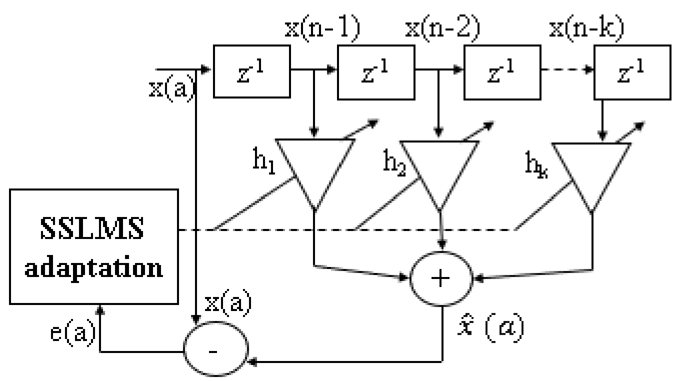

Fig. 3. 17 Adaptive linear predictor

The predictor is constructed with the help of a tapped delay line structure. Least mean square (LMS) algorithm and its variants were used for updating predictor weights and are described by Eq. (3.26), Eq. (3.27), Eq. (3.28), and Eq. (3.29) [108]:

$$LMS\, h(a+1) = h(a) + \mu e(a) x(a) \tag{3.26}$$

$$NLMS\, h(a+1) = h(a) + \beta e(a) \frac{x(a)}{x(a)^2} \tag{3.27}$$

$$SLMS\, h(a+1) = h(a) + \mu \operatorname{sgn}(e(a)) x(a) \tag{3.28}$$

$$SSLMS\, h(a+1) = h(a) + \mu \operatorname{sgn}(e(a)) sgn(x(a)) \tag{3.29}$$

Here, *h(a)* is current predictor coefficient, *h(a +1)* is updated predictor coefficient and μ, β are the step sizes. Based on the performance and hardware complexity, sign-sign least mean square (SSLMS), predictor-based algorithms are chosen [109].

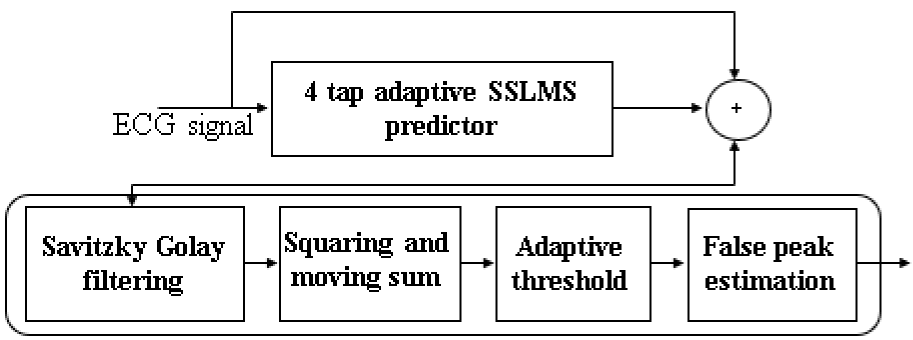

Fig. 3. 18 Block diagram representation of a QRS-complex detector using SSLMS predictor

Block diagram of a QRS-complex detector using SSLMS predictor is shown in Fig. 3.18 [104]. A lossless data compression technique using SSLMS predictor is shown in Fig. 3.19 [104]. The major drawback of lossless compression using SSLMS is its hardware complexity.

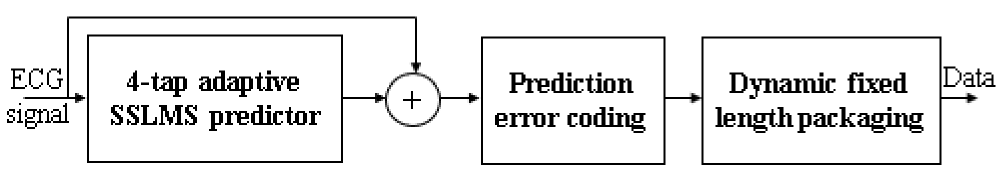

Fig. 3. 19 Block diagram of a lossless data compression Technique using SSLMS predictor

A combined biometric recognition-based ECG signal classification and feature extraction design for single-lead ECG is proposed by Gutta et al. [110]. The focus is on biometric recognition using a single-lead ECG signal as it is easy to acquire in many situations [111]. A real-time QRS-complex detector based on redundant discrete wavelet transform is presented by Junior et al. [112].

Devising a self-effacing cardiac monitoring device is the first stepping stone. Being cost-effective, with a supporting battery, prolonged usage is one of the essential challenges while designing wearable devices. Low power consumption and less hardware complexity are the two crucial attributes of mobile ECG equipment. This sets in the place for integration of inbuilt signal acquisition and required conversion of massive data generated through wearable devices. The seamless power supply sourcing through a wireless transceiver makes it imperative to locally carry out the initial ECG analysis related tasks like QRS-complex detection and R-R interval estimation. The local estimation facilities like ECG signal transmission can be activated only on the need and requirement based on heart rhythm analysis. The massive ECG signal data sets acquired through the continuous watch, and track setup demands a strong need for reliable local storage or needs a data transmission to a storage gateway. Such communication of data exerts a need for continuous battery source, which increases the running cost of such devices. Alliance of ECG chip with a microcontroller enabling burst transfer of ECG signal may increase the cost as some storage class memory needs to be integrated on-chip. A comprehensive review of existing ECG signal denoising and QRS-complex detection is reported in [117]. Increasing ECG signal detection accuracy with the help of sophisticated signal processing techniques is the primary approach. Low power implementation of many ECG signal detection and data compression techniques are reported in [113-116].

3.2 DATABASES TO BENCHMARK ECG DETECTION ALGORITHM

There are plenty of ECG databases available to evaluate the performance of ECG detection algorithms. Some of the standard ECG databases include MIT-BIH arrhythmia database, the American heart association (AHA) database, medical information mart for intensive care (MIMIC) database, Ann Arbor electrogram libraries, long-term ST (LTST) database, and common standards for electrocardiography (CSE) database. Their main characteristics are summarized in Table 3.2.

Table 3.2: Characteristics of the ECG databases

ECG Database	Number of Recordings	Sampling Frequency (Hz)	Duration (min.)	Status
MITDB	48	360	30	Open
QTDB	105	250	15	Open
EDB	90	250	120	Open
TWADB	100	500	2	Open

The most frequently used MIT-BIH arrhythmia database contains forty-eight half-hour excerpts of two-channel ambulatory ECG recordings with *11*-bit resolution over a *10*-mV range at a sampling rate of *360 Hz*. Out of the possible four thousand ECG signals which span a twenty-four-hour data of ambulatory ECG recordings, only twenty-five recordings have a less common arrhythmia, and the remaining are chosen randomly. MIT-BIH database has *116137* QRS-complexes. AHA database [118] used to evaluate detection of ventricular arrhythmia has *155* recordings of ambulatory ECG with *2.5* h recordings of unannotated signal followed by thirty minutes of annotated ECG with a *12*-bit resolution over a *20*-mV range at a sampling rate of *250 Hz*. For the representation of different levels of ectopic excitation, records are arranged into eight groups. For the evaluation of diagnostic ECG analyzer, CSE database [119] contains *1000* multi-lead recordings is used. Electrogram libraries database from Ann Arbor contains a collection of more than *800* intracardiac electrograms and surface ECGs [120]. This database is valuable for the evaluation of algorithms designed for implantable cardiac devices. The MIMIC database introduced in *2001* provides ECG recordings of ICU patients [121] and contains *72* recordings recorded at *500* samples/s with *12*-bit precision and negligible jitter. The LTST database [122] introduced in *2001* is used to develop an evaluation of ischemic and non-ischemic ST event detection algorithms and contains eighty six lengthy ECG recordings of eighty human objects.

Some other libraries like European ST-T database [123], Massachusetts general hospital MGH database [124], QT database [125], and improving control of patient status in critical care (IMPROVE) data library are used to evaluate the detection and classification algorithms. The ST-T database contains ninety recordings and used to evaluate ECG devices which analyze ST waves and T-waves. ECG records in all the databases mentioned above contain information about the occurrences of different artifacts, namely regular heartbeat, premature ventricular contraction (PVC), and changes in signal quality. These databases provide a good testing ground because they contain a large number of beats, various noises, and different pathological states.

3.3 EVALUATION AND COMPARISON OF ECG DETECTION AND DATA COMPRESSION TECHNIQUES

Any recorded ECG signal consists of non-sinus beats and different noises, namely power-line interface, baseline drift, to name a few. To remove noises from an ECG signal, many approaches which include time domain-based, ECG morphology-based, time-frequency domain-based, and some combined methods are proposed in the literature [1–124]. As discussed in Table 3.1, wavelet transform based ECG signal detection algorithms are considered to be more suitable when compared to other reported techniques. Based on wavelet transform, different algorithms for ECG signal detection are discussed in the literature. However, the primary issue is with the selection of proper wavelet transform, which is suitable for ECG signal detection. From the available literature, no suitable reason behind the selection of wavelet transform for ECG signal detection is provided. For example, Rodrigues et al. [66] used the wavelet transform based filter bank for ECG signal denoising, but no further reason for selecting a particular wavelet transform is made. Martinez et al. [69], Min et al. [70], Mahmoodabadi et al. [126] used wavelet transform for ECG signal denoising, but no information on wavelet selection is disclosed. The performance of an ECG detection algorithm is evaluated by using six statistical metrics of the signal for the beat to beat [126]. The statistical metrics to evaluate the performance of an ECG signal detection algorithm are sensitivity (Se), specificity (Sp), positive predictivity (+P), area under the curve (AUC), receiver operating characteristics (ROC), detection error-rate (DER), and overall accuracy (ACC). The mathematical relations that define the above said metrics are given in Eq. (3.30), Eq. (3.31), Eq. (3.32), Eq. (3.33), and Eq. (3.34), respectively.

$$Se(\%) = \frac{TP}{TP + FN} * 100 \tag{3.30}$$

$$+P(\%) = 1 - \frac{FP}{TP + FP} = \frac{TP}{TP + FP} * 100 \tag{3.31}$$

$$SP(\%) = \frac{TP}{N} = \frac{TN}{TP + FP} * 100 \tag{3.32}$$

$$ACC(\%)=\frac{TP}{TP+FP+FN}*100 \tag{3.33}$$

$$DER(\%)=\frac{FP+FN}{Total\,QRS\,complexes}*100 \tag{3.34}$$

Here, *TP* is the number of true positive detection (QRS-complexes detected), *FN* is the number of false negatives (QRS-complexes that are not detected by the detector), *FP* is the number of false positives (a complex wrongly detected as a QRS-complex). The robustness of the ECG signal detector on its noise performance is determined by computing Signal-to-Noise Ratio (SNR) as given by Eq. (3.35).

$$SNR=10\log_{10}\left[\frac{Signal\,energy}{Noise\,energy}\right] \tag{3.35}$$

Table 3.3: Comparison of different ECG detection algorithms

References	**ECG Detection**	**Total Beats**	**Numerical Efficiency**	**Se (%)**	**+P (%)**	**DER (%)**
Liu at al. [12]	Wavelet transform	109492	Medium	99.80	99.86	0.35
Pan and Tompkins [20]	Bandpass filter + filter derivative + squaring + moving average	116137	Medium	99.76	99.56	NR
Li et al. [28]	Wavelet transform	104182	Medium	99.89	99.94	0.17
Afonso et al. [30]	Filter bank	90909	Low	99.59	99.56	NR
Zidelmal et al. [44]	S-transform + Shannon energy	108494	Medium	99.84	99.91	0.25
Poli et al. [50]	NR	109968	High	99.60	99.50	0.90
Satija et al. [61]	CEEMD + decision rules	14068	Medium	99.12	98.56	NR
Rodrigues et al. [66]	Wavelet transform	NR	Medium	99.00	NR	0.4

References	ECG Detection	Total Beats	Numerical Efficiency	Se (%)	+P (%)	DER (%)
Martinez et al. [69]	Wavelet transform	109428	Medium	99.80	99.86	0.34
Min et al. [70]	Dyadic wavelet transform	109496	Medium	99.80	99.86	0.35
Wang et al. [77]	Pan and Tompkins	4509	Low	95.65	99.36	NR
Zou et al. [100]	Wavelet transform	NR	High	99.72	99.49	NR
Deepu et al. [104]	Modified Pan and Tompkins	109508	Medium	99.64	99.81	NR
Mahmoodabadi et al. [126]	Wavelet transform	43438	Medium	94.52	94.30	NR
Faezipour et al. [127]	Modified Pan and Tompkins	104363	medium	99.80	99.79	NR
Ravanshad et al. [129]	LC-ADC	109428	Medium	99.89	99.40	1.71
Suarez et al. [130]	Geometrical matching	60431	Medium	97.94	99.13	2.92
Chen at al. [131]	Moving average + wavelet transform	102125	High	99.35	99.48	0.97
Chouhan and Mehta et al. [132]	Digital filters + threshold	102654	Medium	99.69	99.88	NR
Bahoura et al. [133]	Wavelet transform	109809	Medium	99.83	99.88	0.29
Ghaffari et al. [134]	Continuous wavelet transform	109937	Medium	99.91	99.72	NR
Pan et al. [135]	Biorthogonal spline wavelet transform	102934	Medium	99.72	NR	NR

References	ECG Detection	Total Beats	Numerical Efficiency	Se (%)	+P (%)	DER (%)
Benmalek and Charef [136]	Digital fractional order operators	107632	medium	99.86	99.86	NR
Raj et al. [137]	DCT based DOST + PSO optimized SVM	86113	High	99.82	99.82	1.18
Nayak et al. [138]	Digital differentiator + GMBO	109494	High	99.92	99.92	0.15
Jain et al. [139]	PSO optimisation	109494	high	99.75	99.83	0.42
Chairugi et al. [140]	Bandpass filter + first derivative + multiple thresholds	109494	High	99.76	99.81	NR
Elgendi et al. [141]	TERMA + modified Pan and Tompkins	109775	Medium	99.78	99.92	NR
Tang et al. [142]	Parallel delta modulator + local maximum point	109966	Minimum	99.17	99.55	1.28
Tang et al. [142]	Parallel delta modulator + local maximum point + local minimum point	109966	Minimum	99.17	99.55	1.28
Hou et al. [143]	phase space reconstruction + box-scoring calculation	110008	High	99.32	99.45	NR
Adnane et al. [144]	Modified Pan and Tompkins	109494	Medium	99.77	99.64	0.59
Qin et al. [145]	Wavelet transform + signal monitoring + local maxima location + adaptive threshold selection	86892	Medium	99.83	99.90	NR
Thungtong et al. [146]	Wavelet transform	83292	Medium	99.63	99.78	0.59

*NR: Not reported, DCT: discrete cosine transform, SVM: support vector machine, PSO: particle swarm optimization, GMBO: gases Brownian motion optimization, CEEMD: modified ensemble empirical mode decomposition, TERMA: two-event related moving averages.

Various ECG signal detection algorithms found in the literature are listed in Table 3.3. Most of the works does not mention the reason for selecting a particular wavelet transform. In Table 3.3, various ECG detection algorithms are compared for their numerical efficiency, Se, +P, DER.

The proposed algorithm is evaluated and compared with existing algorithms to find the suitability of proposed algorithm for ECG signal detection. The performance of ECG signal detection algorithms described in the literature is not assessed for some parameters like numerical efficiency, parameter choice, and robustness to noise. "The developed algorithm may have a large number of iterations, parameters to adjust, features extracted, or classification steps. It is desirable to provide numerically efficient (simple, fast, and fewer calculations) algorithms. Of course, computers have become very fast, and therefore numerical efficiency is less important than it used to be. However, if a simple and fast algorithm can achieve good results, there is no need for more complex algorithms. In particular, when the algorithm is used online (in a slightly modified form from the offline version) in a mobile phone embedded system, numerical efficiency is still relevant [64]". Some of the ECG signal detection algorithms are not verified using ECG data from the standard databases. There are many algorithms described in the literature with a very high detection performance. The main drawback of these algorithms is that the high detection performance of the algorithm is achieved by verifying with very limited datasets. For example, in [127], Faezipour et al. claim an accuracy of *99.59%* by testing the algorithm only on very limited ECG data. For example, the algorithm is not verified the most noisy ECG records *207* and *208* from the MIT-BIH arrhythmia database, and therefore, their algorithm may not be superior in its performance.

Furthermore, there are many other works which report high beat detection accuracy and classification *99.44%* and *97.25%*, (Lee et al. [92]) respectively but no information on the data set size is provided. Zou et al. [100] claim an accuracy of *99.72%*, but the performance of the algorithm is not reported. It is required to verify the designed algorithm with ECG record *100* and ECG record *108* of the MIT-BIH arrhythmia database. In the ECG record *100*, QRS-complexes are very clear and easy to determine. Whereas, it is tough to determine the QRS-complexes in ECG record *108*. Detection problems in an ECG signal arise due to noise signals like baseline drift and powerline interface, small amplitude QRS-complexes, pathological signals and sudden level change of the QRS-complex.

In Table 3.3, Se, +P, DER are listed from various works found in the literature. The state-of-the art requirement for Se is greater than *99%*, +P is greater than *99%*, and a nearly zero DER. As the leading cause of death in modern society [104], cardiac diseases have drawn significant attention. Hence, long-term monitoring of ECG is one of the primary requirements for the patients with cardiac diseases. Previously discussed algorithms are used only for ECG detection. Hence, many hardware systems are proposed to record ECG signal and QRS-complex detection. The implementation of such a hardware system should be energy efficient, portable, and record an ECG with high signal quality to aid accurate medical diagnosis.

The performance of any developed ECG signal compression technique is evaluated using seven statistical metrics by comparing the signal for the beat to beat [147]. The statistical metrics are compression ratio (CR), space-saving (S_S), compression gain (C_g), maximum absolute error (MAE), quality score, peak signal to noise ratio (PSNR), and percentage root-mean-square difference (PRD). The relations that define the above said metrics are listed in Eq. (3.36), Eq. (3.37), Eq. (3.38), Eq. (3.39) Eq. (3.40), Eq. (3.41), Eq. (3.42), and Eq. (3.43), respectively.

$$CR = \frac{number\ of\ bits\ in\ the\ original\ file}{number\ of\ bits\ in\ the\ compressed\ file} \tag{3.36}$$

$$S_S = 1 - \frac{1}{CR} = 1 - \frac{number\ of\ bits\ in\ the\ compressed\ file}{number\ of\ bits\ in\ the\ original\ file} \tag{3.37}$$

$$C_g = 100 \log_e \frac{x_i}{compressed\ file} \tag{3.38}$$

$$MAE = \max\left(x_i - y_i\right) \tag{3.39}$$

$$PRD(\%) = \sqrt{\frac{\sum_{i=1}^{n}[x_i - y_i]^2}{\sum_{i=1}^{n}[x_i]^2}} \times 100 \tag{3.40}$$

$$Quality\ score = \frac{CR}{PRD} \tag{3.41}$$

$$RMSE = \sqrt{\frac{1}{n}\sum_{i=1}^{n}(x_i - y_i)^2} \tag{3.42}$$

$$PSNR = 20\log_{10}\frac{\max|x_i|}{root - mean - square - error\,(RMSE)} \tag{3.43}$$

Table 3.4: Comparison of different published ECG data compression algorithms

Method	Algorithm	Data Quality	Computational Complexity	Compression Performance
Direct time-domain methods	Turning Point	Lossy / near-lossless	Medium	Medium
	Amplitude zone time epoch coding (AZTEC)			
	Delta Coding			
Parameter extraction	Linear prediction	Near-lossless or lossless	Complex	High
	Neural network			
	Syntactic method			
	Curvature based ECG signal compression			
	Long-term prediction			
	Hilbert transform		Medium	Medium

Transform methods	Discrete cosine transform	Near-lossless		
	Fast Fourier transform			
	Discrete wavelet transform			
	Hermite transform			
	Walsh transform			
Combine methods	Discrete wavelet transform + run-length encoding	Lossless	Medium	High

Here, x_i and y_i are the original signal and reconstructed signal, respectively.

To compress an ECG signal, many approaches based on direct time-domain approach, transform approach, parameter extraction, and some combined methods are proposed in the literature [147].

The main drawback of direct time domain-based ECG compression method is poor P-wave and T-wave fidelity and reconstruction capabilities (reconstructed signal represents the original signal with distortion). Hence, the performance of the ECG signal compression is degraded. To achieve high compression accuracy, algorithms based on the parameter extraction are proposed, but the major drawback with these approaches is their high computational complexity and power consumption. Transform based techniques are either lossy or near-lossless ECG compression methods. Combined algorithms like wavelet transform with run-length encoding have a high compression performance, medium computational complexity, and good fidelity.

Based on the tradeoff between computational complexity and compression performance, as shown in Table 3.4, wavelet transform and run-length encoding based ECG compression algorithms are considered to be more suitable compared to other reported techniques.

The performance of ECG compression algorithms presented in the literature is not assessed for some statistical parameters like computational complexity, space-saving, parameter choice, and compression gain. Some of the ECG compression algorithms presented in the literature are not verified using ECG data from the standard database.

Table 3.5: Comparison of different ECG compression algorithms

References	**Compression Technique**	**Records Used**	**Performance Metrics**	**Compression Performance**
Lossy ECG compression techniques				
Elgendi et al. [141]	Decimating by a factor *B/K*	48-records of MIT-BIH arrhythmia database	CR, PRD	Medium
Polania et al. [148]	Simultaneous orthogonal matching pursuit	Only one record of MIT-BIH arrhythmia database	CR, PRD	High
Mamaghanian et al. [149]	Compressive sensing	48-records from MIT-BIH arrhythmia database	CR, PRD	Medium
Mishra et al. [150]	Wavelet transform	MIT-BIH arrhythmia database	CR, PRD	Medium
Ansari et al. [151]	Non-uniform binary matrices	NR	CR, PRD	High
Casson et al. [152]	Compressive sensing	Only 3-records of MIT-BIH arrhythmia database	CR, PRD	Low
Kumar et al. [153]	Encoding with modified thresholding	Only 4-records of MIT-BIH arrhythmia database	CR, PRD	High
Chae et al. [154]	Compressive sampling	Only one record of MIT-BIH arrhythmia database	CR, PRD	Low

References	Compression Technique	Records Used	Performance Metrics	Compression Performance
Polania et al. [155]	Compressive sampling matching pursuit	Only 11-records of MIT-BIH arrhythmia database	CR, PRD	High
Manikandan et al. [156]	Wavelet thresholding	Only 2-records of MIT-BIH arrhythmia database and 10-records of qdheart PCG database	CR, PRD, RMSE	High
Lin et al. [157]	lossless and lossy direct compression design	Only 10-records of MIT-BIH arrhythmia database	CR, PRD	High
Lossless ECG compression techniques				
Chua et al. [102]	Delta predictor/Rice Golomb coding	NR	CR, PRD	LOW
Chen et al. [103]	Adaptive predictor/ Huffman coding	NR	CR, PRD	Medium
Deepu et al. [104]	Adaptive predictor	MIT-BIH arrhythmia database	CR, PRD	Medium
Chen et al. [158]	Simple predictor/Huffman coding	NR	CR, PRD	Low
Deepu et al. [159]	Slope predictor/fixed-length packaging	NR	CR, PRD	Medium
Capurro et al. [160]	Universal coding + universal prediction + multivariate recursive least squares	NR	CR	High

Tsai et al. [161]	Adaptive linear prediction + content-adaptive-Golomb-Rice coding + packing format	24-records of MIT-BIH arrhythmia database for lead V1 and 24-records of MIT-BIH arrhythmia for lead V2	CR	High

*NR: Not reported.

Many ECG compression algorithms described in the literature show a high compression performance with a small number of QRS-complexes, as shown in Table 3.5. The main drawback of these algorithms is that the high compression performance of the algorithm is verified using only a few ECG samples.

3.4 DISCUSSION: CHALLENGES AND GAPS

Despite current development in ECG morphology analysis and fast and accurate heartbeat detectors, the use of these algorithms is limited to clinical practice due to the issues related to the hardware implementation of existing algorithms. Apart from business-related concerns and medical approvals, the focus is on related medical concerns. According to medical literature, normal heart rhythm must satisfy the following criterion [128]: Heartrate should lie between *60* to *100 beats per minute* [129-130], impulse speed must be normal, impulses must propagate throughout the normal conducting pathway, and origin of the electrical impulse must lie in the SA node [131].

Heartrate is one of the criteria to identify the behavior of a heart. With the help of heartrate variability analysis, substantial improvements are achieved in identifying the heart-related problems. Even though the heartrate is an important criterion, three other criteria of normal heart rhythm pose a significant impact on ECG signal morphology. For example, if the electrical impulse does not propagate through the normal conducting pathway, it may cause a short PR-segment of ECG signal due to the deficiency of the AV node pause. If the origin of the electrical impulse does not lie in the SA node, then the QRS-complex may not occur exactly after one P-wave. Thus, any issues in collecting one region of ECG waveform affect the other parts of the ECG waveform.

Most of the algorithms which detect QRS-complex are not suitable to detect P-wave and T-wave simultaneously. P-wave indicates atrial related problems, whereas the shape of T-wave represents problems related to beat origin and re-polarization. Detection of these waves is problematic as their amplitude is too small and high attenuation. The amplitude of these waves decreases significantly when the ECG signal is filtered. Recent lifestyle changes are resulting in an issue named Acute Coronary Syndrome (ACS), which is a clinical syndrome. ST-segment is helpful in the detection of ACS [100]. However, there is no proper mechanism available to detect ST-segment. One of the most significant challenges with the ECG analysis is its biometric characteristic, meaning every person has a different ECG signal.

Further, similar ECG signal [133], can be a result of a different medical condition, thus making ECG signal detection more difficult. Most of the researchers gathered around *physionet.org* (an online tool for ECG databases) are considering various challenges. As a result, some other databases might get developed so that the ECG signal analysis can become more realistic to benefit society.

Many algorithms are proposed in the literature to compress ECG signal result in the reduction of the magnitude of transmitted ECG signals. Although, much used and dependable ECG compression techniques are complex and do not fit for wireless transmission. Appropriate compression methods have a directive for high energy consumption or low-compression rate. Thus, it is essential and vital to have a less complex, quicker, coherent, and cost-effective compression procedure fitting the extended ECG signals. Also, the ECG system experiences complications and difficulty with the integration of two definite approaches for QRS-complex detection and data compression. Hence, combined (a joint) technique for ECG signal detection and lossless data compression is required.

3.5 SUMMARY

In the present chapter, existing ECG signal denoising, ECG signal detection, and ECG compression algorithms are summarized. As found in the literature, it is straightforward to achieve sensitivity and specificities of around *99%* for online ECG detectors without significant computational efforts. These specifications may be suitable for clinical applications, but still, hide major problems that are present in the case of pathological signals. A satisfying solution for these challenges is yet to be found. Besides that, it is tough to compare and evaluate the results from various research groups because a large portion of algorithms present in the literature are not tested using standard databases. Long-term monitoring is beneficial for patients suffering from heart diseases. However, the systems that used for long-term monitoring have a limitation on energy consumption. An ECG monitoring system needs to communicate the extracted features to a server and provide a local response. Further, signals from moving patients (for example in an ambulance), abnormal signals have further scope for research. A portable long-term ECG monitoring system either needs local storage or needs a wireless data transfer system. The immediate need is to develop a combine system for both ECG detection as well as data transmission.

CHAPTER 4

ECG SIGNAL DENOISING TECHNIQUES FOR CARDIAC PACEMAKER SYSTEMS

The main reason for medical organizations to focus their research on cardiovascular diseases (CVD) and related problems is increasing worldwide mortality rates due to CVDs. Technological progress in cardiac function assessments has become the nucleus of all leading research studies in the area of CVDs [162]. Use of technologies in hospitals and medical facilities has undergone stupendous advancements, thereby changing the face of the traditional and regular cardiovascular-diagnosis. ECG analysis is the most commonly used clinical cardiac test [163]. ECG signals are the resultant of the heart's electrical activity [164]. An ECG signal provides information on latent operation of the heart and its constituent events that occur and coexist with the succession of depolarization and repolarization of the atria and ventricles. Fig. 4.1 [165] represents different ECG waves produced during a cardiac cycle. The QRS-complex is made up of two troughs, namely, 'Q' and 'S' and a sharp R-wave. The literature identifies a higher detection accuracy of three events, namely, P-wave, QRS-complex, and T-wave during an analysis period less than thirty minutes.

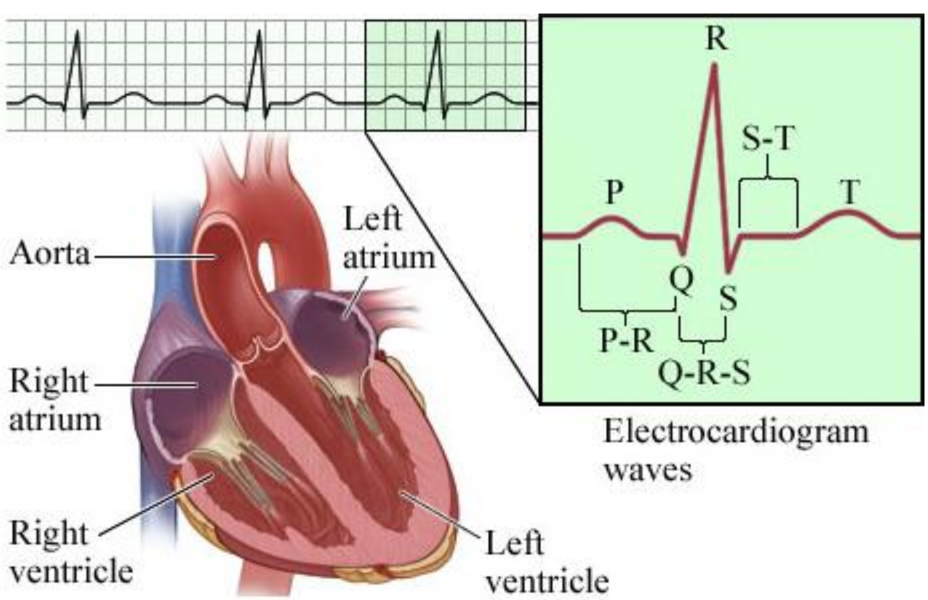

Fig. 4. 1 Graphical representation of a typical ECG signal

Long duration ECG signals are monitored by connecting the electrodes of ECG recorder to a device that banks on the wireless transmission, considered as a fundamental requirement. The technique should be cost-effective, authentic, expandable, and capable of effectual patient tracking with a medical data management tool. Such a tool can facilitate tracking the health of many CVD patients to prevent critical heart failure and to provide rapid medical attention. A model of a wearable ECG monitoring system that can be used for the acquisition, processing, and wireless transmission of ECG data to monitor the health of a CVD subject is shown in Fig. 4.2.

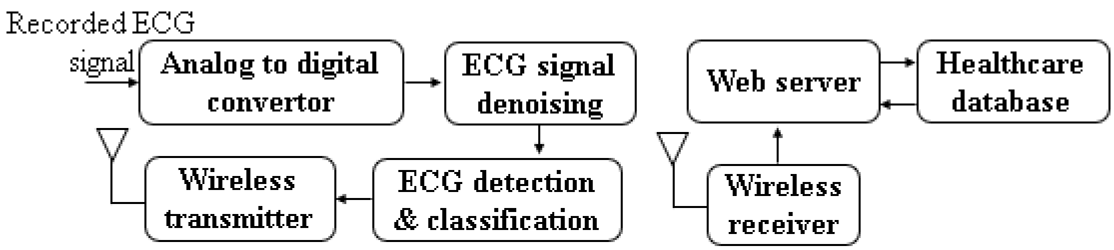

Fig. 4. 2 A model of a wearable ECG monitoring system model

The ECG monitoring system has three main functions, namely, ECG signal analysis, data compression, and wireless transmission. The ECG signal analysis is further divided into two parts, namely, ECG signal denoising and ECG signal detection. The methodology used to develop the proposed design is elucidated below. Combined ECG signal detection and data compression algorithms contain three building blocks, namely, pre-processing, wave detection, and data compression. One of the most important aspects of ECG signal processing is the removal of noises from the signals. In this chapter, different filter bank architectures based on wavelet transform are proposed to remove noise present in an ECG signal.

4.1 ECG SIGNAL DENOISING

Like any electrical signal, an ECG signal is also prone to noise [19] [132]. Various noise removal techniques namely, time-domain, time-frequency domain (wavelet transform), digital filtering, Kalman filtering, fractional calculus, empirical mode decomposition, and Fourier transform are used to remove noise from an ECG signal. Important metrics on which a suitable ECG signal denoising technique is selected are computational complexity, parameter choice, hardware requirements, and robustness to noise. Considering the tradeoff between the above-mentioned statistical parameters as summarized in Table 3.1, wavelet transform based techniques are found to be most suitable for ECG denoising [65].

The methodology used to implement the proposed wavelet transform based ECG signal denoising is presented in this section. Different steps used to denoise the ECG signal are as follows. First, a suitable wavelet transform is selected. A wavelet filter bank with suitable architecture based on a decomposition level is implemented. Thresholding technique is used to detect the QRS-complex. Input ECG signals from a standard database are considered in *.mat* format. As any ECG signal generally contains noise, ECG signals from the database are corrupted by adding random noises. Adding random noise to the signal helps to measure the efficiency of the proposed algorithm to reject noise from the signal. Digitized ECG signals are then applied to the biorthogonal wavelet transform based wavelet filter banks to denoise and decompose into different frequency components. The typical frequency range of an ECG signal is from *0.5 - 150 Hz,* and that of QRS-complex is from *5 - 24 Hz* [166]. After the third level of decomposition, the frequency components which are left behind are in the *45 Hz* range. The output of the third level wavelet filter bank is given as an input to the fourth level wavelet filter bank, and its output contains signals in the frequency range which matches with the frequency range of QRS-complex, then used for further processing.

4.1.1 Criterion to Select Wavelet Transform for ECG Signal Analysis

Accurate analysis of ECG signal with abrupt changes demands a new class of well-localized functions in time and frequency. Wavelet transform with a rapidly decaying wave-like oscillation for a finite duration having zero mean satisfies this condition. Using Fourier analysis, discontinuous, non-smooth waveforms can be converted into a linear combination of extremely smooth functions, namely, the sine waves. Whereas the wavelet transform converts smooth functions into a linear combination of effectively jagged or discontinuous functions. Thus, going from smooth to non-smooth has its place in modern communication and signal processing. The wavelet transform is used in numerous engineering applications like telecommunications, signal processing, geophysics, image and video coding, and astrophysics. Continuous wavelet transform (CWT) and discrete wavelet transform (DWT) are useful to analyze ECG signals. DWT is ideally used to denoise and compress signals and images and useful in representing many naturally-occurring signals with few coefficients.

An ECG signal *s(n)* is decomposed using forward DWT. The standard relations for the forward DWT are as follows.

$$W_\phi(b_0,c)=\frac{1}{\sqrt{M}}\sum_n s(n)\phi_{b_0,c}(n) \tag{4.1}$$

$$W_\psi(b,c)=\frac{1}{\sqrt{M}}\sum_n s(n)\psi_{b,c}(n),\ b\geq b_0 \tag{4.2}$$

Here, $W_\emptyset(b_0,c)$ and $W_\Psi(b,c)$ are the scaling function and wavelet function, respectively. $\psi_{b,c}$ and $\Phi_{b_0,c}$ are the transformation kernel; b_0 is scaling parameter and *n* is shifting parameter. Further,

$$\psi_{b,c}(n)=2^{\frac{b}{2}}\psi(2^b n-c) \tag{4.3}$$

Using Eq. (4.3) in Eq. (4.2) results in

$$W_\psi(b,c)=\frac{1}{\sqrt{M}}\sum_n s(n)2^{\frac{b}{2}}\psi(2^b n-c) \tag{4.4}$$

but

$$\psi(n)=\sum_p h_\psi(p)\sqrt{2}\phi(2n-p) \tag{4.5}$$

If *n* is multiplied by a factor 2^b and with a shift of *c* units, Eq. (4.5) gets modified into

$$\psi(2^b n-c)=\sum_p h_\psi(p)\sqrt{2}\left\{2\left(2^b n-p\right)\right\} \tag{4.6}$$

Let, *p=m-2c*. Substituting in Eq. (4.6), results in

$$\psi(2^b n-c)=\sum_m h_\psi(m-2c)\sqrt{2}\phi(2^{b+1}n-m) \tag{4.7}$$

Using Eq. (4.7) in Eq. (4.4) results in

$$W_\psi(b,c)=\frac{1}{\sqrt{M}}\sum_n s(n)2^{\frac{j}{2}}\left[\sum_m h_\psi(m-2c)\sqrt{2}\phi(2^{j+1}n-m)\right] \tag{4.8}$$

By interchange the order of summation in Eq. (4.8)

$$W_\psi(b,c)=\sum_m h_\psi(m-2c)\left[\frac{1}{\sqrt{M}}\sum_n s(n)2^{b+1}\phi(2^{b+1}n-m)\right] \tag{4.9}$$

Solving Eq. (4.9) results in

$$W_\psi(b,c)=\sum_m h_\psi(m-2c)W_\phi(j+1,m) \tag{4.10}$$

A similar procedure results in

$$W_{\phi}(b_0,c)=\sum_{m}h_{\phi}(m-2c)W_{\phi}(b+1,m) \tag{4.11}$$

Similarly, the transformed signal is reconstructed using inverse DWT. Inverse DWT can be computed using in Eq.(4.12)

$$s(n)=\frac{1}{\sqrt{M}}\sum_{c}W_{\phi}(b_0,c)\phi_{b_0,c}(n)+\sum_{B=b_0}^{\infty}\sum_{c}W_{\psi}(b,c)\psi_{b,c}(n) \tag{4.12}$$

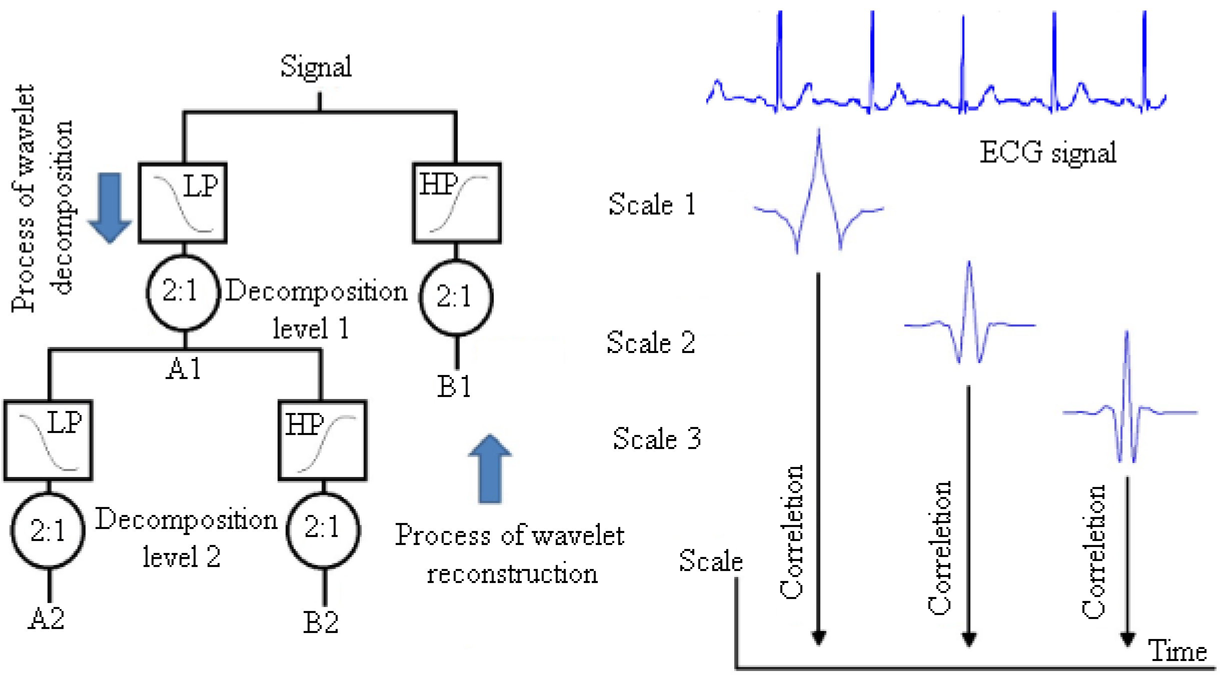

Fig. 4. 3 Decomposition using wavelets

Various wavelet families like Haar, Daubechies, Coiflet, biorthogonal, reverse biorthogonal, Symlet have been used depending on the suitability in various applications like signal analysis, data compression, pattern recognition, medical imaging. Precise estimation of ECG signal parameters demands a suitable choice of basis function [167]. These wavelet families are further categorized into orthogonal, semi-orthogonal, shift orthogonal, and biorthogonal [168]. Orthogonality is used to reconstruct an ECG signal from wavelet coefficients by conserving the energy of the ECG signal. As shown in Fig. 4.3, ECG signal is first decomposed using scaling coefficients *(h(n))* and wavelet coefficients *(g(n))* and then down-sampled by the scaling and wavelet coefficients. In the next step, *h(n)* and *g(n)* are down-sampled to get *A1* and *B1* also known as *TREND* and *DETAIL*. The *TREND* signal *A1* is further down sampled. In each step, the signal *TREND* is further down sampled until the ECG signal in the desired frequency band is obtained. The process to reconstruct the ECG signal is in reverse order to that of decomposition.

The orthogonal wavelets are neither regular nor symmetric, hence introduce a non-linear phase shift during analysis. The non-linear phase shift results in a temporal shape change in the transformed ECG signal, which is not desired. The non-linear phase shift can be eliminated by using the biorthogonal wavelet transform as biorthogonal wavelet is regular as well as symmetric. Another valuable property of wavelet transform that plays a crucial role while analyzing ECG signal is the time-frequency localization and the ability to localize temporal and spectral information. Time localization is inversely related to frequency localization and the smoothness of the wavelet function. A signal whose events are separated by narrow frequency margins need frequency localization. The signals need time localization in which transitory events are important. For the selection of a wavelet transform for ECG signal denoising and detection, properties of an ECG signal need to be examined. The three essential properties of an ECG signal which play a vital role in the selection of wavelet transform are (i) slope of QRS-complex, (ii) the shape and spectrum of ECG signal [169] and (iii) event localization in time [31]. The wavelet transform on an ECG signal should result in a linear phase. Hence such a wavelet transform is non-orthogonal. Time localization is vital because of the transient nature of ECG events. As biorthogonal wavelets are symmetric, nonorthogonal, and localized in time, biorthogonal wavelets satisfy the above-listed criterion. Biorthogonal scaling and wavelet function coefficients are calculated using Eq. (4.13) and Eq. (4.14), respectively.

$$g(n) = (-1)^{1-n} h(1-n) \tag{4.13}$$

$$h(n) = (-1)^{1-n} g(1-n) \tag{4.14}$$

With the increase in the order of the wavelet transform based filter, the desired frequency response becomes sharper. A higher-order wavelet results in a large number of coefficients, thus increasing the computational time and power consumption. Hence there is a tradeoff between the order of the filter and frequency response. Quadratic spline wavelet transform is useful in avoiding the tradeoff between the order of the filter and frequency response, but the shape of the wavelet function is not suitable for ECG signal detection. Biorthogonal wavelet transform has a shape that resembles that of an ECG signal when compared to other wavelet transforms. It is observed from [31] that almost all wavelet transforms have a similar detection accuracy of

90% of the ECG signals available in a database. For the remaining 10% of ECG signals, biorthogonal wavelet transform gives less error compared to other wavelet transforms.

Important properties of selected wavelet transforms are listed in Table 4.1. It is evident from Table 4.1 that biorthogonal wavelet transform satisfies all the criterion required for the ECG signal denoising and detection. Signal analysis has greatly benefitted by wavelet transform in the form of ampleness of the base wavelet developed in the past few years. This has resulted in well documented thirteen wavelet families getting a particular reference in the wavelet transform literature. This abundance puts an intriguing and obvious question related to the selection criteria of the best-fitted wavelet for examining a specific signal. Thus, the most challenging aspect in the selection of a proper wavelet. The present research is a result of comprehensive study and enriched analysis of different properties of the wavelet transform, which has formed the necessary basis for selecting the suitable wavelet transform. The properties like symmetricity, shape of the wavelet transform, slope of the QRS-complex, number of coefficients, event localization, signal to noise ratio (SNR), root mean square error (RMSE) and percentage root-mean-square difference (PRD) are studied. They are thereby making biorthogonal 3.1 wavelet transform as the most proper choice for ECG signal detection.

Table 4. 1: Classification of wavelets base on their properties

Wavelet Transform	**Compact Support**	**Key Properties**	**Implementation**
Orthogonal	No	Symmetry and regularity + orthogonality	IIR/FIR
Semi-orthogonal	Analysis or synthesis	Symmetry and regularity + optimal time-frequency localization	Recursive IIR/FIR
Shift-orthogonal	No	Symmetry and regularity + Quasi-orthogonality +fast decaying wavelet	IIR
Biorthogonal	Yes	Symmetry and regularity + linear + compact support + optimal time-frequency localization	FIR

*IIR: Infinite impulse response, FIR: Finite impulse response.

4.1.2 Criterion for Selecting Wavelet Filter Bank Architecture

ECG signal contains both high frequency and low-frequency responses. The low-frequency responses are more likely to last over an extended region in time hence form the low-frequency components of the ECG signal. The high-frequency response in the ECG response lasts for a small duration in time and thus forms the high-frequency components of the ECG signal. Hence, it is desirable to separate the high frequency and low-frequency components of the ECG signal. To separate the frequency components, a system of filters which possess a specific individual characteristic as well as collective characteristics is required. Such a system is known as a filter bank. A filter bank, as opposed to a single filter in discrete-time signal processing, has a common input and summation output. Two filter banks are required for denoising, one for analysis and the other for synthesis form central core to multirate discrete signal processing.

To denoise an ECG signal, different wavelet filter bank architectures like, two-channel filter bank [67], quadrature mirror filter bank [170], Mallat's wavelet filter bank [67], parallel filter bank, decimator wavelet filter bank [66], undecimator wavelet filter bank [70], and pyramid filter bank [171] are proposed by various researchers. One of the primary concerns with all these filter bank architectures is that the hardware requirement and the circuit complexity. To reduce the overall circuit complexity of a wavelet filter bank, the wavelet filter bank needs to be designed in such a way that it can detect all the useful features of an ECG signal, namely P-wave, Q-wave, R-wave, S-wave, and T-wave. Wavelet filter bank architectures are verified using all the seventy-eight wavelet transforms. Based on the SNR and circuit complexity, a modified wavelet filter bank is found suitable for ECG signal denoising. The methodology used to implement the proposed technique is discussed in the flowchart as shown in Fig. 4.4 (a). Block diagram representation of the wavelet filter bank is shown in Fig. 4.4 (b) and the proposed modified biorthogonal *3.1* wavelet transform based wavelet filter bank is shown in Fig. 4.4 (c). The proposed wavelet filter bank uses a parallel combination of lowpass and highpass filters in wavelet filter bank four, which helps contain both high frequency as well as low-frequency components. Also, the use of booth multiplier instead of simple add-shift multiplier makes the circuit fast and power-efficient [76].

The lowpass and highpass filter used in the wavelet filter bank of the modified biorthogonal *3.1* wavelet is designed using transfer function given in Eq. (4.15) and Eq.(4.16), respectively.

$$H(z) = 1.06 + 1.53z^{-1} + 1.06z^{-2} \tag{4.15}$$

$$G(z) = 1 - z^{-1} \tag{4.16}$$

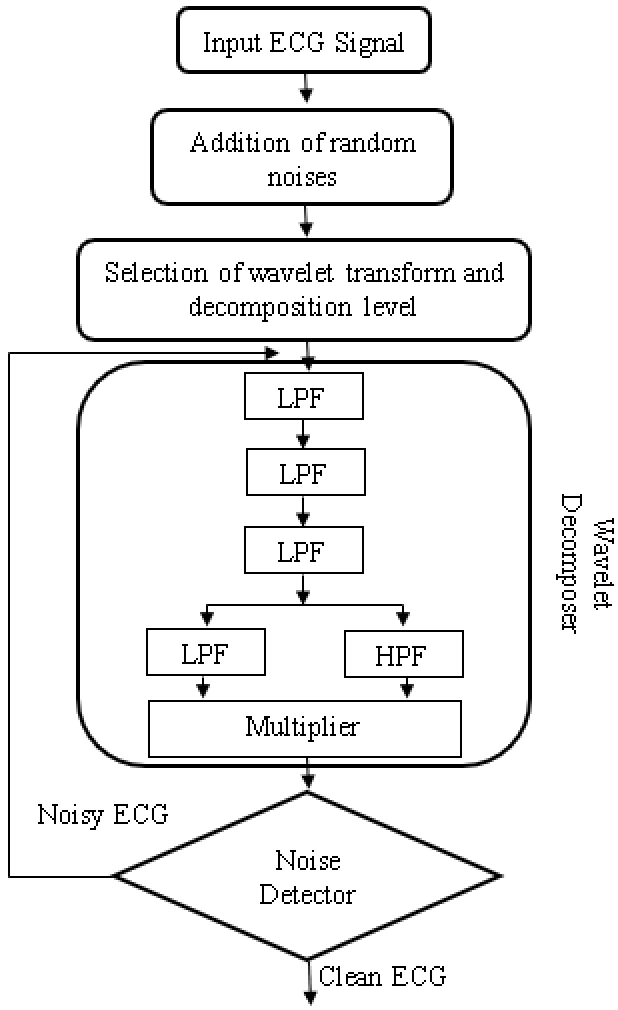

(a)

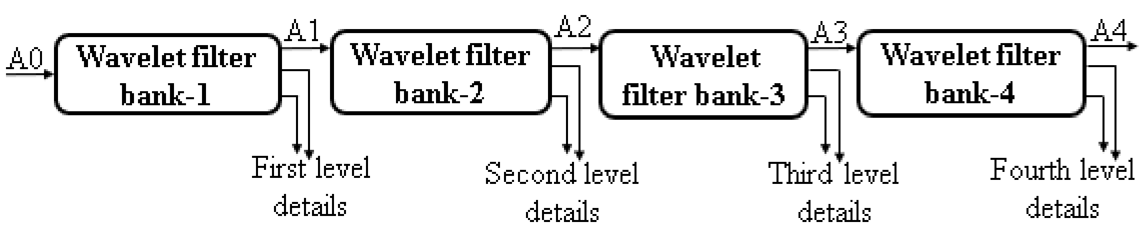

(b)

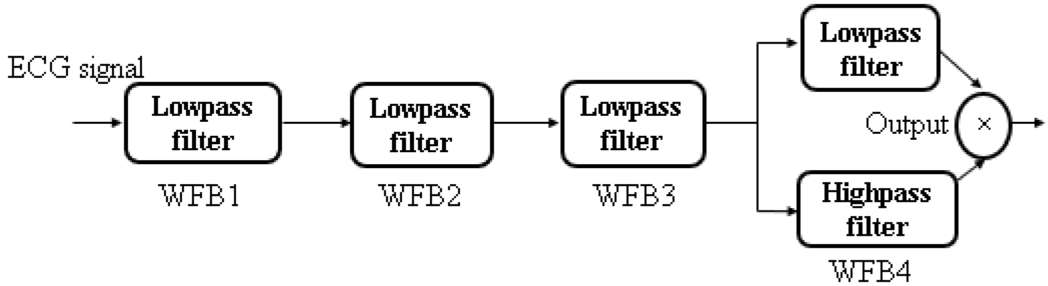

(c)

Fig. 4. 4 (a) Flowchart of the proposed technique. (b) Basic block diagram of wavelet filter bank. (c) Proposed modified biorthogonal 3.1 wavelet transform based wavelet filter bank used to denoise the ECG signal

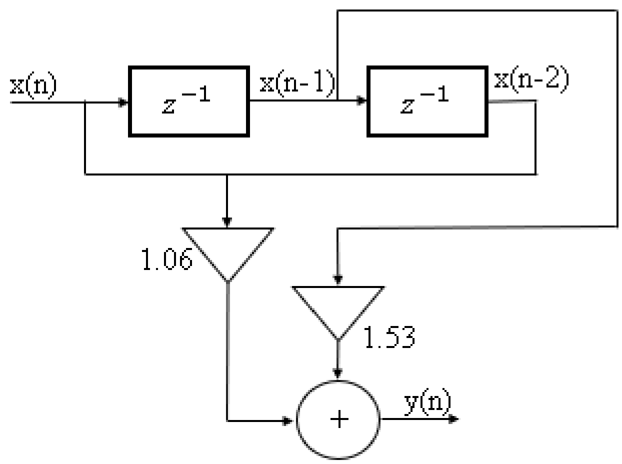

(a)

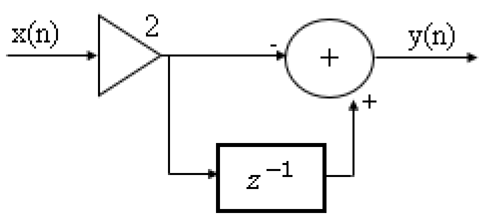

(b)

Fig. 4. 5 Linear phase structure realizations, (a) lowpass filter, (b) highpass filter

4.1.3 Simulation Results and Performance Evaluation of the Proposed Modified 3.1 Wavelet Transform Based Wavelet Filter Bank

Performance of the proposed modified biorthogonal *3.1* wavelet transform based filter bank used to denoise the ECG signal is evaluated using the signal to noise ratio (SNR), root mean square error (RMSE), and percent root mean square difference (PRD).

The proposed design is implemented using Matlab® and tested by using various ECG signals from different databases, namely, MIT-BIH database, BIDMC congestive heart failure database, PTB diagnostic ECG database, and St.-Petersburg Institute of Cardiological Techniques *12*-lead arrhythmia database [188]. The frequency range of raw ECG data taken from these databases lies between *250 - 1000 Hz*. In addition to the forty-eight records and *109494* beats of MIT-BIH arrhythmia database, the *105* records from the QT database, twelve records from the NSTB, *549* records from the PTB database are also used to evaluate the proposed technique and compared with the existing techniques.

ECG signals of three different duration (ten seconds, one minute, and full-length ECG signal) are used to calculate the SNR. For the worst-case consideration, white Gaussian noise and random noise are generated and added to the original ECG signal. Then, the noisy ECG signal is denoised using a conventional wavelet transform based filter bank. White Gaussian noise is first added to *100.mat* and *215.mat* ECG signals from the MIT-BIH database. Then using all seventy-eight wavelet transforms the above-mentioned ECG signals are denoised using conventional wavelet filter bank, and their SNR performance is studied. Table 4.2 lists the SNR performance of all seventy-eight wavelet transforms.

Random noise is added to *100.mat* ECG signal from MIT-BIH database. Then using all seventy-eight wavelet transforms, the ECG signal is denoised, and the SNR performance is studied. Table 4.3 lists the SNR performance of all seventy-eight wavelet transforms.

As observed from Table 4.2 and Table 4.3, different wavelet transforms resulted in an SNR ranging between *26.68* to *41.12 dB* by using the conventional wavelet filter bank on *100.mat* and *215.mat* ECG signals from MIT-BIH arrhythmia database. Out of the wavelet transform, biorthogonal *3.1* wavelet transform has the highest SNR; hence, used in the proposed work. Some modifications have made in the biorthogonal *3.1* wavelet transform based on the requirements of the ECG signal, as explained below. To denoise, an ECG signal, not all the coefficients of a biorthogonal *3.1* wavelet transform are required. Wavelet coefficients which do not exist in the frequency range of an ECG signal are made zero. After selecting the wavelet transform and its architecture, selection of decomposition level is also essential.

Table 4. 2: Signal to noise ratio analysis of different wavelet transforms using 100.mat MIT-BIH signal added with white Gaussian noise

Wavelet	**SNR (dB) of 100.mat Signal**	**SNR (dB) of 215.mat Signal**	**Wavelet**	**SNR (dB) of 100.mat Signal**	**SNR (dB) of 215.mat Signal**
Haar	34.00	36.91	Coif3	29.49	34.59
Db1	33.41	36.95	Coif4	29.82	34.73
Db2	34.21	35.99	Coif5	31.0	34.89
Db3	31.98	35.83	Bior1.1	33.40	37.00
Db4	32.38	35.64	Bior1.3	34.49	36.08
Db5	33.42	35.26	Bior1.5	33.01	35.83
Db6	32.55	35.31	Bior2.2	34.33	37.00
Db7	31.30	35.28	Bior2.4	33.18	36.15
Db8	32.21	34.99	Bior2.6	32.57	35.80
Db9	33.02	34.92	Bior2.8	31.55	35.45
Db10	31.55	34.99	**Bior3.1**	**37.92**	**41.12**
Db11	31.09	34.79	Bior3.3	34.66	38.57
Db12	32.42	34.68	Bior3.5	33.88	36.58
Db13	32.19	34.70	Bior3.7	33.00	35.96
Db14	31.53	34.70	Bior3.9	32.80	36.28
Db15	32.03	34.52	Bior4.4	31.19	34.29
Db16	32.89	34.60	Bior5.5	32.70	36.24
Db17	31.00	34.54	Bior6.8	32.88	35.36
Db18	30.28	34.59	RBior1.1	31.09	38.97
Db19	33.37	34.39	RBior1.3	33.02	36.24
Db20	31.85	34.42	RBior1.5	33.44	35.99
Sym2	35.13	35.85	RBior2.2	34.57	36.18
Sym3	34.05	35.95	RBior2.4	33.02	35.91
Sym4	32.88	35.74	RBior2.6	32.42	35.75
Sym5	31.32	35.22	RBior2.8	32.39	35.95
Sym6	35.02	35.40	RBior3.1	36.11	40.56

Wavelet	SNR (dB) of 100.mat Signal	SNR (dB) of 215.mat Signal	Wavelet	SNR (dB) of 100.mat Signal	SNR (dB) of 215.mat Signal
Sym7	33.98	34.99	RBior3.3	35.01	38.35
Sym8	32.98	35.03	RBior3.5	34.42	36.69
Sym9	33.15	34.80	RBior3.7	32.30	33.55
Sym10	34.84	35.59	RBior3.9	33.10	35.61
Sym11	31.58	34.82	RBior4.4	32.48	36.00
Sym12	32.08	34.89	RBior5.5	29.07	33.27
Sym13	33.13	35.61	RBior6.8	32.65	35.28
Sym14	33.00	34.60	Sym18	32.36	34.55
Sym15	32.41	34.71	Sym19	30.33	34.48
Sym16	31.59	35.21	Sym20	33.11	34.35
Sym17	32.25	34.45	Coif1	32.89	36.06
Coif2	33.18	34.97			

As discussed earlier, usually, the typical frequency range of an ECG signal is from *0.5 - 150 Hz*, and that of QRS-complex is from *5 - 24 Hz*. Frequency components at every wavelet filter bank output are shown in Fig. 4.6. Hence, after the fourth level of decomposition, the frequency will be in the *0* - 22*.5 Hz* range. Therefore, only outputs of the fourth level wavelet filter bank are

Table 4. 3: Signal to noise ratio analysis of different wavelet transforms using 100.mat MIT-BIH signal added with random noise

Wavelet	SNR (dB) of 100.mat Signal	Wavelet	SNR (dB) of 100.mat Signal
Haar	36.23	Sym14	32.31
Db1	36.23	Sym15	29.87
Db2	29.88	Sym16	28.93
Db3	27.24	Sym17	34.88
Db4	28.59	Sym18	36.59
Db5	29.17	Sym19	28.86
Db6	28.53	Sym20	32.37

Wavelet	SNR (dB) of 100.mat Signal	Wavelet	SNR (dB) of 100.mat Signal
Db7	28.11	Coif1	31.89
Db8	26.68	Coif2	27.18
Db9	27.92	Coif3	28.17
Db10	27.94	Coif4	27.76
Db11	27.94	Coif5	28.05
Db12	27.97	Bior1.1	31.19
Db13	27.57	Bior1.3	35.66
Db14	28.11	Bior1.5	36.13
Db15	28.16	Bior2.2	31.77
Db16	35.14	Bior2.4	32.52
Db17	28.60	Bior2.6	32.60
Db18	30.55	Bior2.8	34.87
Db19	28.28	**Bior3.1**	**39.05**
Db20	28.31	Bior3.3	35.53
Sym2	33.12	Bior3.5	34.88
Sym3	26.99	Bior3.7	35.87
Sym4	36.27	Bior3.9	35.51
Sym5	35.36	Bior4.4	32.69
Sym6	32.62	Bior5.5	32.75
Sym7	28.47	Bior6.8	32.84
Sym8	36.22	RBior1.1	35.11
Sym9	35.43	RBior1.3	36.26
Sym10	36.20	RBior1.5	35.42
Sym11	29.44	RBior2.2	31.48
Sym12	32.35	RBior2.4	31.86
Sym13	30.37	RBior2.6	32.10
RBior2.8	34.20	RBior3.9	36.58
RBior3.1	37.07	RBior4.4	31.98
RBior3.3	36.00	RBior5.5	34.77

used for further processing as their frequency component matches the frequency of the QRS-complex.

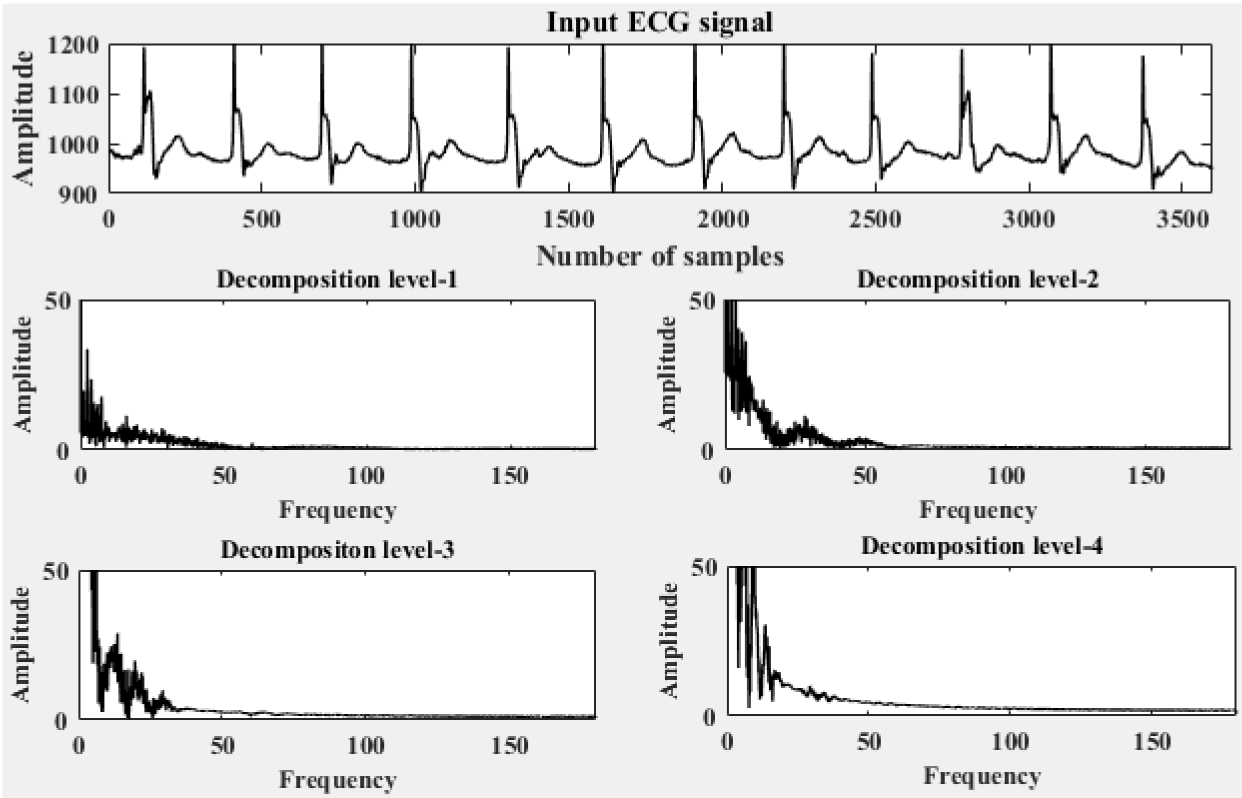

Fig. 4. 6 Frequency component at each wavelet filter bank output

Table 4.4 summarizes the SNR of different ECG signals after different levels of decomposition. The effect of biorthogonal 3.1 wavelet decomposition level on ECG signal is further studied by using ECG signals of ten second duration. Random noise is added to all of the ECG signals.

As observed from Table 4.4, SNR increases until the fourth level of wavelet decomposition and decreases from the fifth level of the wavelet decomposition. By using the modified *3.1* wavelet transform based filter bank, at the fourth level of wavelet decomposition, SNR ranging from *36.01* - *53.92 dB* is obtained for different ECG signals.

From Table 4.4, it is clear that the fourth level of wavelet decomposition has the highest SNR compare to other levels. As the fourth level of decomposition results in the required frequency range and also provides maximum SNR, the fourth level wavelet filter bank is used to denoise ECG signal denoising in the present work.

Table 4. 4: SNR of ten seconds ECG signal based on modified biorthogonal 3.1 wavelet transform

ECG Signal	SNR (dB) at Level 2	SNR (dB) at Level 3	SNR (dB) at Level 4	SNR (dB) at Level 5	SNR (dB) at Level 6
100.mat	50.39	50.46	**50.59**	49.35	49.10
101.mat	49.09	49.31	**50.16**	48.92	48.76
102.mat	50.21	50.39	**50.72**	50.18	49.87
103.mat	45.81	45.94	**46.11**	45.18	45.00
104.mat	44.52	44.81	**45.00**	44.38	44.18
105.mat	45.97	46.10	**46.18**	45.66	45.39
106.mat	40.79	40.43	**41.11**	40.69	40.53
107.mat	37.15	37.44	**38.00**	36.83	36.51
108.mat	50.55	50.70	**50.78**	49.93	49.61
109.mat	43.85	43.99	**44.12**	43.59	43.28
111.mat	50.16	50.31	**50.81**	50.42	50.05
112.mat	47.88	48.00	**48.06**	46.62	46.19
113.mat	43.08	43.22	**43.46**	42.63	42.39
114.mat	53.71	53.82	**53.92**	52.95	52.49
115.mat	45.66	45.79	**45.85**	45.29	45.03
116.mat	38.95	39.23	**39.57**	38.64	38.51
117.mat	46.96	47.08	**47.14**	46.51	46.09
118.mat	36.75	36.89	**37.22**	36.84	36.01
119.mat	40.88	41.17	**41.41**	40.43	40.21
121.mat	47.26	47.49	**47.54**	46.99	46.59
122.mat	43.59	43.83	**43.96**	43.00	42.66
123.mat	45.07	45.20	**45.38**	45.00	44.79
124.mat	43.14	43.39	**43.53**	42.96	42.39
200.mat	42.98	43.13	**43.29**	42.65	42.43
201.mar	40.62	40.85	**41.17**	40.71	40.34
202.mat	48.50	48.62	**48.76**	48.05	47.79
205.mat	49.57	49.70	**49.77**	49.17	49.01

ECG Signal	**SNR (dB) at Level 2**	**SNR (dB) at Level 3**	**SNR (dB) at Level 4**	**SNR (dB) at Level 5**	**SNR (dB) at Level 6**
207.mat	45.93	46.15	**46.23**	45.53	45.40
208.mat	41.46	41.88	**42.04**	41.00	39.89
209.mat	47.88	48.04	**48.19**	47.53	47.25
210.mat	51.49	51.77	**52.08**	51.67	51.29
212.mat	45.20	45.43	**45.51**	44.80	44.44
213.mat	40.22	40.71	**40.96**	40.00	39.77
214.mat	42.38	42.54	**42.88**	42.06	41.87
215.mat	48.05	48.16	**48.30**	47.87	47.51
217.mat	40.50	40.64	**41.06**	40.15	40.01
219.mat	41.76	41.93	**42.12**	41.49	41.26
220.mat	45.00	45.21	**45.28**	44.75	44.61
221.mat	46.15	46.35	**46.44**	45.98	45.81
222.mat	51.46	51.57	**51.68**	51.02	50.92
223.mat	43.10	43.35	**43.49**	42.83	42.73
228.mat	50.17	50.28	**50.44**	50.00	49.89
230.mat	51.44	51.86	**52.00**	51.73	51.21
231.mat	46.57	46.69	**46.74**	46.29	46.03
232.mat	53.11	53.21	**53.62**	53.00	52.85
233.mat	40.33	40.53	**40.81**	40.11	40.00
234.mat	46.27	46.29	**46.46**	46.02	45.82

(* Here, Level-2 through Level-6 indicate different wavelet decomposition levels)

Using the fourth level filter bank, ECG signals of different duration are denoised. All the ECG signals are taken from the MIT-BIH arrhythmia database. Random noise is added to all the signals. Table 4.5 shows the SNR of one-minute ECG data of the MIT-BIH arrhythmia database, whereas, Table 4.6 shows the SNR of one hour ECG data.

As observed in Table 4.5 and Table 4.6, the proposed modified biorthogonal *3.1* wavelet transform based filter bank is used to analyze different ECG signals from MIT-BIH arrhythmia resulted in an SNR ranging between *36.89* and *53.81 dB*.

Table 4. 5: SNR of one-minute ECG signal of MIT-BIH arrhythmia database after denoising using the fourth level of decomposition

ECG Signal	SNR (dB)	ECG Signal	SNR (dB)	ECG Signal	SNR (dB)
100.mat	51.53	116.mat	44.84	219.mat	37.58
101.mat	49.34	117.mat	47.20	220.mat	44.95
102.mat	49.97	119.mat	37.64	221.mat	46.40
103.mat	45.54	121.mat	48.19	222.mat	52.09
104.mat	50.63	122.mat	42.22	223.mat	38.17
105.mat	45.87	123.mat	45.58	228.mat	45.21
106.mat	45.69	124.mat	43.61	230.mat	49.76
107.mat	36.89	205.mat	49.80	231.mat	46.55
108.mat	50.17	209.mat	48.02	233.mat	52.00
109.mat	43.42	210.mat	47.84	234.mat	45.91
111.mat	48.77	212.mat	45.55	114.mat	53.81
112.mat	48.31	213.mat	40.92	115.mat	45.52
113.mat	37.54	214.mat	51.66	215.mat	47.02
114.mat	48.79	115.mat	39.48		

The modified wavelet filter bank achieves a high SNR for both one-minute and one-hour ECG signals.

Table 4.7 summarizes the performance of ECG signal denoising technique based on biorthogonal wavelet transform *3.1*. In this analysis, ECG signals from different ECG databases with a randomly generated noise and white Gaussian noise are considered.

From Table 4.7, the proposed modified biorthogonal *3.1* wavelet transform based ECG denoising technique is evaluated using different ECG databases which results in the average SNR ranging between *45.12* and *46.88 dB* against the input SNR of -10 dB, the average RMSE is ranging between *0.002 and 0.008,* and the average PRD ranging between *11.853 and 12.210*.

The output of the proposed wavelet filter bank for two different ECG signals, one each from the MIT-BIH arrhythmia database and QT database are shown in Fig. 4.7 and Fig. 4.8 respectively.

Table 4. 6: SNR of one-hour ECG signal of MIT-BIH arrhythmia database after denoising using the fourth level of decomposition

ECG Signal	SNR (dB)	ECG Signal	SNR (dB)	ECG Signal	SNR (dB)
100.mat	49.39	116.mat	37.44	219.mat	41.81
101.mat	48.93	117.mat	46.73	220.mat	44.95
102.mat	49.61	119.mat	48.52	221.mat	51.66
103.mat	47.52	121.mat	38.57	222.mat	52.00
104.mat	47.54	122.mat	47.53	223.mat	43.31
105.mat	48.91	123.mat	45.31	228.mat	45.01
106.mat	44.54	124.mat	38.11	230.mat	45.11
107.mat	38.05	205.mat	49.24	231.mat	45.55
108.mat	46.07	209.mat	47.93	233.mat	50.76
109.mat	49.61	210.mat	39.11	234.mat	49.87
111.mat	47.43	212.mat	45.55	114.mat	52.81
112.mat	49.55	213.mat	40.88	115.mat	40.18
113.mat	43.68	214.mat	50.48	215.mat	46.92

Table 4. 7: Performance of ECG denoising technique based on modified biorthogonal 3.1 wavelet transform

ECG database	Duration	Average SNR (dB)	Average RMSE	Average PRD (%)
MIT-BIH	10-seconds	46.88	0.008	12.141
MIT-BIH	1-minute	45.94	0.003	11.943
MIT-BIH	One-hour	46.06	0.002	12.008
Fantasia	One-hour	46.27	0.008	11.853
Apnea ECG	One-hour	45.12	0.006	12.210
ADB	One-hour	45.92	0.003	11.943
QT-database	One-hour	45.52	0.002	11.871

Fig. 4.7 (a) contains input ECG signal of ten second duration, base at *1024 mV,* and sampling frequency of *360 Hz* for MIT-BIH. Random noise is shown in Fig. 4.7 (b) is generated and added to the original ECG signal and Fig. 4.7 (c) represents the noisy ECG signal. Finally, the denoised ECG signal is shown in Fig. 4.7 (d).

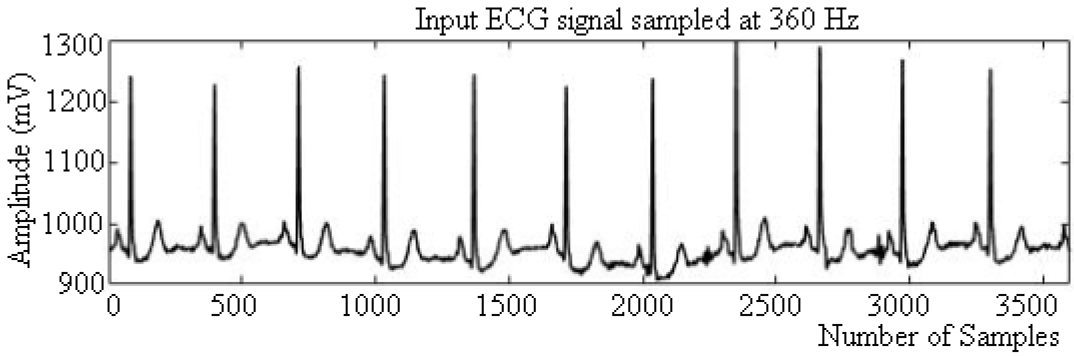

(a)

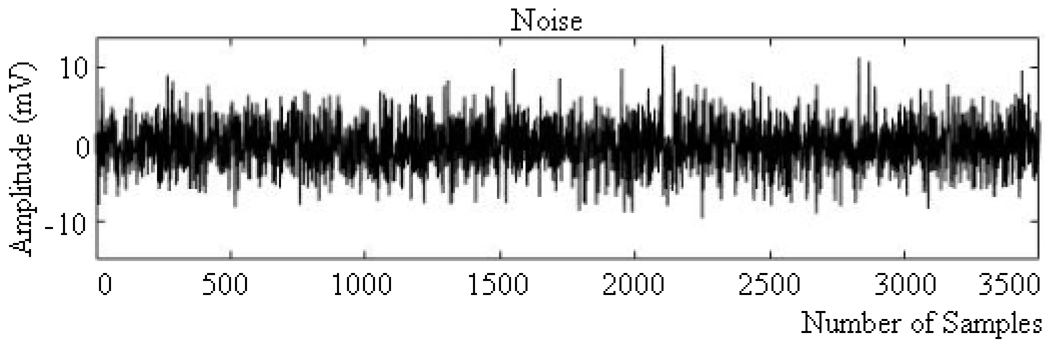

(b)

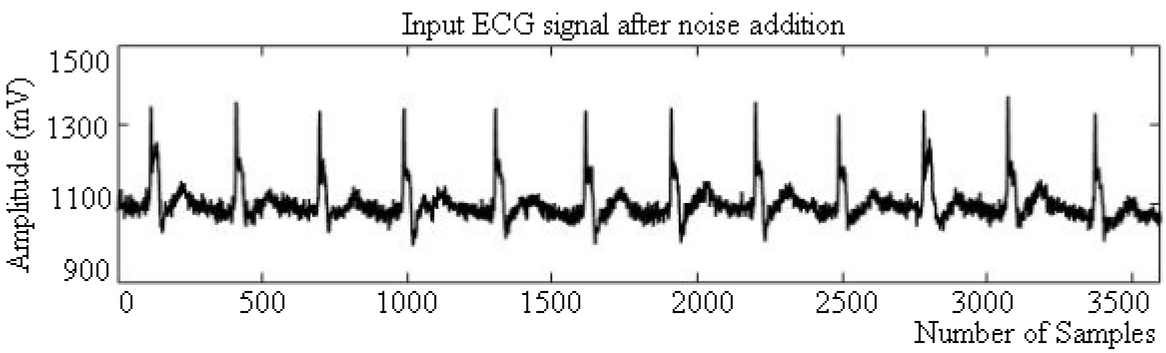

(c)

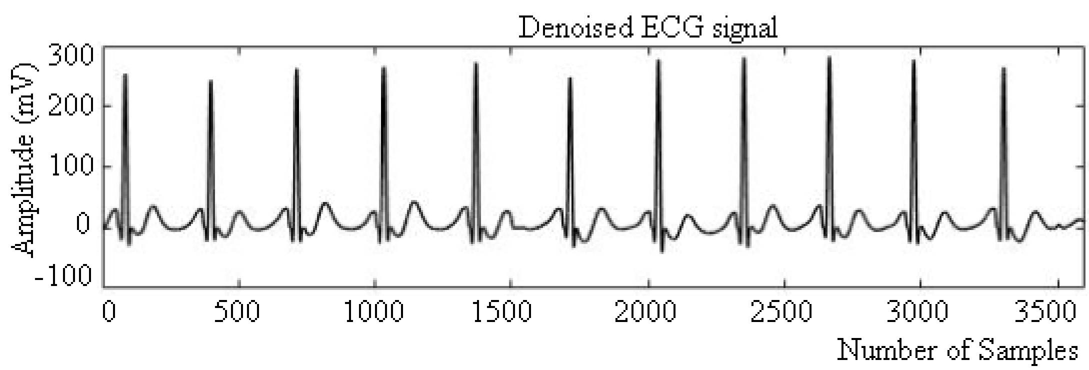

(d)

Fig. 4. 7 (a) Input ECG signal is taken from the MIT-BIH arrhythmia database, (b) random noise source, (d) input ECG signal after noise addition, (d) denoised ECG signal

Fig. 4.8 (a) contains input ECG signal of ten-second duration, base at *1024 mV* and sampling frequency of *250 Hz* for QT database. The random noise is shown in fig. 4.8 (b) is added to the original ECG signal. Fig. 4.8 (c) represents the noisy ECG signal. Finally, the denoised ECG signal is shown in Fig. 4.8 (d).

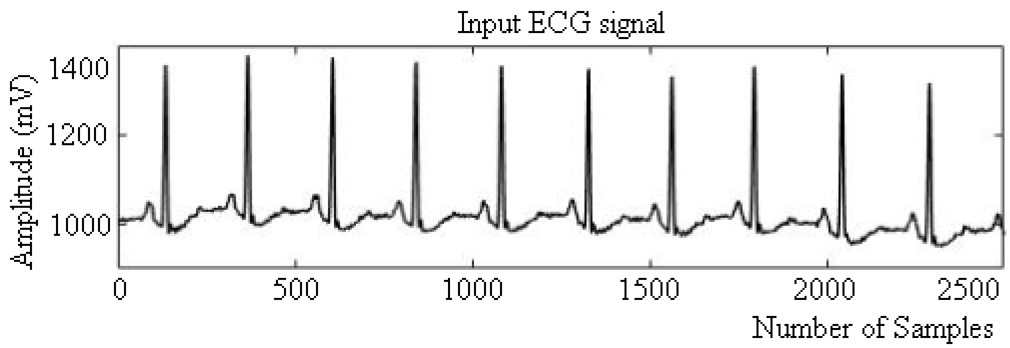

(a)

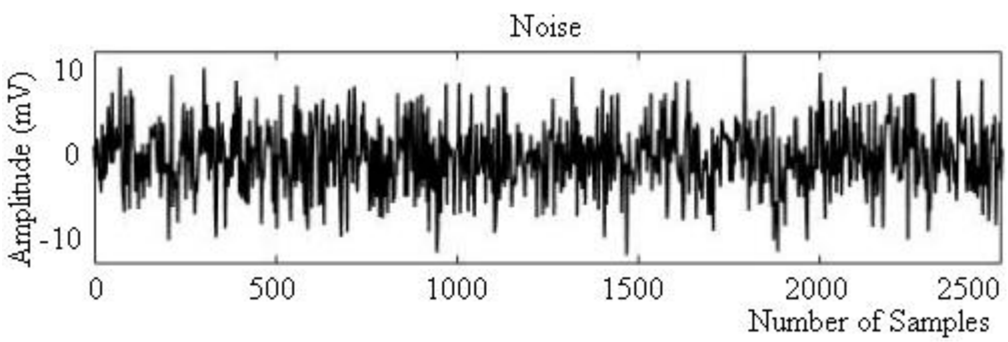

(b)

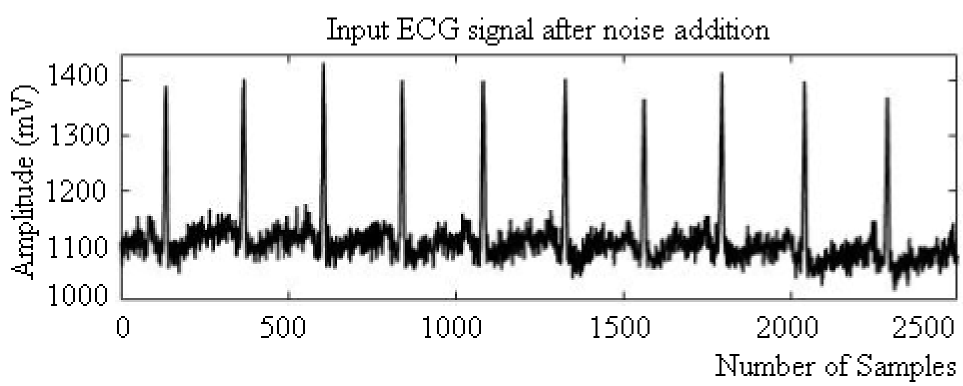

(c)

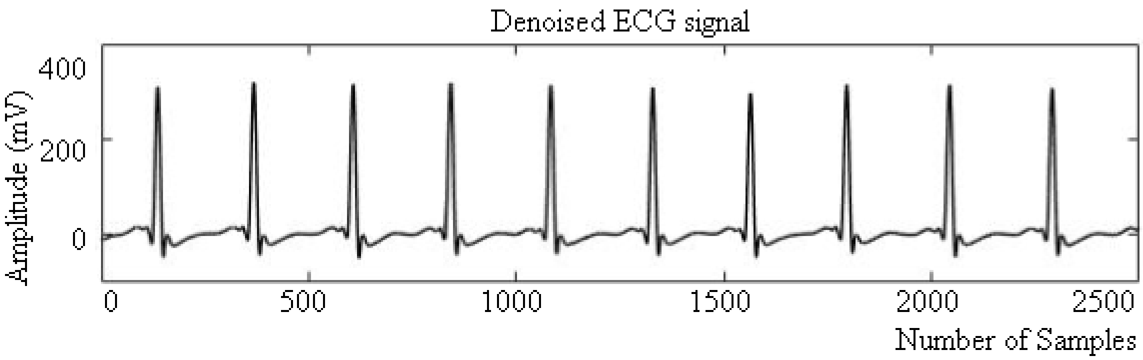

(d)

Fig. 4. 8 (a) Input ECG signal is taken from QT database, (b) random noise source, (d) input ECG signal after noise addition, (d) denoised ECG signal

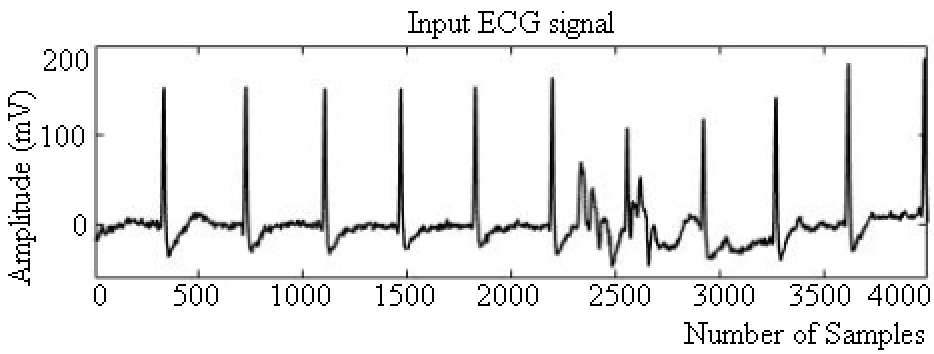

(a)

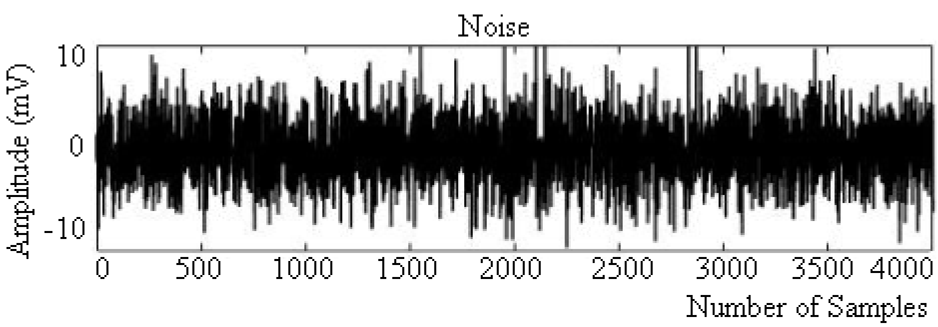

(b)

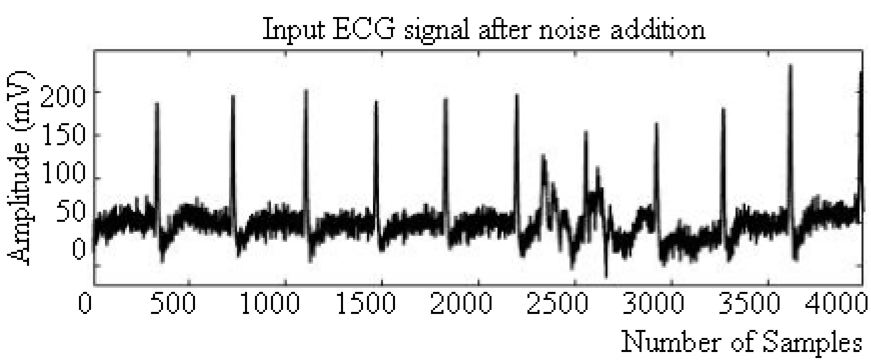

(c)

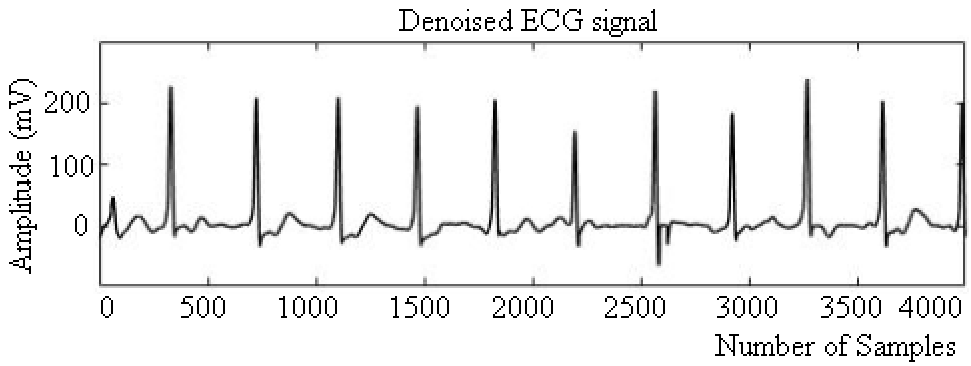

(d)

Fig. 4. 9 (a) Input ECG signal is taken from fantasia database, (b) random noise source, (d) input ECG signal after noise addition, (d) denoised ECG signal

Fig. 4.9 (a) contains input ECG signal of long duration, a gain of *2000*, and a sampling frequency of *250 Hz* from fantasia database. The random noise shown in fig. 4.9 (b) is added to the original ECG signal. Fig. 4.9 (c) represents the noisy ECG signal. Finally, the denoised ECG signal is shown in Fig. 4.9 (d).

Table 4. 8: Hardware comparison of proposed modified 3.1 wavelet transform based filter bank with existing ones

Method	Lowpass Filters	Highpass Filters	Adders	Multipliers	Delay Elements
Pipelined [32]	3	1	16	16	24
Undecimator [67]	3	4	16	13	13
Decimator [75]	3	4	16	13	13
Conventional [76]	3	4	16	13	13
Proposed modified WFB	**4**	**1**	**5**	**9**	**9**

Table 4. 9: Area comparison of adders and multipliers of proposed wavelet filter bank with existing ones

Method	Adders	Area Required for Adders	Multipliers	Area Required for Multiplier
Pipelined [32]	16	1260.16 μm^2	16	76313.76 μm^2
Undecimator [67]	16	1260.16 μm^2	13	62004.93 μm^2
Decimator [75]	16	1260.16 μm^2	13	62004.93 μm^2
Conventional [76]	16	1260.16 μm^2	13	62004.93 μm^2
Proposed modified WFB	**5**	**393.8 μm^2**	**9**	**42926.49 μm^2**

Hardware comparison of the proposed modified biorthogonal *3.1* wavelet transform based filter bank with the existing denoising technique is listed in Table 4.8. It is observed from Table 4.8 that the proposed architecture for the wavelet filter bank required five adders, nine delay elements, and nine multipliers. In *180 nm* technology, the total area required to realize these adders and multipliers is $393.8\ \mu m^2$ and $42926.49\ \mu m^2$, respectively, which is comparatively lower than the previously reported methods [67,75,76,32]. From Table 4.9, it is clear that the proposed wavelet filter bank architecture uses less hardware compared to the existing wavelet filter banks. The area required to realize the adders ($78.76\ \mu m^2$ per adder [189]) of the proposed wavelet filter bank is $393.8\ \mu m^2$ and the area required to realize the multipliers ($4769.61\ \mu m^2$ per Multiplier [190]) of the proposed wavelet filter bank is $42926.49\ \mu m^2$.

4.2 DEMAND BASED WAVELET FILTER BANK

Circuit complexity is the primary concern with the modified biorthogonal *3.1* wavelet transform based wavelet filter bank architecture. As discussed earlier, the use of a multiplier to multiply lowpass and highpass filter outputs of wavelet filter bank-four in the modified *3.1* wavelet transform based wavelet filter bank increases the hardware cost of the ECG signal denoising technique. Hence, to reduce the overall circuit complexity of the wavelet filter bank, a new demand-based wavelet filter bank architecture is proposed for ECG signal denoising that utilizes a cascade connection of three lowpass filters which requires less hardware and consume low power. Block diagram representation of the proposed wavelet filter bank is shown in Fig. 4.10.

Fig. 4. 10 Proposed biorthogonal 3.1 wavelet transform based demand-based wavelet filter bank architecture

In the proposed biorthogonal *3.1* wavelet transform based demand-based wavelet filter bank architecture; ECG signal is first filtered using a lowpass filter to yield lowpass sub-bands. As per Nyquist criterion, after filtering, half the samples are thrust aside. While realizing the filters, due to the smaller number of coefficients, the resultant implementation has a reduced computational complexity. These filters can also be used to reconstruct the sub-bands while canceling any aliasing which occurs due to down sampling. In the next level of decomposition, the sub-bands are iteratively filtered by the demand-based wavelet filter bank to yield narrow sub-bands. Demand-based wavelet filter bank architecture is verified for all wavelet transforms. The efficiency of a filter bank is determined by finding SNR, PRD, RMSE, and circuit complexity. The transfer function of lowpass filter *H(z)* and highpass filter *G(z)* used in the proposed biorthogonal wavelet filter bank architecture is given by Eq. (4.17) and Eq. (4.18).

$$H(z) = -0.12 + 0.99z^{-1} + 0.99z^{-2} - 0.15z^{-3} \tag{4.17}$$

$$G(z) = -0.17 + 0.53z^{-1} - 0.53z^{-2} + 0.17z^{-3} \tag{4.18}$$

Here, z^{-1}, z^{-2} and z^{-3} are delay elements.

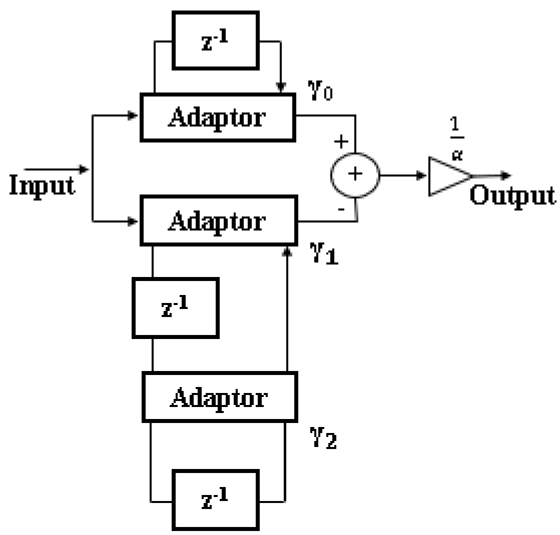

Fig. 4. 11 Wave digital filter realization of a third-order lowpass filter

However, the cascading of filters increases hardware complexity and power consumption in the circuit [173]. To further reduce the circuit complexity of proposed filter bank architecture, lowpass filters are realized using wave digital filter (WDF). WDF realization is advantageous as it requires less number of the multipliers and delay elements when compared to other filter realization techniques reported prior [57]. As a result, the WDF realization reduces the overall circuit complexity of the filter bank. Wave digital filter realization of a third-order lowpass filter is shown in Fig. 4.11.

Various hardware components required to realize the wavelet filter bank architecture are listed in Table 4.10. It is observed from Table 4.10 that the proposed architecture for the wavelet filter bank requires ten adders, four multipliers, and three delay elements.

Table 4. 10: Hardware comparison of proposed demand-based wavelet filter bank with existing ones

References	Lowpass Filters	Highpass Filters	Adders	Multipliers	Delay Elements
Rodrigues et al. [66]	3	4	32	26	NR*
Min et al. [70]	3	4	16	13	13
Bhavtosh et al. [76]	3	4	16	13	13
Proposed demand-based WFB [210]	**3**	**0**	**10**	**4**	**3**

*NR = Not reported, WFB = Wavelet filter bank.

It is evident from Table 4.10 that the proposed demand based wavelet filter bank realization uses less hardware compared to the other existing filter bank realizations. The results of this work are published in [210].

4.2.1 Criterion to Select Wavelet Decomposition Level

The decomposition level of the wavelet transform plays a vital role in the detection of the number of waves and their location in an ECG signal. Selecting the desired decomposition level is associated with the frequency components necessary for the ECG signal analysis for a given number of samples.

Biorthogonal wavelet transform satisfies the relationship as in Eq. (4.19).

$$2^N = p \tag{4.19}$$

Here, 'p' is the number of signal samples, and 'N' is the decomposition level. An ECG signal after different levels of decomposition is shown in Fig. 4.8. Usually, the typical frequency range of an ECG signal is from *0.5 - 150 Hz,* and that of QRS-complex is from *5 - 24 Hz* [174]. Since most of the QRS-complex frequencies lie between *0 - 24 Hz,* the third level of decomposition gives an optimal performance, hence, selected for the proposed work.

4.2.2. Wavelet Thresholding Techniques

Wavelet thresholding is used to retain the wavelet coefficients of a signal whose amplitude is higher than a particular preset value, called as a threshold. If the amplitude of the wave is smaller than the threshold, then the corresponding wavelet coefficients are made zero. Ideally, the threshold value is chosen such that the noise coefficients are discarded, and the signal is estimated from the remaining wavelet coefficients [175]. If the threshold value is too small, then the wavelet coefficients also contain the noise. Thus, the estimated signal is not noise-free. On the other hand, if the value of the threshold is large, then the signal is over smoothened, which may lead to the loss of valid information. Thus, the selection of an optimal threshold value becomes vital to reduce the mean square error (MSE) [176]. There are five different types of thresholding techniques, namely, hard thresholding [177], soft thresholding [177], sure shrink [177], hybrid thresholding [177], and wavelet Wiener filter. The hard thresholding method smoothens the signal, but may result in spurious blips in the output. Soft threshold method overcomes this drawback. Sure shrink, and hybrid shrink methods smoothen the signal but do not reduce RMSE.

In the case of ECG signal interference with power-line noise, it is observed that applying hard, soft, sure shrink thresholding methods results in large variance and RMSE increases. In case of an ECG signal interference with EMG signal noise, it is observed that applying hard, soft, sure shrink thresholding methods, the variance and bias square value either simultaneously increases or decreases, and MSE increases. In wavelet-Wiener filter thresholding method, both variance and bias square value decreases, and thus the RMSE is small, hence, used in the proposed work.

4.2.3 Simulation Results and Performance Evaluation of the Proposed Demand-Based Wavelet Filter Bank

The simulation procedure of the proposed demand-based wavelet filter bank architecture is as follows. Initially, the collected ECG data are further classified into five types: normal, atrial premature contraction (APC), premature ventricular contraction (PVC), left bundle branch block and right bundle branch block. Table 4.11 categorizes different ECG signals available in the MIT-BIH database.

SNR, RMSE, PRD are the three performance evaluation indexes of the proposed ECG signal denoising technique. The proposed demand-based wavelet filter bank-based ECG denoising technique is compared with the existing literature [191-196] to validate the denoising capabilities. To ensure a fair comparison between various ECG denoising methods given in [191-196], all these methods are implemented under the same conditions using MATLAB®.

Table 4. 11: Detail of different types of ECG signals

Type of ECG Signal	ECG Record	Total Number of Beats
Healthy	100, 101, 108, 112.	2000
Atrial Premature Contraction	103, 121, 124, 200, 201, 202, 205, 207, 209, 213, 215, 219, 220, 222, 223, 228, 231, 232, 233	2000
Premature Ventricular Contraction	106, 107, 200, 201	2000
Right Bundle Branch Block	118, 207, 212	2000
Left Bundle Branch Block	109, 111, 207, 214	2000

Performance of the proposed demand-based wavelet filter bank is evaluated in five different conditions, namely, normal ECG signal, ECG signal with random noise, ECG signal with white Gaussian noise (WGN), ECG signal with baseline wandering noise (BWN) and ECG signal with power line interference noise (PLI). All the above four noises are generated and added to the raw ECG signal. Table 4.12 presents the performance comparison of the proposed demand wavelet filter bank-based ECG denoising technique with the existing techniques.

Table 4. 12: Performance comparison of the proposed demand-based wavelet filter bank with the existing techniques

References	Random Noise		WGN		BWN		PLI	
	SNR	MSE	SNR	MSE	SNR	MSE	SNR	MSE
Komaty et al. [191]	NA	NA	1.21	NA	NA	0.02	NA	NA
Chang et al. [192]	NA	NA	6.85	NA	NA	0.002	NA	NA
Weng et al. [193]	10.01	0.002	8.12	0.0002	14.02	0.003	10.01	0.002
Nguyen et al. [194]	9.12	0.001	NA	0.0020	11.50	NA	9.12	0.001
Tan et al. [195]	NA	NA	NA	0.0039	8.51	NA	NA	NA
Wang et. al. [196]	9.00	0.002	6.18	0.0016	12.98	0.002	9.00	0.002
Proposed demand WFB	**30.00**	**0.0008**	**32.6**	**0.0003**	**28.38**	**0.002**	**30.00**	**0.0008**

Table 4.13 presents the PRD comparison of the proposed demand wavelet filter bank-based ECG signal denoising technique with the existing techniques. It is evident from Table 4.12 and Table 4.13 that the proposed demand wavelet filter bank-based ECG denoising technique achieves highest SNR, lowest MSE, and lowest PRD as compared to the previously designed ECG denoising techniques.

Table 4. 13: PRD comparison of the proposed demand wavelet filter bank-based technique with the existing techniques

References	PRD
Komaty et al. [191]	1.28
Chang et al. [192]	2.69
Weng et al. [193]	3.93
Nguyen et al. [194]	2.47
Tan et al. [195]	6.31
Wang et al. [196]	2.86
Proposed demand WFB	**0.47**

Area comparison of adders and multipliers of the proposed demand-based filter bank with the existing denoising technique is listed in Table 4.14. It is observed from Table 4.14 that the proposed architecture for the wavelet filter bank required ten adders, and four multipliers.

Table 4. 14: Area comparison of adders and multipliers of proposed demand-based wavelet filter bank with existing ones

Method	Adders	Area Required for Adders	Multipliers	Area Required for Multiplier
Pipelined [32]	16	1260.16 μm^2	16	76313.76 μm^2
Undecimator [67]	16	1260.16 μm^2	13	62004.93 μm^2
Decimator [75]	16	1260.16 μm^2	13	62004.93 μm^2
Conventional [76]	16	1260.16 μm^2	13	62004.93 μm^2
Demand based WFB	10	787.6 μm^2	**4**	**19078.44 μm^2**

In *180nm* technology, the total area required to realize these adders and multipliers is *787.6* μm^2 and *19078.44* μm^2, respectively, which is comparatively lower than the existing reported methods [67,75,76,32]. From Table 4.14, it is clear that the proposed wavelet filter bank architecture uses less hardware compared to the existing wavelet filter banks.

The output of the proposed demand-based wavelet filter bank is shown in Fig, 4.12. Fig. 4.12 (a) contains an input ECG signal with a sampling frequency of *360 Hz* taken from the MIT-BIH arrhythmia database. Random noise is shown in Fig. 4.12 (b) is generated and added to the original ECG signal and Fig. 4.12 (c) represents the noisy ECG signal. Finally, Fig. 4.12 (d) represents the denoised ECG signal.

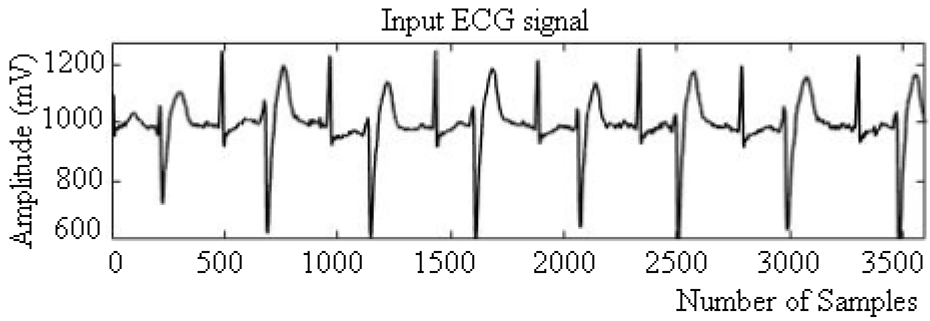

(a)

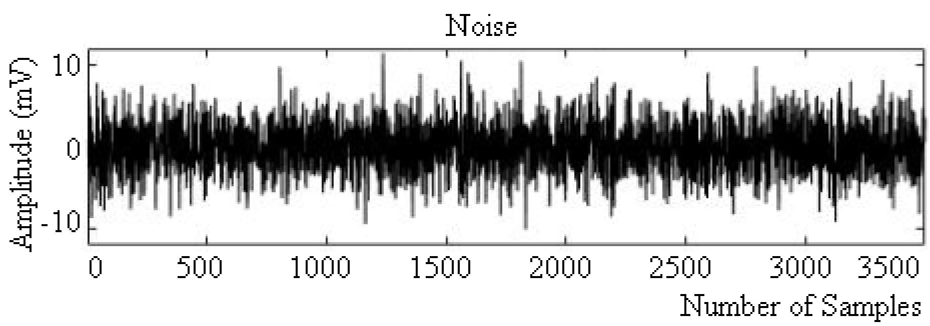

(b)

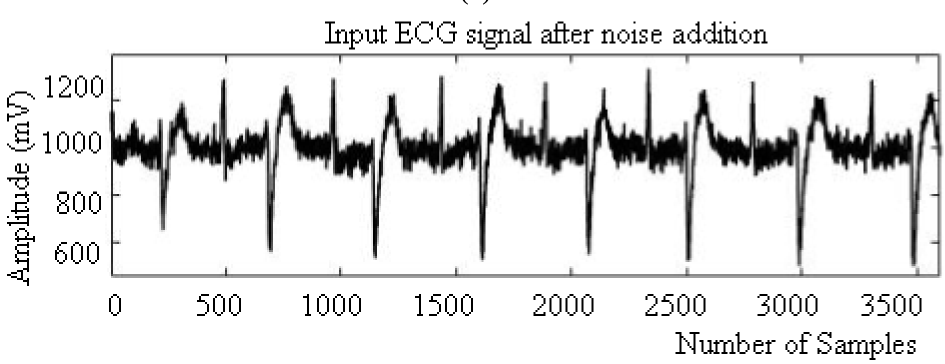

(c)

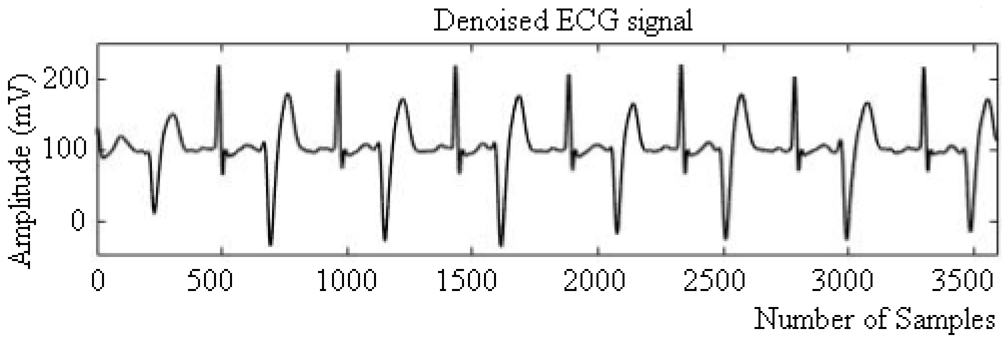

(d)

Fig. 4. 12 Output of the proposed heartrate monitoring and Therapeutic Devices, (a) input ECG signal, (b) noise source, (c) noise added ECG signal, (d) Denoised ECG signal

4.3 SUMMARY

The wavelet transform-based filter bank architecture suitable for ECG signal denoising is proposed in this chapter. The proposed demand-based wavelet filter bank uses only three lowpass filters for the filtering purpose. A digitized ECG signal is applied to the demand-based wavelet filter bank which separates the QRS-complexes from the noises. One of the main advantages of the demand-based wavelet filter bank architecture is that multiplexer and multiplier circuit are not required for further processing. The proposed architecture consumes less area and is relatively fast compared to existing wavelet filter bank architectures.

CHAPTER 5

ECG SIGNAL DETECTION AND LOSSLESS DATA COMPRESSION TECHNIQUES FOR IMPLANTABLE CARDIAC PACEMAKER SYSTEMS

Clinical procedures have a prominent and essential space to biomedical signal transmission techniques. Signal transmission techniques enable a remote clinical assessment using biomedical signals. Healthcare processes generate substantial data, thus demand a massive data transmission. Thus, the application of data compression techniques on biosignal transmission can make a remote clinical assessment cost-effective. For example, several hours of cardiac activity is recorded using multiple channel ECG recorder generates an enormous amount of data. Thus, it is imperative that an ECG recording system is equipped with sufficient storage capacity clubbed with channel bandwidth. As real-time monitoring requires large memory and ample bandwidth to transfer raw data, a proper compression technique is required for transmission and data storage. Further, to enable secure off-line data storage through ECG archives, the ECG data needs to be compressed for a cost-effective solution. Thus, there is an obvious requirement for data compression in biomedical signals. This chapter presents the theoretical aspects, simulation results and performance analysis of the proposed ECG signal detection and lossless data compression methods. The chapter is divided into two sections, namely, ECG signal detection, and lossless data compression. Performance of the proposed methods is verified using different ECG databases.

5.1 ECG SIGNAL DETECTION

P-wave, QRS-complex, T-wave are the main features in an ECG signal which provide information about the cardiac health of a person. Automatic detection of P-wave, QRS-complex and T-wave is the essential aspect of ECG signal processing and analysis. The performance of any ECG detection algorithm mainly relies on the accuracy of QRS-complex detector. A comprehensive review of the existing ECG signal detection techniques is found in literature [63, 64, 65]. Many ECG signal detection algorithms present in the literature detect QRS-complex. Most of the QRS-complex detection techniques include one of the following methods:

thresholding based, neural network, hidden Markov model (HMM), matched filter, zero-crossing, multiplication of backward difference, syntactic method and singularity-based approach [63, 64, 65]. Finding a robust algorithm to detect a QRS-complex is difficult. Thus, most of the ECG detection methods are not universally accepted. Hence, continuous efforts are made by various researchers to improve the detection capabilities and other vital features of an ECG signal.

The use of thresholding approach for ECG signal detection is recommended, as thresholding techniques are simple, numerically efficient to detect different waves present in an ECG signal and provide high detection accuracy. The methodology used to implement the proposed ECG signal detection techniques is as follows. The threshold value is determined after passing the ECG signal through a wavelet filter bank. The amplitude of incoming denoised ECG waves from the wavelet filter bank is compared with a threshold value. Two types of threshold values, namely hard threshold and soft threshold can be used to compare the amplitude of the ECG signal. The waves with amplitude value less than the threshold value are counted as zero in both hard and soft thresholds. Thus, the functionality of both hard and soft threshold values is the same in the case of those waves with amplitude less than the set threshold. For the ECG waves with an amplitude value larger than a set threshold, hard threshold and the soft threshold result in different functionality. In case of the hard threshold, those waves having an amplitude value larger than the set threshold are forced to approach towards "one" thus detecting the presence of a wave. In doing so, some features of the signal are lost and hence using a hard threshold degrades the detection accuracy. In the soft threshold, the value of the wave is retained if the value of the amplitude is larger than the threshold value. Thus, a soft threshold is more advantageous than the hard threshold. Hence in the proposed QRS-complex detector, soft thresholding technique is used. Eq. (5.1) defines the threshold value used in this work. This work is published in [216].

$$V_{th} = 0.8 \times A(\max) \tag{5.1}$$

Here, *A(max)* is the maximum amplitude of the denoised ECG signal.

A wave having an amplitude higher than the defined threshold value is considered to be QRS-complex. Thus, by identifying the QRS-complex, the time interval between two consecutive R-waves is calculated.

The reason for selecting the above-said threshold values is as follows. Different values of the threshold are used to detect the QRS-complex. The threshold value neither should result in a false QRS-complex detection nor should miss a QRS-complex. Further, setting a large value of threshold increases the probability to miss a wave, thus increasing the error rate of detection. Setting a small value of threshold results in increased computation complexity and false detection, thus reducing the detection efficiency of the system. Different values of V_{th}, ranging from *0.7 - 0.9,* are considered. V_{th} close to *0.7* resulted in an increased false QRS-complex detection, while, V_{th} close to *0.9* resulted in the missed QRS-complex. Hence the threshold value is fixed at $0.8 \times A(max)$. As the V_{th} value is fixed, this method is called as fixed threshold method. Further, analysis of a large dataset may result in an optimized value of V_{th}.

5.1.1 Simulation Results and Performance Evaluation of the Proposed Soft-Thresholding Based QRS-Complex Detection Technique

The proposed technique is tested with three different types of ECG signals from the MIT-BIH arrhythmia database and QT database. The ECG signal duration in short time data is for ten seconds, medium data is one-minute, and full-length data is one-hour.

Further, false negative (FN) and false positive (FP) detections are also used to evaluate the detection performance. FP is the number of extra detected waves, and FN is the number of missed waves. Further, FN and FP are used to compute the sensitivity (Se %), positive predictivity (+P %), data error rate (DER %), the probability of missed detection (PD), and the probability of false alarms (PFA).

QRS-complex detection results for all records and the different size of data, namely, ten seconds, one minute, and full-length ECG data of MIT-BIH arrhythmia is summarized in Table 5.1, Table 5.2 and Table 5.3, respectively.

As shown in Table 5.1, the proposed soft-thresholding based QRS-complex detector achieves the sensitivity and positive predictivity of 99.31% and 99.65% with the MIT-BIH arrhythmia database of ten seconds. 108.mat and 214.mat signals from the MIT-BIH arrhythmia database contains maximum noise [21]. The proposed soft-thresholding based QRS-complex detector achieves the sensitivity and positive predictivity of 90.90 % and 100 % on 108.mat and 100 % sensitivity and 100 % positive predictivity on 214.mat.

Table 5. 1: Performance of the proposed soft-thresholding based QRS-complex detection technique using ten-second MIT-BIH database

Record No.	Total (beats)	TP	FN	FP	Se (%)	+P (%)	DER (%)
100	13	13	0	0	100	100	0
101	11	11	0	0	100	100	0
102	12	12	0	0	100	100	0
103	11	11	0	0	100	100	0
104	13	13	0	0	100	100	0
105	14	14	0	0	100	100	0
106	10	10	0	0	100	100	0
107	12	11	1	0	91.66	100	0.83
108	11	10	1	0	90.90	100	0.09
109	16	16	0	1	100	94.11	0.06
111	12	12	0	0	100	100	0
112	14	14	0	0	100	100	0
113	09	09	0	0	100	100	0
114	10	10	0	0	100	100	0
115	10	10	0	0	100	100	0
116	14	14	0	0	100	100	0
117	9	9	0	0	100	100	0
118	12	12	0	0	100	100	0
119	10	10	0	0	100	100	0
121	10	10	0	0	100	100	0
122	15	15	0	0	100	100	0
123	9	8	1	0	90	100	0.11
124	8	8	0	0	100	100	0
200	15	15	0	0	100	100	0
201	14	14	0	0	100	100	0
202	7	7	0	0	100	100	0
205	15	15	0	0	100	100	0

Record No.	Total (beats)	TP	FN	FP	Se (%)	+P (%)	DER (%)
207	10	10	0	0	100	100	0
208	13	12	1	0	92.30	100	0.07
209	15	15	0	0	100	100	0
210	16	16	0	0	100	100	0
212	15	15	0	0	100	100	0
213	18	18	0	0	100	100	0
214	13	13	0	0	100	100	0
215	18	18	0	0	100	100	0
217	12	12	0	0	100	100	0
219	13	13	0	0	100	100	0
220	12	12	0	0	100	100	0
221	13	13	0	0	100	100	0
222	13	13	0	0	100	100	0
223	13	13	0	0	100	100	0
228	12	12	0	0	100	100	0
230	14	14	0	0	100	100	0
231	10	10	0	0	100	100	0
232	9	9	0	1	100	90	0.11
233	17	17	0	0	100	100	0
234	15	15	0	0	100	100	0
Total	**587**	**583**	**4**	**2**	**99.31**	**99.65**	**1.02**

From Table 5.2, the proposed soft-thresholding based QRS-complex detector achieves sensitivity and positive predictivity of *99.65%* and *99.65%* with the MIT-BIH arrhythmia database of one minute. Also, the proposed soft-thresholding based QRS-complex detector achieves sensitivity and positive predictivity of *100 %* on *108.mat* and *100 %* sensitivity and positive predictivity on *214.mat* to existing detection algorithms. Summary of Se, +P, and DER of the proposed soft-thresholding based QRS-complex detection technique with different sizes of ECG dataset is shown in Fig. 5.1.

Table 5. 2: Performance of the proposed soft-thresholding based QRS-complex detection technique using one-minute MIT-BIH database

Record No.	Total (beats)	TP	FN	FP	Se (%)	+P (%)	DER (%)
100	74	74	0	0	100	100	0
101	70	70	0	1	100	98.59	0.01
102	73	73	0	0	100	100	0
103	70	70	0	0	100	100	0
104	74	73	1	0	98.64	100	0.01
105	83	83	0	0	100	100	0
106	69	67	2	0	97.10	100	0.02
107	71	71	0	0	100	100	0
108	58	58	0	0	100	100	0
109	91	91	0	0	100	100	0
111	69	69	0	0	100	100	0
112	85	85	0	0	100	100	0
113	58	58	0	0	100	100	0
114	55	55	0	0	100	100	0
115	63	63	0	0	100	100	0
116	79	79	0	0	100	100	0
117	50	50	0	0	100	100	0
118	73	73	0	0	100	100	0
119	65	65	0	0	100	100	0
121	60	59	1	0	98.33	100	0.01
122	87	87	0	0	100	100	0
123	49	48	1	0	97.95	100	0.02
124	50	50	0	0	100	100	0
202	53	53	0	0	100	100	0
205	89	89	0	0	100	100	0
209	92	92	0	0	100	100	0
210	91	89	2	0	97.80	100	0.02

Record No.	Total (beats)	TP	FN	FP	Se (%)	+P (%)	DER (%)
212	90	90	0	0	100	100	0
213	111	111	0	0	100	100	0
214	76	76	0	0	100	100	0
215	106	106	1	4	99.06	96.36	0.04
217	72	72	0	0	100	100	0
219	74	74	0	0	100	100	0
220	72	72	0	0	100	100	0
221	79	78	1	0	98.73	100	0.01
222	75	75	0	0	100	100	0
223	80	80	0	0	100	100	0
228	71	69	2	3	97.18	95.83	0.07
230	79	79	0	0	100	100	0
231	63	63	0	0	100	100	0
233	103	103	0	0	100	100	0
234	92	92	0	0	100	100	0
Total	**3144**	**3140**	**11**	**11**	**99.65**	**99.65**	**0.006**

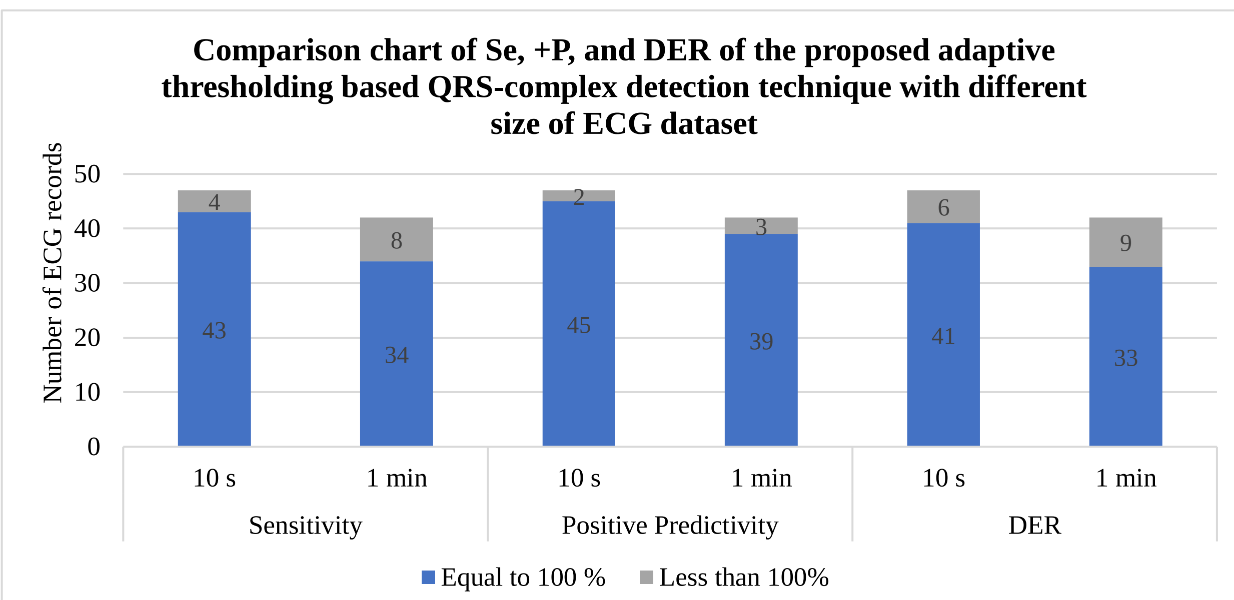

Fig. 5. 1 Comparison chart of Se, +P, and DER of the proposed soft-thresholding based QRS-complex detection technique with different size of ECG dataset

From Fig. 5.1, it is noticed that the proposed soft-thresholding based QRS-complex detection technique achieves a 100% sensitivity and 100% positive predictivity on the maximum number of ECG signals of different length. From Table 5.3, the proposed soft-thresholding-based QRS-complex detector achieves the highest sensitivity and positive predictivity of *99.75%* and *99.98%*, respectively, with the MIT-BIH arrhythmia database of one-hour length.

Table 5. 3: Performance of the proposed soft-thresholding based QRS-complex detection technique using the one-hour MIT-BIH database

Record No.	Total Beats	TP	FN	FP	Se (%)	+P (%)	DER (%)
100	2273	2273	0	0	100	100	0
102	2191	2187	4	0	99.8174	100	0.1826
103	2090	2083	7	0	99.665	100	0.3349
107	2139	2136	3	0	99.8597	100	0.1403
113	1795	1795	0	0	100	100	0
117	1538	1533	5	3	99.6749	99.8047	0.5202
122	2478	2476	2	0	99.9193	100	0.0807
123	1518	1518	0	0	100	100	0
220	2068	2048	20	0	99.0329	100	0.9671
234	2763	2752	11	0	99.6019	100	0.3951
Total	**20853**	**20801**	**52**	**3**	**99.75**	**99.98**	**0.26**

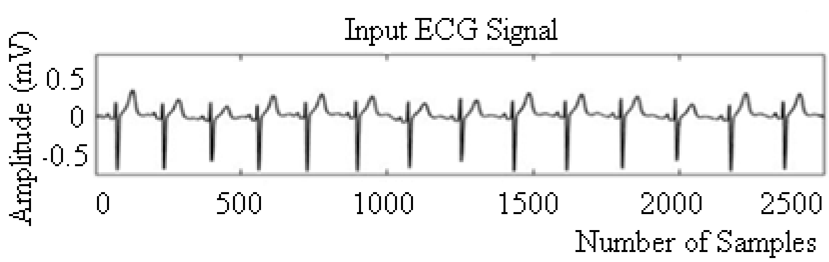

(a)

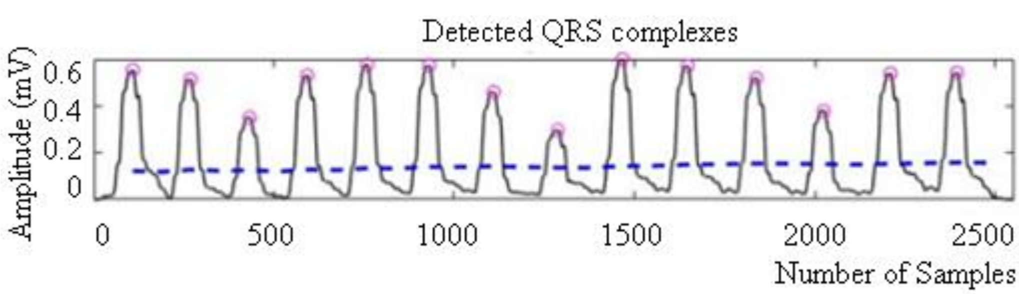

(b)

Fig. 5. 2 (a) 108 series of input ECG signal taken from the MIT-BIH arrhythmia database, (b) detected QRS-complexes

The performance of the proposed soft-thresholding based QRS-complex detector under noisy conditions is shown in Figure 5.2.

Fig. 5.2 (a) pictorially represents the *108.mat* input ECG signal taken from the MIT-BIH arrhythmia database. Fig. 5.2 (b) shows the detected QRS-complexes in ten seconds of ECG data. Table 5.1 also shows the same number of QRS-complexes for the *108.mat* ECG data.

Table 5. 4: Performance comparison of proposed soft thresholding technique with existing techniques

Method	Se (%)	+P (%)
Soft-thresholding (Proposed)	**99.75**	**99.98**
Multirate processing using filter banks [30]	99.59	99.56
Quadratic spline wavelet [50]	99.31	99.70
Genetic algorithm [99]	99.60	99.51
Wavelet denoising [131]	99.50	99.49
Real-time [173]	97.63	97.33
Mathematical morphology [197]	97.80	97.80

As shown in Table 5.4, the proposed soft-thresholding technique has a better detection performance compared to existing techniques. Some techniques like genetic algorithm, multirate processing using filter bank also offer excellent performance, but their computational complexities are relatively high compared to the proposed technique. The proposed soft-thresholding technique requires less hardware when compared to the existing techniques like [66], [70]. Usage of modified demand-based wavelet filter bank architecture and linear phase structure realization are the main reasons for the hardware complexity reduction. Hence, the proposed soft-thresholding technique is better for both implantable as well as wearable cardiac pacemaker applications.

5.1.2 Dynamic Dual Thresholding Based ECG Signal Detection

The performance of the soft thresholding technique has been evaluated on three different ECG data types, namely, low-quality versus high-quality ECG data, normal ECG data versus arrhythmic ECG data and normal ECG data versus paced rhythm ECG data. For the low-quality and high-quality ECG data, the soft thresholding technique achieves a higher detection accuracy. The soft thresholding technique has some limitations to differentiate between normal ECG data and abnormal ECG data. Some ECG data (*107.mat*, *109.mat,* and *219.mat*) from MIT-BIH arrhythmia database are recommended as normal ECG data by Physicians, but the soft thresholding technique detects all these ECG data as abnormal ECG data. Hence, a precise, exact, and coherent ECG signal detection algorithm is required. The dynamic dual thresholding technique-based ECG signal detection can overcome the problem mentioned above. Variable threshold value forms the central part of the dynamic dual thresholding method [178]. Flowchart of the dynamic dual thresholding technique-based ECG signal detector is shown in Fig. 5.3. The results of this work are published in [217]. The methodology used to implement the proposed dynamic dual thresholding-based ECG signal detection is as follows.

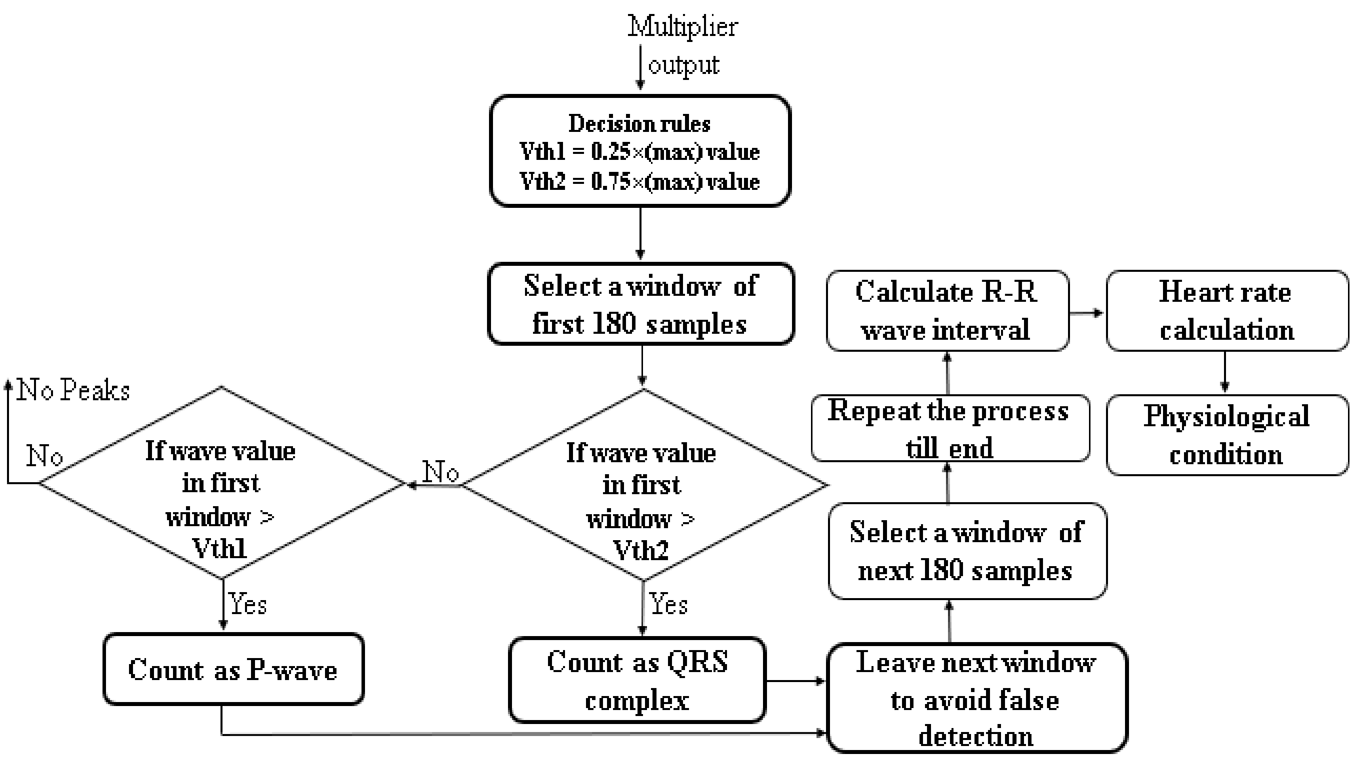

Fig. 5. 3 Flowchart of the proposed dynamic dual thresholding ECG detection technique

Two different threshold values are selected to which a booth multiplier's output is compared to detect different waves in the ECG signal. In this work, the variable threshold method is used to detect different waves in an ECG signal. The threshold value to detect QRS-complex (V_{th2}) is set at *0.75* times that of the maximum value of booth multiplier's output. To detect P-wave and T-wave of the ECG signal, *0.25* times the maximum value of booth multiplier's output is selected as the threshold value (V_{th1}). The reasons for selecting the above-said threshold values are as follows. Different values of the threshold are used to detect QRS-complex, P-wave, and T-wave. The threshold value should neither result in false wave detection nor should miss a wave. Further, setting a large value of threshold results in missed waves thus increasing the error rate, whereas, setting a small value of threshold results in increased computation complexity and false detection, thus reducing the detection accuracy of the system. Threshold values other than the used in this work is either detecting an extra number of ECG waves or detecting less number of ECG waves, thus reducing the detection accuracy of the algorithm.

Then after, windowing is applied to the first *180* samples of the ECG signal. The reason for the selection of *180* samples is that none of the ECG signals has an R-R wave interval less than *0.5* seconds or heartrate of *120* beats per minute. Then all the waves within the selected window are compared with the threshold values. If the amplitude of a wave is higher than the threshold value V_{th2}, the wave is counted as QRS-complex. Those waves whose value lies between V_{th1} and V_{th2} are counted as P-waves. After the detection of one QRS-complex or P-wave, the next *180* samples are left to avoid false detection. Then again, a window of next *180* samples are selected, and the same procedure is repeated until the end of the ECG signal. By calculating the time difference between two successive R waves, the heartrate (HR) can be calculated by using the relation given by Eq. (5.2).

$$HR = \frac{60}{\text{Average value of R-R } wave \text{ interval}} \tag{5.2}$$

Heartrate helps to measure the physiological condition of the subject. If the number of waves exceeds above *100* beats per minute (bpm) regularly, then the subject is suffering from sinus tachycardia, and if the number of waves is below 50 bpm, then the subject is suffering from sinus bradycardia. Thus, the proposed dynamic dual thresholding can detect the presence of a particular sinus arrhythmia in the subject.

5.1.3 Simulation Results and Performance Evaluation of the Proposed Dynamic Dual Thresholding Based ECG Signal Detection Technique

A dynamic dual thresholding technique-based ECG signal detector is proposed to overcome the shortcomings related to the soft-thresholding technique. Table 5.5 summarize the ECG signal detection results for all recordings of different size of ECG signals ten seconds, one minute, full length ECG signal of different ECG databases.

Table 5. 5: Measured detection accuracy of proposed dynamic dual thresholding-based ECG detector on different ECG databases

ECG Database	Duration	Total Waves	Se (%)	+P (%)	DER (%)	Avg. R-R Interval (Sec.)	Heartrate
MIT-BIH	10 seconds	532	99.43	99.43	0.011	0.8711	73.77
MIT-BIH	One minute	2871	99.86	99.86	0.002	0.8715	70.65
MIT-BIH	One hour	96581	99.95	99.92	0.001	0.8711	73.77
Fantasia	One hour	19445	99.96	99.84	0.002	0.8307	72.22
Apnea DB	One hour	703750	99.94	99.85	0.001	0.9280	64.65
ADB	One hour	197009	99.80	99.72	0.004	0.8388	71.59
QT-DB	One minute	124	99.19	98.40	0.020	0.6327	96.30

*DB: Database,

Table 5. 6: Performance comparison of proposed dynamic dual thresholding-based ECG detector with existing ECG detectors

Method	Se (%)	+P (%)
Dynamic dual thresholding (Proposed)	**99.95**	**99.98**
Multirate processing using filter Banks [30]	99.59	99.56
Genetic algorithm [50]	99.60	99.51
Quadratic spline wavelet [99]	99.31	99.70
Elgendi et al. [141]	99.90	99.84
Elgendi et al. [166]	99.79	99.88
Multiscale morphology [179]	99.81	99.80
Elgendi et al. [188]	99.78	99.87
Elgendi et al. [198]	99.90	99.56
Bandpass filtering/ search-back [199]	99.69	99.77
Pulse train approach [200]	98.58	99.55
Soft thresholding [216]	99.75	99.98

From Table 5.5, the proposed dynamic dual thresholding-based ECG detector achieves an average sensitivity ranging from 99.43% - 99.96% and average positive predictivity ranging from *99.43%-99.92%* with the different ECG databases of different durations. Fig. 5.4 shows the performance of the proposed dynamic-dual thresholding-based ECG signal detection technique.

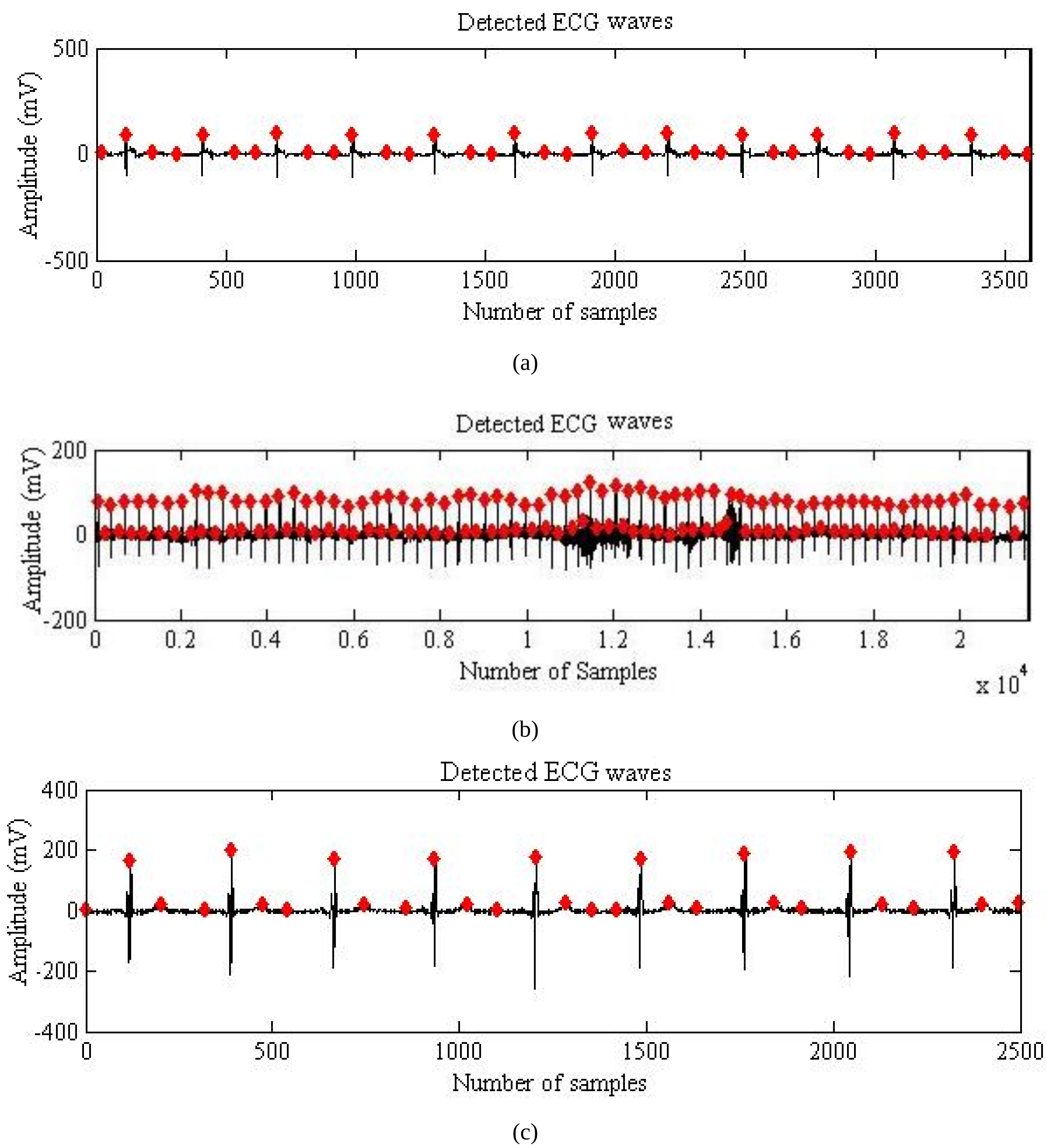

Fig. 5. 4 Outputs of proposed ECG detector, (a) with 10 seconds of MIT-BIH data, (b) with 1 minute of MIT-BIH data, (c) with 10 minutes of QT data

Comparison of dynamic-dual thresholding-based ECG detection technique with the existing techniques is discussed in Table 5.6.

From Table 5.6, it is evident that the dynamic dual thresholding-based ECG signal detection technique has better performance compared to the existing ECG signal detection techniques. Table 5.7 shows the P-wave detection performance of the proposed dynamic-dual thresholding based ECG signal detection technique.

Table 5. 7: measured detection accuracy of the proposed dynamic dual thresholding-based p-wave detector on full-length ECG signal

Record No.	Total	TP	FN	FP	Se (%)	+P (%)	DER (%)
100	2273	2273	0	0	100	100	0
101	1865	1865	0	0	100	100	0
102	2187	2187	0	0	100	100	0
103	2084	2084	0	1	100	99.95	0.004
104	2230	2229	0	0	100	100	0
105	2572	2566	6	25	99.76	99.03	0.012
106	2027	2027	0	0	100	100	0
107	2137	2137	0	0	100	100	0
108	1774	1771	3	0	99.83	100	0.001
109	2532	2532	0	0	100	100	0
111	2124	2124	0	0	100	100	0
112	2539	2539	0	0	100	100	0
113	1795	1795	0	0	100	100	0
114	1879	1877	2	2	99.89	99.89	0.002
115	1953	1953	0	0	100	100	0
116	2412	2402	10	0	99.58	100	0.004
117	1535	1535	0	0	100	100	0
118	2278	2278	0	0	100	100	0
119	1987	1987	0	0	100	100	0
121	1863	1863	0	0	100	100	0

Record No.	Total	TP	FN	FP	Se (%)	+P (%)	DER (%)
122	2476	2476	0	0	100	100	0
123	1518	1516	2	0	99.86	100	0.003
124	1619	1619	0	0	100	100	0
200	2601	2601	0	0	100	100	0
201	1963	1963	0	40	100	98	0.02
202	2136	2136	0	0	100	100	0
205	2656	2656	0	0	100	100	0
207	2332	2324	8	0	99.65	100	0
208	2301	2301	0	0	100	100	0
209	3004	3004	0	0	100	100	0
212	2748	2748	0	0	100	100	0
213	3251	3251	0	0	100	100	0
214	2265	2265	0	0	100	100	0
215	3363	3363	0	0	100	100	0
217	2209	2209	0	0	100	100	0
219	2154	2154	0	0	100	100	0
220	2048	2048	0	0	100	100	0
221	2427	2426	1	3	99.95	99.87	0.001
222	2483	2480	3	0	99.87	100	0.001
223	2605	2605	0	0	100	100	0
228	2053	2053	0	0	100	100	0
231	1571	1571	0	0	100	100	0
233	2426	2426	0	0	100	100	0
234	2753	2753	0	0	100	100	0
Total	**96582**	**96546**	**35**	**71**	**99.96**	**99.92**	**0.001**

From Table 5.7, the proposed dynamic dual thresholding for P-wave detection algorithm achieves sensitivity and positive predictivity of *99.96%* and *99.92%*, respectively, with the MIT-BIH arrhythmia database. Table 5.8 shows the detection performance of the T-wave.

From Table 5.8, the proposed dynamic dual thresholding for T-wave detection algorithm achieves the highest sensitivity and positive predictivity of *99.97%* and *99.93%*, respectively, with the MIT-BIH arrhythmia database.

Table 5. 8: Measured detection accuracy of proposed dynamic dual thresholding-based T-wave detector on full-length ECG signal

Recording No.	Total	TP	FN	FP	Se (%)	+P (%)	DER (%)
100	2274	2274	0	0	100	100	0
101	1865	1865	0	0	100	100	0
102	2188	2188	0	0	100	100	0
103	2084	2084	0	1	100	99.95	0.004
104	2230	2229	0	0	100	100	0
105	2572	2568	4	20	99.84	99.22	0.009
106	2027	2027	0	0	100	100	0
107	2137	2137	0	0	100	100	0
108	1774	1772	2	0	99.88	100	0.001
109	2532	2532	0	0	100	100	0
111	2125	2125	0	0	100	100	0
112	2539	2539	0	0	100	100	0
113	1795	1795	0	0	100	100	0
114	1879	1877	2	2	99.89	99.89	0.002
115	1953	1953	0	0	100	100	0
116	2412	2410	2	0	99.91	100	0.0008
117	1535	1535	0	0	100	100	0
118	2278	2278	0	0	100	100	0
119	1987	1987	0	0	100	100	0
121	1863	1863	0	0	100	100	0
122	2476	2476	0	0	100	100	0
123	1518	1516	2	0	99.86	100	0.003
124	1619	1619	0	0	100	100	0
200	2601	2601	0	0	100	100	0

Recording No.	Total	TP	FN	FP	Se (%)	+P (%)	DER (%)
201	1963	1963	0	40	100	98	0.02
202	2136	2136	0	0	100	100	0
205	2656	2656	0	0	100	100	0
207	2332	2324	8	0	99.65	100	0
208	2301	2301	0	0	100	100	0
209	3005	3005	0	0	100	100	0
212	2749	2749	0	0	100	100	0
213	3251	3251	0	0	100	100	0
214	2265	2265	0	0	100	100	0
215	3363	3363	0	0	100	100	0
217	2209	2209	0	0	100	100	0
219	2154	2154	0	0	100	100	0
220	2048	2048	0	0	100	100	0
221	2427	2426	1	3	99.95	99.87	0.001
222	2483	2480	3	0	99.87	100	0.001
223	2605	2605	0	0	100	100	0
228	2053	2053	0	0	100	100	0
231	1571	1571	0	0	100	100	0
234	2753	2753	0	0	100	100	0
Total	**96587**	**96562**	**25**	**65**	**99.97**	**99.93**	**0.0009**

The proposed dynamic dual thresholding method can detect P-wave, QRS-complex, and T-wave, thus detecting the ECG wave. Further, the computational complexity of the proposed ECG detector is controlled with the help of data compression to achieve low power. The additional logic required for data compression is minimal. Hence, the proposed dynamic dual thresholding is better suited for ECG detection when compared to the existing techniques.

5.1.4 Adaptive Thresholding Based ECG Signal Detection Technique

The major disadvantage of dynamic dual thresholding is to effectively address the balance between missing ECG waves and false ECG wave detection. To overcome false wave detection problem, an adaptive slope prediction based thresholding technique is used to detect different waves of an ECG signal. Two different threshold values, namely, the downward threshold (V_{th1}) and the upward threshold (V_{th2}) are selected with which the denoised ECG signal is compared to detect different waves in the ECG signal. Eq. (5.3) gives the downward threshold and upward threshold. Both the upward as well as downward threshold values are calculated using continuous assessment of the ECG signal peak and noise peak.

$$\begin{aligned} \mathrm{V}_{\mathrm{th1}} &= NP + 0.25(SP - NP) \\ \mathrm{V}_{\mathrm{th2}} &= 0.50\mathrm{V}_{\mathrm{th1}} \end{aligned} \tag{5.3}$$

Here, NP is the continuous assessment of the noise peak, and SP is the continuous assessment of the ECG signal peak. NP and SP are continuously estimated by using Eq. (5.4).

$$\begin{aligned} NP &= 0.25\, of\ overall\ peak + 0.85\, of\ NP, if\ overall\ peak\ is\ the\ noise\ peak \\ SP &= 0.25\, of\ overall\ peak + 0.85\, of\ SP, if\ overall\ peak\ is\ the\ signal\ peak \end{aligned} \tag{5.4}$$

Then denoised ECG signal is compared with both the threshold values. If the compared value is higher than V_{th2}, then the QRS-complex is identified, and a wave is counted. Those waves whose value lies between V_{th1} and V_{th2} are counted as a P-wave. All the other waves that may occur within the refractory period (*0.2 seconds*) are disregarded. This process is repeated until the end of the ECG signal. By calculating the rising and falling edge of the detected wave, the actual presence of a wave can be determined. The process of proposed adaptive slope prediction threshold-based ECG signal detection is shown in Fig. 5.5. The results of this work are published in [210].

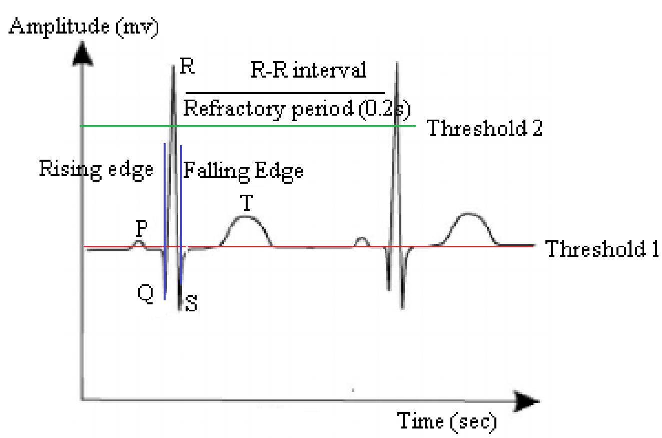

Fig. 5. 5 Proposed adaptive slope prediction threshold-based ECG detection

By calculating the time difference between two successive QRS-complexes, the heartrate in beats per minute (bpm) can be calculated by using Eq. (5.2). Physiological condition of a subject is measured by using the heartrate. If heartrate regularly exceeds *100* bpm, then the subject is suffering from sinus tachycardia, and if the heartrate is below *50* bpm, then the subject is suffering from sinus bradycardia. This system thus can identify the presence of particular sinus arrhythmia disease in the subject.

5.1.5 Simulation Results and Performance Evaluation of the Proposed Adaptive Thresholding Based ECG Signal Detection Technique

An adaptive slope prediction thresholding based ECG detector is proposed to overcome the concerns related to those mentioned above dynamic dual thresholding based ECG detector. The output of the proposed ECG detector is shown in Fig. 5.6.

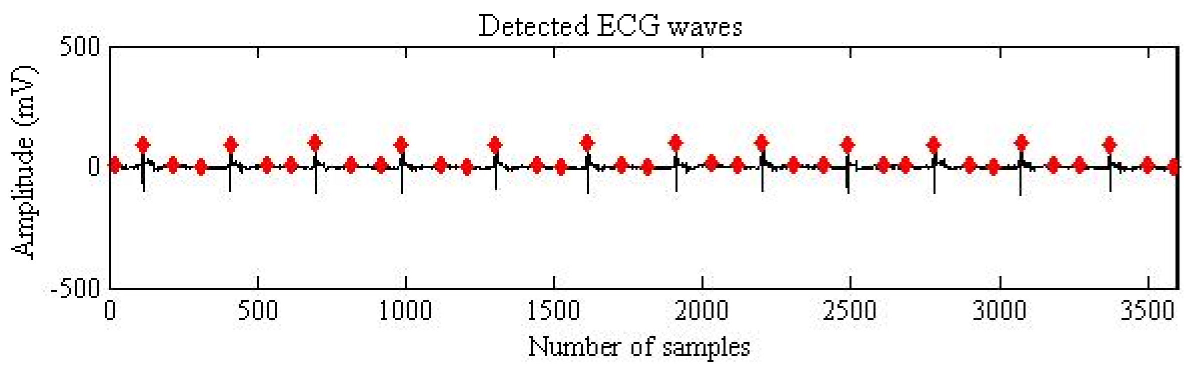

Fig. 5. 6 Output of the proposed adaptive slope prediction thresholding-based ECG detector

Table 5. 9: performance evaluation of the proposed adaptive slope prediction thresholding-based ECG detector

Type of ECG Beat	Number of Beats	TP	FP	FN	+P (%)	Error	SE (%)
Healthy	104363	104296	60	40	99.98	0.001	99.99
MI	40182	40150	30	20	99.98	0.0014	99.99
CAD	41545	41496	41	32	99.98	0.0020	99.98
CHF	89237	89177	42	38	99.99	0.0012	99.99
Total	**275327**	**275119**	**208**	**154**	**99.98**	**0.0013**	**99.98**

* MI: Myocardial infarction, CAD: Coronary artery disease, CHF: Congestive Heart Failure.

Performance evaluation of the proposed adaptive slope prediction thresholding-based ECG detector is depicted in Table 5.9. Total *275327* ECG beats out of which *104363* healthy beats, *41545* coronary artery disease beats, *89237* Congestive Heart Failure beats, and *40182* myocardial infarction beats are used to evaluate the performance of the proposed ECG detector.

It is observed from Table 5.9 that the proposed adaptive slope prediction thresholding-based ECG detection technique achieves a sensitivity of 99.98%, positive predictivity of 99.98% and an overall error of 0.0013.

Table 5.10 compares the ECG wave detection performance of the proposed adaptive slope prediction thresholding-based ECG detector with the existing detectors.

Table 5. 10: Comparison of the proposed adaptive slope prediction thresholding-based ECG detector with the existing detectors

Method	SE (%)	+P (%)	Error
Adaptive slope prediction (Proposed)	**99.98**	**99.98**	**0.0013**
Soft thresholding proposed in this thesis [216]	99.75	99.98	NR
Dynamic dual thresholding proposed in this thesis [217]	99.95	99.98	NR
Pan Tompkins [20]	99.74	99.60	NR
Genetic algorithm [50]	99.61	99.79	NR
Quadratic spline wavelet [99]	99.29	99.72	NR
Faezipour et al. [127]	99.79	99.78	0.4000
Wavelet denoising [131]	99.56	99.53	NR
Search-back [199]	99.72	99.79	NR
Pulse train approach [200]	99.57	99.56	NR
Cvikl et al. [201]	99.81	99.79	NR
Iliev et al. [202]	99.16	99.53	NR

It is observed from Table 5.10 that the proposed detector with an adaptive slope prediction threshold is capable of accurately distinguishing between healthy, myocardial infarction, congestive heart failure and coronary artery disease subjects with sensitivity, positive predictivity, and error of *99.94%*, *99.92%* and *0.0013* respectively. The key benefit of an adaptive slope predication threshold based detector is that the false wave detection is controlled by comparing the rising and falling edge of the ECG signal.

5.2 LOSSLESS DATA COMPRESSION

Long-term monitoring of the ECG signal is highly desirable for those subjects who are suffering from cardiovascular diseases [12, 179]. Few long term ECG monitoring systems are presented in the past few years. An ECG monitoring system is mainly categorized into recording and analyzing systems. A recording system is primarily used for acquisition, processing, and wireless transmission of an ECG signal [180]. Whereas, the analyzing system is used to extract the vital features of an ECG signal. Raw data transmission used in early ECG recording systems [13] consumes a large amount of data as raw ECG data is large in quantity thus requiring high data rate, hence not suitable for long term ECG signal monitoring. To deal with the substantial power requirements of ECG signal transmission, the ECG signals need compression to minimize the data transfer rate for transmission, thus reducing the power requirements of the system. To achieve a high compression ratio, lossy data compression techniques are considered. The ECG signal reconstructed after lossy data compression results in an ECG signal that contains a sizable amount of noise, and crucial diagnostic data is lost, thus lacking regulatory conformity. Thus, Medical applications demand the usage of lossless data compression techniques. The world of wearable sensors is experiencing new waves with high-efficiency, decreased power operation, and modest convolution in the application. Hence, it is much required to find a better fit and balance between the complexity and compression ratio (CR). Hence, data compression is an essential requirement to make the system power efficient.

Many lossless ECG compression techniques presented in the literature have focused on achieving a high compression ratio. Here in the proposed work, various data compression techniques, namely wavelet transform, Huffman coding/simple predictor, Huffman coding/adaptive predictor, slope predictor/fixed length packaging, and run-length encoding, are tested. Run-length encoding is chosen based on its simplicity and high compression ratio. In this method, the detected QRS-complexes are represented by "*1*" and "*0*" represent the rest of the data. This data is then compressed by replacing the zeros between two waves by the number of zeros between the waves. Run length encoding (RLE) is a well known, simple, and quick form of lossless data compression technique which offers a significant amount of compression for a specific type of data stream (in which the same data value occurs in many consecutive data elements). The run length encoding decreases the size of a given signal, while at the same time not losing any information. Each packet of run-length encoding consists of two components, namely, *run_count*, which denotes the number of characters in the run, and *run_value*, which indicates the common value of the characters in the run. For example, using RLE, the string of data "*1111111111110000111111100000001100*" encoded after string compression results in *1214071602120*. This can be interpreted as a sequence of twelve *1s*, four *0s*, seven *1s*, six *0s*, two *1s*, and two *0s*. After that, RLE is applied to the binary matrix.

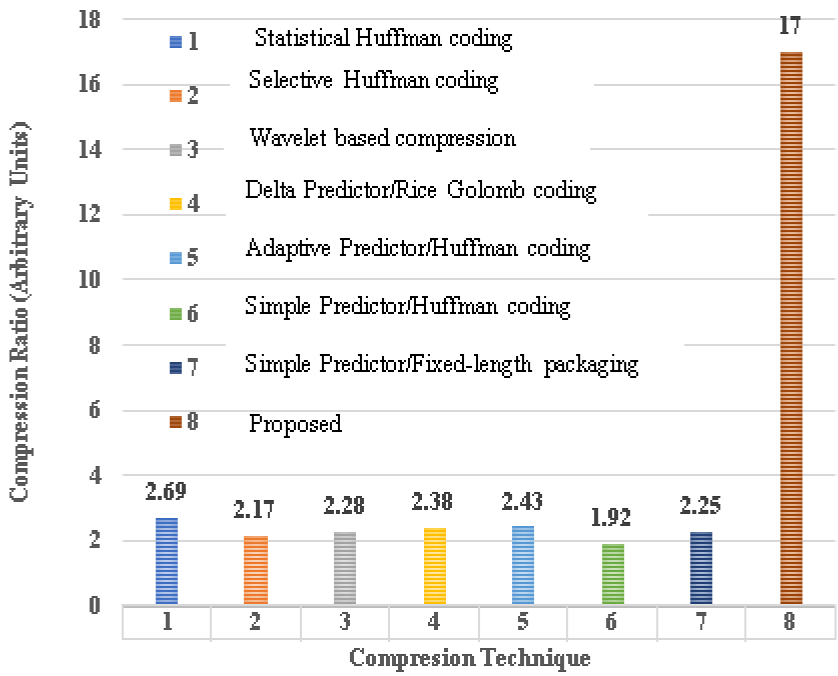

Fig. 5. 7 Comparison of the proposed technique with existing techniques

5.2.1 Simulation Results and Performance Evaluation of the Proposed RLE Based Lossless Data Compression Technique

The proposed RLE based ECG data compression technique is tested using the QT database and the MIT-BIH arrhythmia database. Comparison of proposed RLE compression technique with existing techniques is shown in Fig. 5.7. The proposed RLE based lossless data compression Technique achieves a higher compression ratio. The proposed RLE based ECG data compression technique attains a high compression ratio of *17.1*. The other existing data compression techniques provide a low compression ratio, which is *2.66* for statistical Huffman coding, *2.17* for selective Huffman coding, and *2.28* for wavelet-based data compression technique. The performance of the algorithm is not compared for other statistical parameters like PRD, MAE, space-saving, and compression gain, to name a few. This work is published in [216].

5.2.2 LZMA Based Lossless Data Compression Technique

Generally, RLE is not the best option for lossless ECG data compression because when no repeating values are present in the data string, it leads to increase in the number of bits and hence, decrease the compression ratio. Comparison of some lossless data compression techniques based on the three parameters, namely, compression ratio, compression speed, and memory usage, are presented in Table 5.11.

Table 5. 11: Comparison of different data compression techniques

Compression Technique	Compression Speed	Compression Ratio	Memory Usage
Lempel–Ziv–Welch (LZW)	Medium	Medium	Medium
Lempel–Ziv–Oberhumer (LZO)	Fast	Low	Low
Lempel–Ziv–Markov chain algorithm (LZMA)	Medium	High	Low
LZFX	Fast	Low	Not Reported
Bzip2	Medium	High	High
LZ4	Fast	Low	Low
Run-length encoding (RLE)	Medium	High	Medium
Huffman coding	High	Medium	High

It is observed from Table 5.11 that all three criteria cannot be achieved simultaneously. Considering the tradeoff among the above three criteria, LZMA data compression technique is used for the ECG data compression. Block diagram representation of LZMA data compression technique used in this work is as shown in Fig. 5.8. LZMA data compression Technique has medium compression speed, high compression ratio, and low memory usage. The results of this work are published in [210].

During compression, detected ECG samples are taken. Then, a window of eight ECG samples is selected, and the compression process is applied to the window. The first value of the window is unchanged, and the next bit value is subtracted from the previous bit value as described below

$$Delta\ (0) = W(0)$$
$$Delta\ (i) = W(i) - W(i\text{-}1)$$

$$1 \le i \le 7$$

End

For example, a window of input ECG samples *"5, 6, 7, 8, 9, 8, 7, 6"* is selected, and the encoded output sequence is *"5, 1, 1, 1, 1, -1, -1, -1"*.

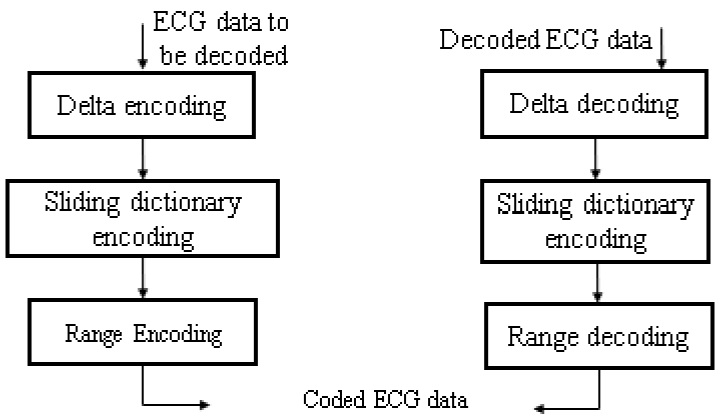

Fig. 5. 8 Block diagram representation of LZMA data compression technique

The delta encoding provides encoded output sequences in the form of differences from previous data, as shown in the example. Then the sliding dictionary algorithm is applied to the encoded output sequence of the delta encoding. Finally, the sliding dictionary output is used as an input of a range encoder which encodes the symbols of the ECG signal into numbers based on the frequency at which the symbols occur.

5.2.3 Simulation Results and Performance Evaluation of the Proposed LZMA Lossless ECG Data Compression Technique

The output of the proposed LZMA data compression technique is shown in Fig. 5.9. Fig. 5.9 (a) contains an input ECG signal with a sampling frequency of *360 Hz* taken from the MIT-BIH arrhythmia database. The compressed ECG signal using LZMA data compression technique is shown in Fig. 5.9 (b).

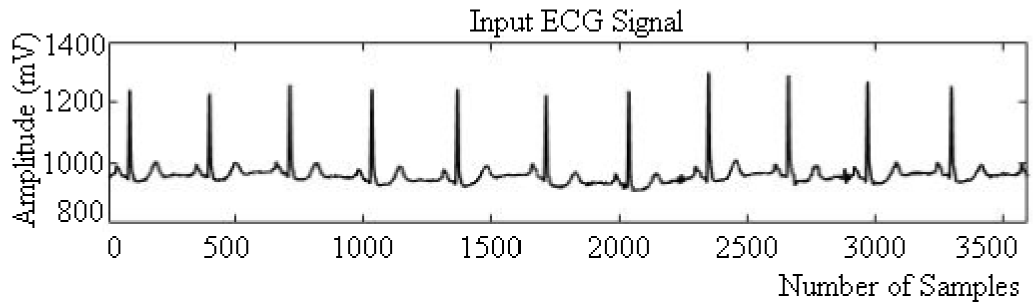

(a)

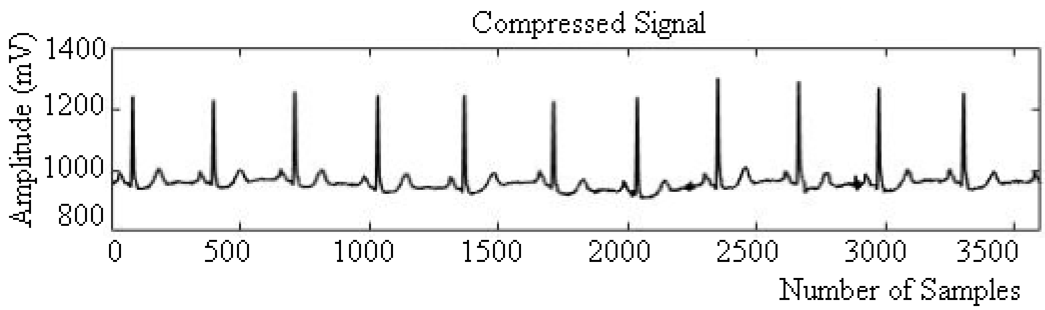

(b)

Fig. 5. 9 Output of the proposed LZMA data compression technique, (a) input ECG signal, (b) compressed ECG signal

Table 5. 12: performance comparison of proposed LZMA lossless ECG compression technique with existing techniques

Method	Compression ratio	Quality score
Lossy Compression Techniques		
m-AZTEC [203]	5.8	0.30
Mukhopadhyay et al. [204]	15.83	2.0
Mukhopadhyay et al. [205]	22.81	3.10
Near-lossless Compression Techniques		
USZZQ and Huffman coding of DSM [156]	11.09	4.16
SPIHIT [206]	8.06	6.78
Lossless Compression Techniques		
LZMA (Proposed)	**88.89**	**44445**
Rice Golomb Coding [102]	2.38	NR
Sang Joon Lee et al. [207]	16.5	27.15
JPEG2000 [208]	8.05	9.29

The significant challenges involved in wireless data transmission are data conversion and power consumption. A lossless compression technique with high bit compression ratio is highly required. Here in the proposed work, LZMA lossless data compression technique is used, and comparison of the proposed data compression technique with the existing techniques is presented in Table 5.12. It is evident from Table 5.12 that the proposed LZMA based ECG data compression technique has a high compression ratio, and quality score.

5.2.4 Biorthogonal 3.1 Wavelet Transform Based Lossless ECG Data Compression Technique

It is found that using two different approaches for ECG signal detection and compression increases the overall system complexity. Hence, the wavelet transform is selected for ECG signal detection and compression. The wavelet transform is extensively used in ECG signal compression due to the inherent irregularities in the ECG signal. DWT is preferred over CWT because the information stored in the coefficient of DWT is not repeated. Also, DWT allows a complete reconstruction of the ECG signal without any loss. These properties of DWT motivated to develop a wavelet-based ECG signal compression algorithm. Different wavelet transforms, namely, Haar wavelet transform, Daubechies wavelet transform, biorthogonal wavelet transform, reverse biorthogonal wavelet transform are available in the literature. Therefore, selecting an efficient wavelet transform is an essential requirement.

As the shape of the modified biorthogonal *3.1* wavelet transform resembles that of an ECG signal, is used for the ECG compression. Further, modified biorthogonal *3.1* wavelet transform can construct symmetrical wavelet functions, generate different multi-resolution analyses, higher SNR, and only a few wavelet coefficients, make it suitable for ECG applications. The process of ECG compression is as follows. Initially, for the decomposition of detected ECG signal, the detected ECG signal is passed through a parallel combination of a specially designed lowpass and highpass filters called scaling function and wavelet function. The output of both the lowpass and highpass filters are then down sampled by two, which provides a band of *0 – 180 Hz* for the lowpass filter and *180 - 360 Hz* for a highpass filter, named as wavelet filter bank-one (WFB01).

Further, the downsampled output of lowpass filter is passed through a parallel combination of lowpass and highpass filters. Similarly, the outputs of lowpass and highpass filters are downsampled by two, which provide a frequency band of *0 - 90 Hz* for lowpass filter and *90 - 180 Hz* for highpass filter, called as wavelet filter bank-two (WFB02). The same procedure is repeated until wavelet filter bank-four (WFB04), which provides a frequency band of *0 - 22.5 Hz* for lowpass filter and *22.5 – 45 Hz* for a highpass filter is achieved.

The architecture of a WFB plays a significant role while compressing an ECG signal. Various wavelet filter bank architectures are available for the ECG signal compression, namely decimator based wavelet filter bank, undecimator based wavelet filter bank architecture. The undecimator based wavelet filter bank architecture has the advantage of translation-invariance over decimator based wavelet filter bank. The requirement of a large number of registers, delay elements, adders, and multipliers is the significant drawback of the undecimator wavelet filter bank architecture. To reduce the number of delay elements, adders, and multipliers; in the present work, lowpass and highpass filters are realized using a linear phase structure realization. The undecimator wavelet filter bank architecture with linear phase structure realization is shown in Fig. 5.10. This work is published in [217].

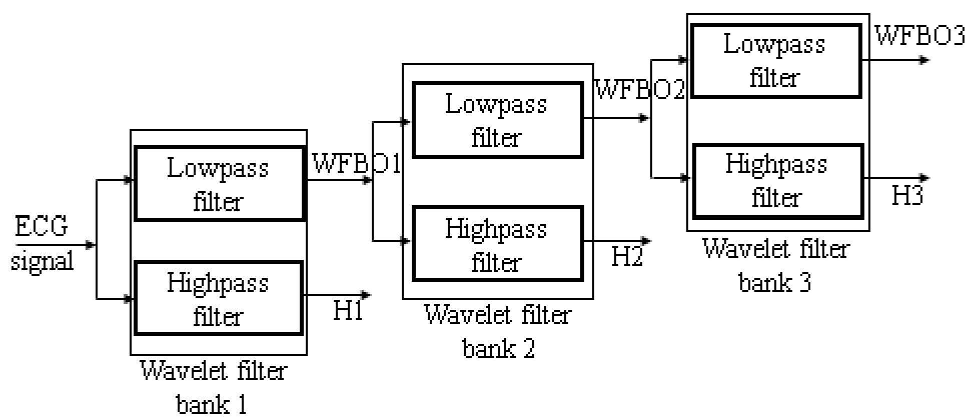

Fig. 5. 10 Compression of detected ECG signal using undecimator wavelet filter bank architecture

After wavelet decomposition, run-length encoding (RLE) technique is used for further data compression. In this method, the detected QRS-complexes are represented by '*1*' and '*0*' represents the rest of the data. This data is then compressed by replacing a '*0*' between two waves by the number of zeros between the waves.

The process of reconstruction of the transmitted ECG signal is as follows. The decomposed lowpass and highpass outputs say *L4* and *H4* are first upsampled by two and then passed through a parallel combination of lowpass and highpass filters. After that, the output of lowpass and highpass filters are added. This whole process is known as reconstruction. As shown in Fig. 5.11, this process is repeated three more times to reconstruct the original ECG signal.

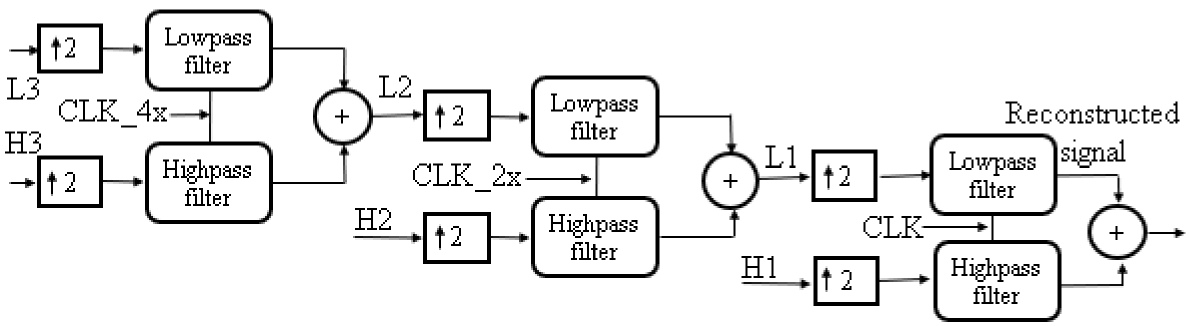

Fig. 5. 11 Reconstruction of transmitted ECG signal using undecimator wavelet filter bank architecture

5.2.5 Simulation Results and Performance Evaluation of the Proposed Biorthogonal 3.1 Wavelet Transform Based Lossless ECG Data Compression Technique

The performance of the proposed data compression algorithm is evaluated using CR. The proposed modified biorthogonal *3.1* wavelet transform and RLE based data compression algorithm achieve the highest CR of *16.271*. In the proposed biorthogonal *3.1* wavelet transform and RLE based data compression algorithm, all the detected QRS-complexes are represented using *1's*, and the rest of the data is represented using *0,* as shown in Fig. 5.12.

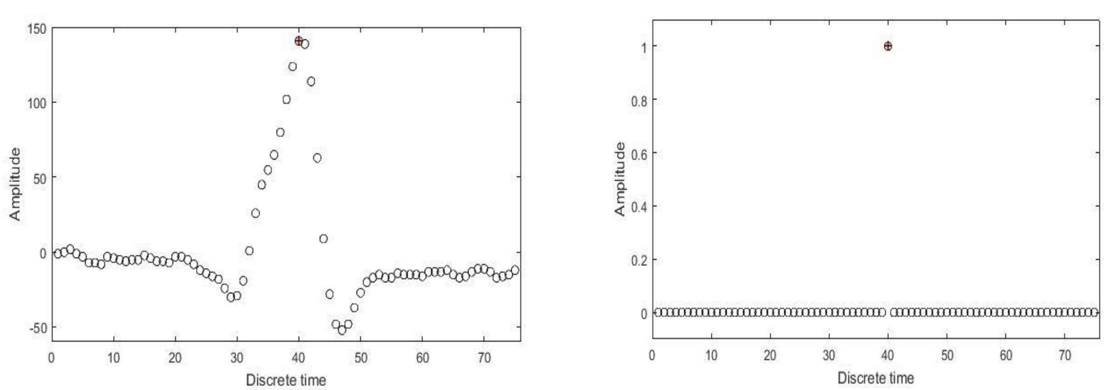

Fig. 5. 12 The output of the compressed ECG data

The performance of the proposed modified biorthogonal *3.1* wavelet transform and RLE based lossless data compression algorithm with the existing algorithms are shown in Table 5.13. Table 5.13 shows that the proposed modified biorthogonal *3.1* wavelet transform and RLE based compression algorithm results in a high CR of *16.271* compared to the existing data compression algorithms.

The output of the proposed modified biorthogonal *3.1* wavelet transform based data compression algorithm is shown in Fig. 5.13. Fig. 5.14 shows the reconstructed ECG signal.

Table 5. 13: Comparison of compression performance of proposed wavelet transform and RLE based technique with published works

Compression Method	Compression Ratio (CR)
Proposed modified biorthogonal 3.1 + RLE	**16.271**
Wavelet transform [11]	10.3
Quadratic spline wavelet transform [100]	1
Delta predictor [102]	2.38
Huffman coding/Adaptive predictor [103]	2.43
JQDC based [104]	2.28
Elgendi et al. [141]	4.5
Kumar et al. [153]	6.06
Huffman coding/simple predictor [158]	1.92
Fixed-length packaging [159]	2.25
Elgendi et al. [198]	6
Brajovic et al. [209]	6.2

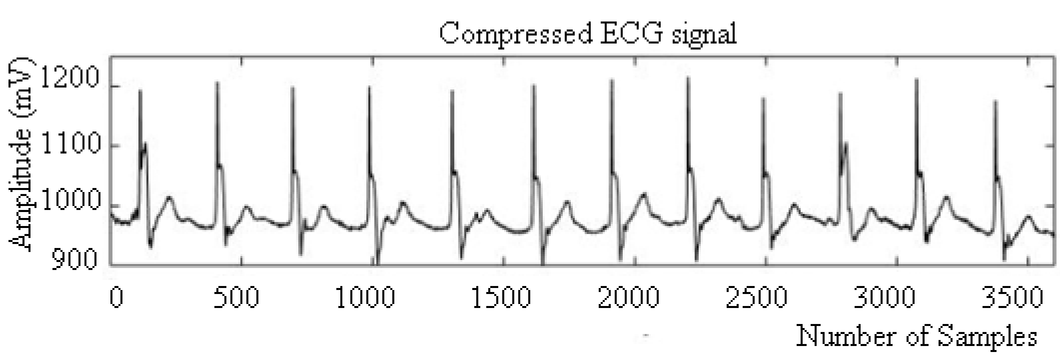

Fig. 5. 13 Output of the proposed modified biorthogonal 3.1 wavelet transform based data compression algorithm

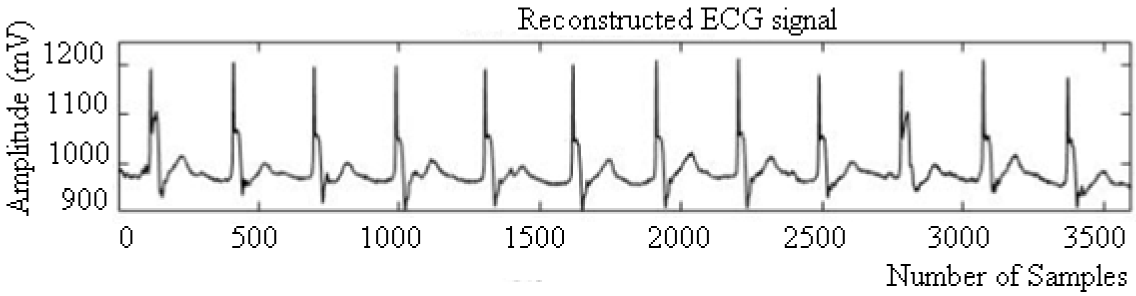

Fig. 5. 14 Reconstructed ECG signal

5.3 THREE-TAP WAVELET FILTER BANK BASED LOSSLESS ECG DATA COMPRESSION TECHNIQUE

Current literature uses two-band WFBs to analyze ECG signals [181, 182]. Poor resolution ($\Delta\omega = \pi/2$) of low and high-frequency bands during signal decomposition is the major drawback of two-band WFBs. In two-band WFBs, cascading and wavelet packet decomposition are required to improve the resolution of lower and higher frequency bands, respectively. Cascading increases the computation complexity of the design. To reduce the computation complexity, three-band WFBs with linear phase, less computational complexity, higher energy in high-frequency bands and better frequency resolution of ($\Delta\omega = \pi/3$) in lower and higher frequency bands are preferred over two-band WFBs [183].

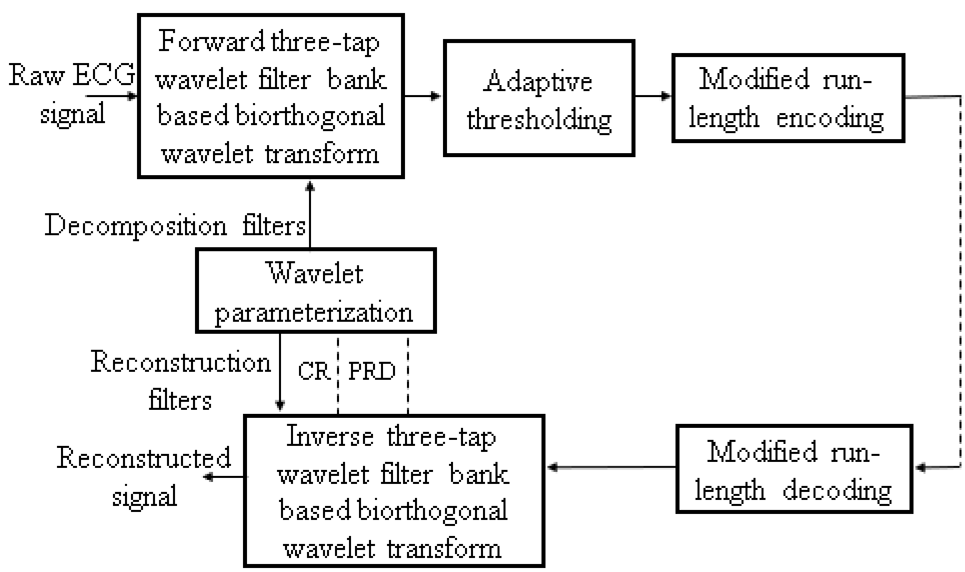

Fig. 5. 15 Proposed three-tap biorthogonal wavelet filter bank-based ECG compression Technique

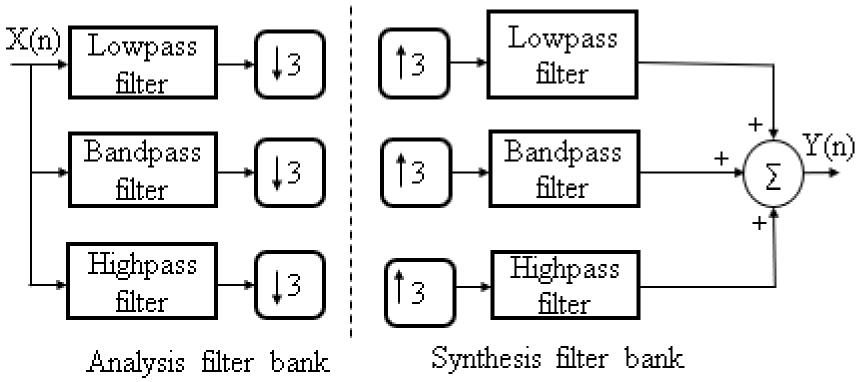

Fig. 5. 16 Proposed three-tap biorthogonal wavelet filter bank

Literature has supported the involvement of three-band time-frequency localized WFBs in numerous applications, namely, classification of EEG signals [184], digital watermarking [185], and image denoising [186]. The advantages of combined time-frequency localized three-band biorthogonal WFB motivates us to compress the ECG signal using three-band WFBs. The objective of this study is to develop a computer-aided ECG compression algorithm to use in the real systems by evaluating the performance of combine time-frequency localized three-band biorthogonal WFBs on different performance evaluation metrics like compression ratio, quality score, compression time, MSE, signal-to-noise ratio (SNR), maximum absolute error, and percentage root-mean-square difference (PRD). The signal processing flow of the proposed ECG compression technique, the corresponding three-tap wavelet filter bank, and decomposition of ECG signal up to the fourth level are shown in Fig. 5.15, Fig. 5.16 and Fig. 5.17, respectively.

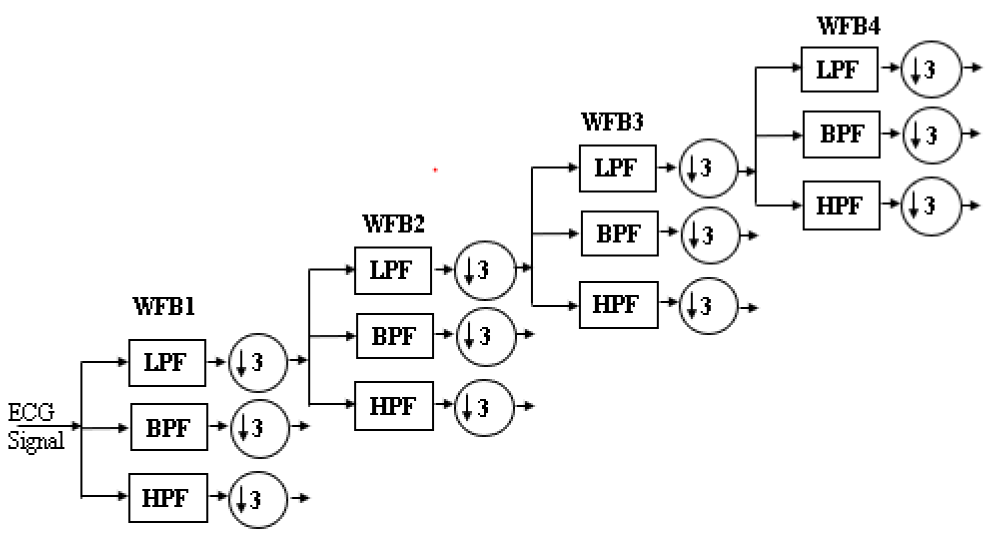

Fig. 5. 17 Decomposition of ECG signal up to the fourth level

The process used to compress the ECG signal is the same as used in [187] with some modifications proposed in the work. The modifications are as follows: digitized ECG signal is decomposed into four subbands using a novel combine time-frequency localized three-band biorthogonal WFB. The transfer function of lowpass, bandpass and highpass filters, respectively, are obtained as shown in Eq. (5.5), Eq. (5.6), and Eq. (5.7), respectively.

$$H_0(z) = -0.0074 + 0.4559z^{-1} + 0.7292z^{-2} + 0.4559z^{-3} - 0.0074z^{-4} \tag{5.5}$$

$$H_1(z) = -0.0178 - 0.3588z^{-1} - 0.3558z^{-3} - 0.0178z^{-4} \tag{5.6}$$

$$H_2(z) = 0.0098 - 0.4125z^{-1} + 0.1179z^{-2} - 0.4125z^{-3} + 0.0098z^{-4} \tag{5.7}$$

The decomposed ECG signal is adaptively thresholded, and the absolute values greater than the threshold are considered as digital high (logic high and represented as “1”) and all the other remaining values are considered as digital low (logic low and represented as “0”). The digitized data is then compressed using run-length encoding Technique.

5.3.1 Simulation Results and Performance Evaluation of the Proposed Three-Tap Wavelet Filter Bank Based Lossless ECG Data Compression Technique

Compression rate (CR), maximum absolute error (MAE), quality score (QS), root mean square error (RMSE), compression time and percentage root mean square difference (PRD) are the parameters used to demonstrate the validity of the novel approach.

Table 5. 14: Performance evaluation of the proposed approach

Performance Parameters	Three-Tap WFB	Kumar et al. [210]
Average CR	**22.61**	18.89
Average QS	**18841**	20.47
Average Ct (ms)	**327.29**	494.22
Average MAE	**0.013**	0.0002
Average PRD	**0.0015**	NA
Average RMSE	**0.0016**	0.029

Performance results of the proposed three-tap WFB based ECG compression approach are summarized in Table 5.14, where the proposed three-tap WFB based approach achieves a better result compared to the existing techniques in the literature [210]. The proposed design achieves an average CR, average QS, respectively, of *22.61* and *18841*. Also, the proposed design has an average Ct, average MAE, average RMSE and PRD, respectively of, *327.29ms*, *0.013*, *0.0016*, and *0.0015*.

The output of the proposed combine time-frequency localized three-band biorthogonal WFBs based ECG compression approach is shown in Fig. 5.18. Fig. 5.18 (a) is an input ECG signal having a sampling frequency of *100 Hz*. Fig. 5.18 (b) represents the reconstructed ECG signal and Fig. 5.18 (c) represents the error between the original ECG signal and the compressed ECG signal.

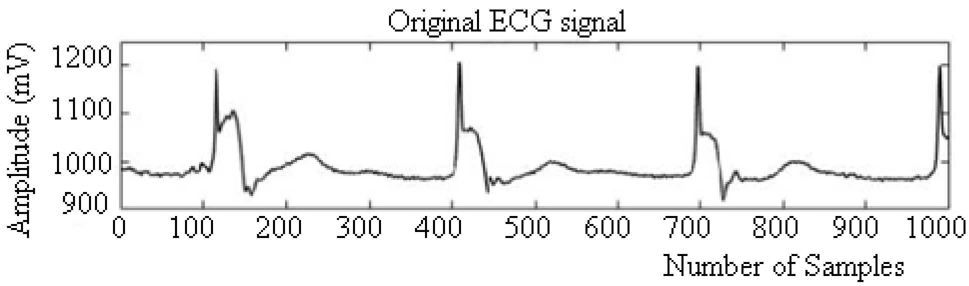

(a)

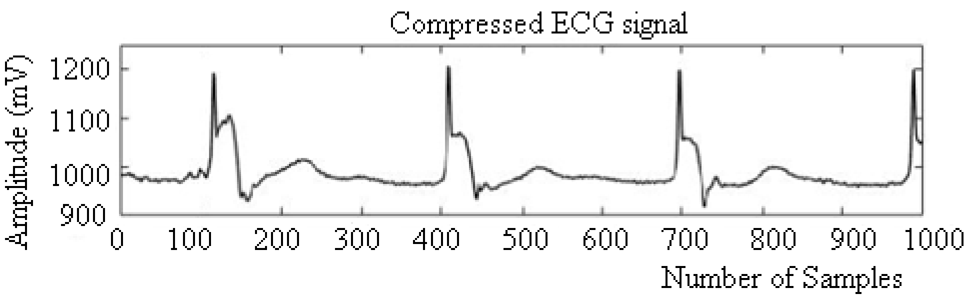

(b)

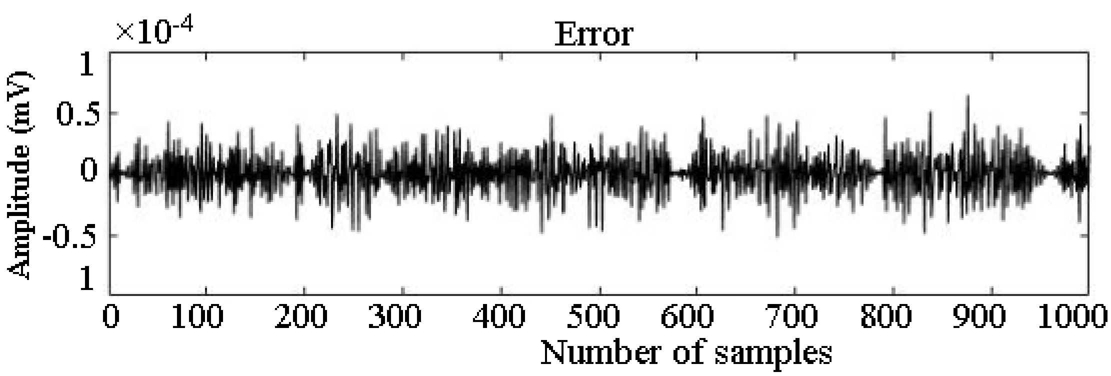

(c)

Fig. 5. 18 Original ECG signal, (b) compressed ECG signal and (c) error

5.4 SUMMARY

In this work, *DER* is used to evaluate the accuracy, *Se* is used to evaluate the ability to detect true waves of the proposed algorithm, and *+P* is used to evaluate the ability to differentiate between true and false waves of the proposed algorithm. Unlike previous articles in the literature [11, 70, 76, 104, 102, 103, 158, 159, 211], in this work, the performance of ECG signal detection algorithms is mainly assessed for detection accuracy and circuit complexity. In the available literature, some parameters like efficiency, parameter choice, and robustness to noise are not considered while evaluating the performance of an ECG detector. There are many algorithms described in the literature that show unusually high detection performance with the total number of detected QRS-complexes but are not reliable as they cannot detect ECG signals with noise.

The use of adaptive slope prediction threshold values in the ECG detector showed excellent performance on different databases, achieving sensitivity and specificity of *99.94%* and *99.92%* respectively on *96542* annotated beats, and an error of *0.0013 %*.

Also, the use of two different techniques for ECG signal denoising, ECG signal detection, and data compression results in higher overall system complexity. Hence, a combine approach for ECG signal denoising, ECG signal detection, and data compression is proposed. Proposed is a combine time-frequency localized three-tap biorthogonal WFB, adaptive thresholding and modified RLE based method for ECG compression. According to extensive experimental simulations, the proposed approach gives an excellent performance. The proposed algorithm gains a high CR compare to other existing algorithms. A combine time-frequency localized three-tap modified biorthogonal *3.1* WFB based lossless data compression achieves a high CR of *22.61*. To best of our knowledge, this is the first of its kind combine ECG denoising, ECG detection, lossless data compression algorithm for cardiac pacemaker system.

CHAPTER 6

FPGA IMPLEMENTATION OF COMBINE ECG SIGNAL DENOISING, PEAK DETECTION TECHNIQUE FOR CARDIAC PACEMAKER SYSTEMS

Different medical research fields are marking their importance in the development of cardiovascular devices for monitoring and regulating symptoms of heart diseases [212]. Wearable ECG monitoring devices are going to become a norm, and the research has taken the nucleus of every medical research study on CVDs. Medical practitioners are widely open in accepting the usage of wearable ECG devices for biosignal acquisitions, as a better patient examining and supervising device in real-time. Medical institutions require an automated cardiac function assessment to improve conventional cardiovascular analysis. Holter devices are incapable of providing real-time diagnose and information of arrhythmia, thus limiting their usage in critical conditions. Hence, there is an immediate requirement to develop energy-efficient ECG detection algorithms for implantable and portable cardiac devices. Block diagram of an implantable/portable cardiac device is represented in Fig. 6.1.

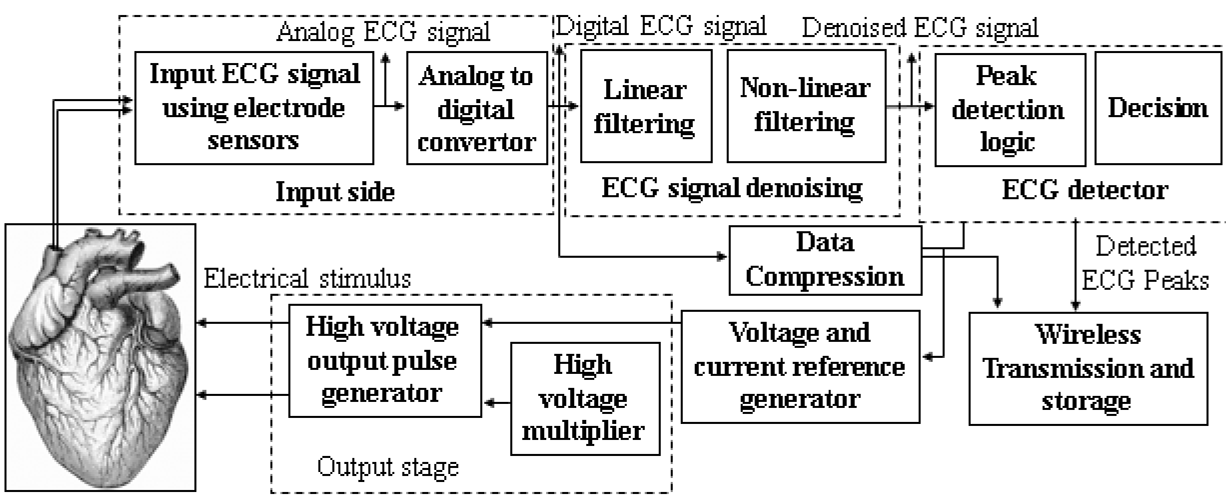

Fig. 6.1 Block diagram representation of the implantable/portable cardiac device

Periodic and administered electric stimulus made the implantable device a reality in today's globally emerging world of portable and implantable cardiac devices. The present implantable and portable cardiac pacemakers are bulky, and expensive so not within reach of many. Thus, to become a real lifesaver, portable, and implantable cardiac pacemaker needs to be cheap and yet reliable. The new archetype of these portable devices requires higher circuit densities and technological breakthroughs so that all the lacunas like single-chamber, asynchronous, non-programmable pacing can be left behind. Technology adds more flavor and variations in the device with benefits like dual-chamber multi-programmability for enhanced efficiency and reliability. Such newer and advanced devices have amplified the storage of important medical data for a much reliable and accurate diagnosis. The contemporary pacing system has three integral components: a pulse generator, lead, and programmer as part of its device architecture. The pulse generator provides a real pulse to the device and contains energy management system. With complex circuits sensing electrical activity of the heart, which composes and generates suitable patterned response leading to stimulus and a transceiver. The channel from the generator to the heart is connected through a thin insulated wire responsible for transferring and sending indelible cardiac signals back to the generator.

Various literature discusses power-efficient ECG signal detection techniques. An extensive review of the ECG detection techniques presented till date is available in [61, 63-65, 117]. Different research groups introduced various ECG signal detection techniques based on time-domain [110, 213-214], ECG morphology (neural network) [26, 62, 215], time-frequency (Hilbert transform, wavelet transform) [216-220], and some combined algorithms (Bandpass filtering and wavelet transform) [11]. The first real-time ECG signal detection technique presented by J. Pan [20] was based on the time-domain analysis. In this technique, high order bandpass filter and thresholding technique are utilized to detect various waves of an ECG signal. The major difficulty encountered with the time domain-based ECG signal detection techniques is that, if these techniques are implemented using finite impulse response filters, computational delay and ringing effects are caused due to the long impulse response.

On the other hand, infinite impulse response filter can cause non-linear phase distortion. The issues mentioned above are addressed using zero-phase bidirectional filters. However, the problem of tuning the bandwidth of the filter remains an issue. In order to reject the time-varying noises and retain the ECG signal features of the same frequency range, adaptive filters have been utilized in [221-223]. These adaptive filtering techniques require models of different noises to generate reference signals. The need for reference signals increases the computational complexity of the algorithm. The other disadvantages of adaptive algorithms are low convergence speed and fixed step size.

Further, ECG signal morphology and combined ECG signal detection techniques have been presented to achieve high signal detection accuracy. Implementing these techniques on the integrated circuit is too complicated. Time-frequency analysis techniques, namely, Hilbert transform, empirical mode decomposition, and its modified versions, wavelet transform, are also used to analyze ECG signals. As for ECG signal detection, the performance of wavelet transform technique is far superior to Hilbert transform or empirical mode decomposition in terms of time-frequency resolution and thus can provide better results.

In this chapter, a biorthogonal wavelet transform based modified wavelet filter bank (WFB) [210] to suppress the various low, and high-frequency noises present in the ECG signal is implemented on field-programmable gate array (FPGA) platform. Quantitative measures, namely, Shannon entropy, uncertainty, cross-correlation, relative entropy, mutual information, and distribution error, are considered to select the optimal base wavelet.

Steps involved in ECG signal denoising using wavelet transform are as follows:

1. The approximation and the detail coefficients are obtained using multi-level wavelet decomposition.
2. Using a discrete wavelet transform, the ECG signal was split into a lowpass sub-band (approximation level) and highpass sub-band (detail level). Further decomposing the approximation sub-band at multiple scales results in a fine-scale analysis.
3. A suitable thresholding technique is selected by analyzing the detailed coefficients to reconstruct the ECG signal.

After denoising the ECG signal using biorthogonal wavelet transform, an adaptive slope prediction criterion is utilized to check the location of different waves present in the ECG signal. The proposed ECG denoising and ECG signal detection technique is implemented using System Verilog HDL and synthesized in FPGA on Xilinx® Virtex®-7 platform.

6.1 FPGA IMPLEMENTATION OF AN ECG SIGNAL DETECTION TECHNIQUE

The input ECG signals are recorded using iworx® IX-TA-*220* recorder. The ECG data is then digitized at *360 Hz* sampling frequency with *11*-bit resolution over a *10-mV* range. Various other

ECG databases available on *physionet.org* [224] are also used to evaluate the performance of the proposed Technique. Based on different physiological conditions, input ECG data are then classified into normal ECG signal, ECG signal with right bundle branch block, ECG signal with left bundle branch block, ECG signal with premature atrial contraction and ECG signal with premature ventricular contraction [210]. Different white Gaussian noise signals are generated and added to the input ECG signal. Adding different Gaussian noise signals alters the input SNR of the ECG signal, thus allowing to test the proposed Technique for critical cases. Noisy ECG signals are then decomposed using biorthogonal wavelet filter bank to suppress the noises. The procedure for selecting wavelet and wavelet filter bank architecture are discussed below.

6.2 SELECTION OF WAVELET TRANSFORM

Wavelets developed in the recent past have paved the way for applying a wavelet transform to biomedical signal analysis. The study so far in the literature put forward a clear perspective for selecting the best-suited base wavelet for functional signal processing.

Table 6. 1: Classification of wavelets based on their properties

Wavelet Family	Compact Support	Regularity	Symmetry	Number of Vanishing Moments
Haar	Yes	No	Yes	1
Daubechies	Yes	No	No	N
Coiflets	Yes	No	No	2N-1
Symlets	Yes	No	No	N
Biorthogonal / reverse biorthogonal	Yes	Yes	Yes	N_r
Discrete Meyer wavelet	No	No	Yes	NA

*: NA: Not Available, N_r: Reconstruction Order

The fundamental properties support only the qualitative acceptance and fitment for a specific application, thus making a study of quantitative measures in the selection of base wavelet a much-required approach. The present visual differentiation and contrast studies are not sufficient to accurately match the shape of a signal to that of a base wavelet transform, thus establishing an accurate quantitative matching is much required. The selection criteria of a wavelet suitable for ECG signal analysis made by considering important properties like symmetry, regularity, orthogonality, compact support, a support width, filter length, the shape of wavelet transform and number of vanishing moments. Classification of wavelet transforms on their main properties are listed in Table 6.1. From Table 6.1, it is clear that biorthogonal wavelet transform satisfies most of the properties required and selected for analyzing ECG signals.

Mathematically, energy, Shannon entropy, cross-correlation, minimum description length, mutual information, and relative entropy are the quantitative measures used to evaluate the performance of base wavelet for ECG signal denoising [224].

6.2.1 Energy and Shannon Entropy:

Features of a signal are characterized using the energy content of a signal. The energy content (E_{energy}) of a signal *s(t)* is calculated using wavelet coefficients is given by Eq. (6.1).

$$E_{energy}s(t)=\sum_{k=1}^{M}\left|wt(j,k)\right|^{2} \tag{6.1}$$

Here, *M* stands for the number of wavelet coefficients and *wt(j,k)* stands for the wavelet coefficients.

Shannon entropy ($E_{entropy}s(t)$) is a measure of uncertainty associated with random variables. Hence, Shannon entropy helps to describe the energy distribution of wavelet coefficients, which is calculated using Eq. (6.2).

$$E_{entropy}s(t)=-\sum_{k=1}^{M}P_k.\log_2 P_k \tag{6.2}$$

Here, P_k stands for the energy probability distribution of wavelet coefficients and is calculated using Eq. (6.3).

$$P_k=\frac{\left|wt(j,k)\right|^{2}}{E_{energy}s(t)} \tag{6.3}$$

With $\sum_{k=1}^{M} P_k = 1$, and if $P_k = 0$, then $P_k log_2 P_k = 0$. Then, entropy of the wavelet coefficients are bounded in the range $0 \leq E_{entropy} s(t) \leq log_2 M$. The base wavelet that satisfies the condition of maximum energy, minimum Shannon entropy should be the appropriate wavelet transform for ECG signal denoising.

6.2.2 Mutual Information and Relative Entropy:

The amount of information that signal '*S*' contains about signal '*X*' is measured using mutual information (I_{mutual}) and is calculated using Eq. (6.4)

$$I_{mutual} = \sum_{s \in S} \sum_{x \in X} p(s,x) \log p(s,x) - \sum_{s \in S} \sum_{x \in X} p(s,x) \log[p(s)p(x)] \tag{6.4}$$

The average mutual information between two signals *S* and *X* can be calculated by subtracting the entropy of pair from the sum of two self-entropies. The amount of shared information contained by signals *S* and *X*, respectively, in the wavelet thresholding, is represented by mutual information.

The distance between the probability distributions of two signals *S* and *X* is measured using relative entropy ($E_{relative}$). Relative entropy is zero only when the probability distributions of both the signals are equal.

$$E_{relative} = D(S \| X) = \sum_{s \in S} p(s) \log\left(\frac{p(s)}{p(x)}\right) \tag{6.5}$$

6.2.3 Cross-correlation:

Cross-correlation (r) between the ECG signal and wavelet filter is computed as follows:

$$r = \frac{\sum_i \left[\left(s(i) - ms\right) * \left(x(i-d) - mx\right)\right]}{\sqrt{\sum_i \left(s(i) - ms\right)^2} \sqrt{\sum_i \left(x(i-d) - mx\right)^2}} \tag{6.6}$$

Here, *ms* is mean of signal *S*, and *mx* is mean of signal *X*, *d* is the delay. Mathematically, *ms* and *mx* are expressed using Eq. (6.7) and Eq. (6.7), respectively.

$$ms = \frac{1}{n} \sum_{i=1}^{n} s(i) \tag{6.7}$$

$$mx = \frac{1}{n}\sum_{i=1}^{n} x(i) \tag{6.8}$$

Base wavelet with maximum cross correlation coefficients is selected in the proposed work.

6.2.4 Minimum Description Length (MDL):

Optimal base wavelet is the one which provides the shortest description of ECG data and base wavelet. Mathematically, MDL is expressed using Eq. (6.9).

$$\begin{gathered} MDL(p,m) = \min\left\{\frac{3}{2} p \log M + \frac{M}{2}\log\left\| a_m - a_m^{(p)} \right\|\right\}; \\ 0 \le p < M; 1 \le m < N \end{gathered} \tag{6.9}$$

Mathematically, a_m and $a_m^{(p)}$ are expressed using relation in Eq. (6.10).

$$\begin{aligned} a_m &= W_m f \\ a_m &= \Theta^{(p)} a_m \end{aligned} \tag{6.10}$$

Here W_m is the wavelet filter of length m, M is the signal length, N is the count of wavelet filter used, $\Theta^{(p)}$ is a thresholding operation parameter, and f is a discrete model which is mathematically expressed using Eq. (6.11).

$$f = a + g \tag{6.11}$$

Here a is an unknown true signal to be estimated, g is noise.

6.3 SELECTION OF WAVELET FILTER BANK ARCHITECTURE

Various wavelet filter bank architectures for different signal processing applications have been presented in the existing literature. For a given precision, VLSI implementation of a wavelet filter bank architectures requires minimization of area, power, and memory. A conventional wavelet filter bank architecture is shown in Fig. 6.2. The performance of a conventional wavelet filter bank can be improved using undecimator and decimator-based wavelet filter banks [67, 69]. Although the use of undecimator wavelet filter bank architecture provides the benefit of translation-invariance, the requirement of a large number of register and a constant clock are its major drawbacks. The limitations posed by an undecimator wavelet filter bank architecture are overcome by using decimator wavelet filter bank architecture. However, the use of the parallel combination of lowpass and highpass filters to decompose signal at each level of decomposition requires nearly the same amount of hardware. Hence, a modified wavelet filter bank architecture to suppress different noises present in the ECG signal is required.

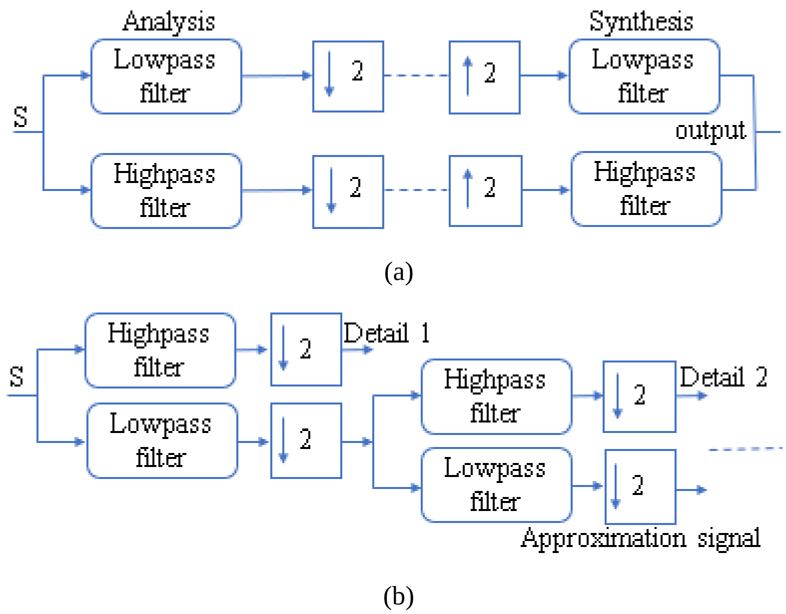

Fig. 6.2 Signal decomposition using discrete wavelet transform (DWT), (a) 1-D, 1-level decomposition and reconstruction using DWT, (b) 1-D, m-level decomposition using DWT

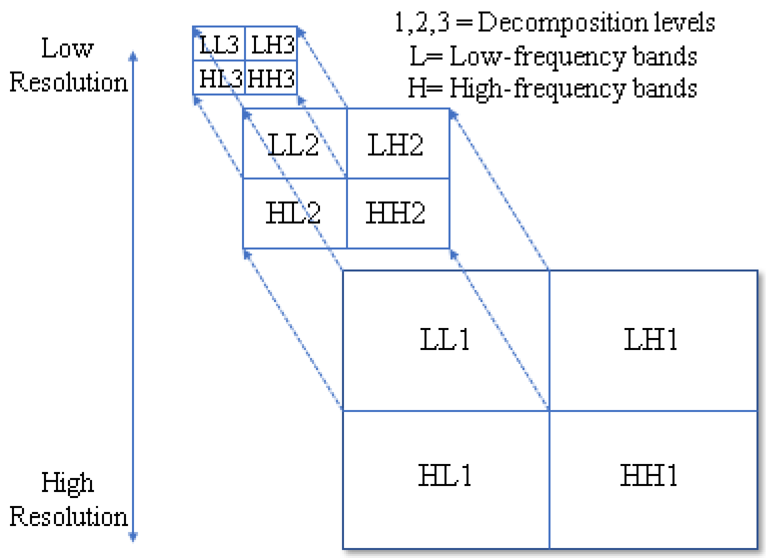

Fig. 6.3 Demand-based wavelet filter bank architecture

A demand-based wavelet filter bank architecture that decomposes the noisy ECG signal using only three lowpass filters is proposed in this present work. Fig. 6.3 represents a demand-based wavelet filter bank architecture. ECG signal '*S'* is first filtered with a special lowpass filter to yield lowpass sub-bands. Half of the samples are discarded after filtering as per the Nyquist criterion. A filter which typically has a small number of coefficients results in a better computational performance.

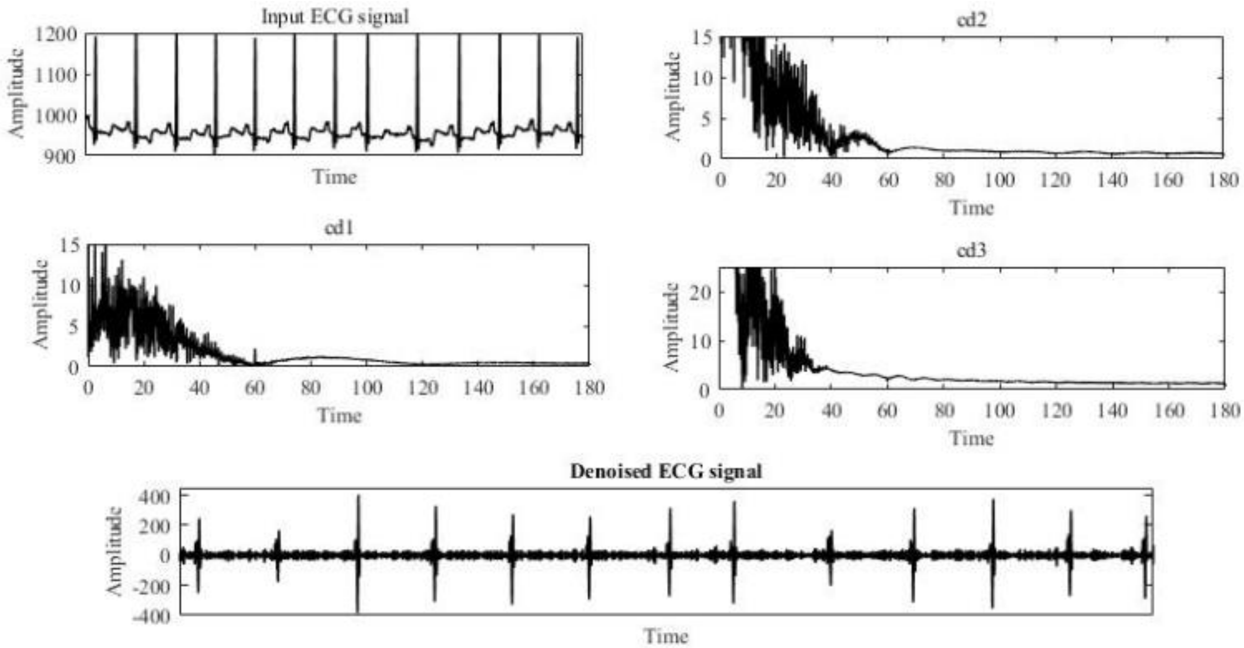

Fig. 6.4 Frequency response of ECG signal for different wavelet decompositions

The filter can reconstruct the sub-bands while canceling any aliasing that occurs due to down-sampling. The process repeats itself for the next two decomposition levels. Reason for modifying the wavelet filter bank architecture and selecting the third level of wavelet decomposition is as follows. As per the existing literature, the ECG signal has a frequency range of *0.05 -150* Hz and out of which QRS-complex has a frequency range of *5 - 32* Hz [166]. The proposed wavelet filter bank provides a frequency range of *0 - 45* Hz, which is similar to the frequency range of the QRS-complex, as shown in Fig. 6.4. Also, the proposed wavelet filter bank architecture decreases the hardware complexity by reducing the count of highpass filters from four to zero.

6.4 ECG SIGNAL DETECTION

Many algorithms are presented in the literature to detect all the waves present in an ECG signal. Some of the ECG signal detection techniques are thresholding based, neural network, HMM, matched filter, zero- crossing, multiplication of backward difference, syntactic method, and singularity-based approach. Hence, finding a robust algorithm for ECG signal detection is difficult as most of the ECG signal detection methods are not universally accepted. Hence, continuous efforts are made by various researchers to improve the detection capabilities of the vital features of an ECG signal. The use of thresholding approaches for ECG wave detection is preferred due to the following reasons: simple, numerically efficient for the detection of different waves present in an ECG, minimum memory storage, and provide a high detection accuracy. The present work utilizes an adaptive slope prediction criterion to check the location of different waves present in the ECG signal. Similar slope predication criterion to detect different waves present in an ECG signal is used in [210]. In this work, a few changes have been made to improve the signal detection accuracy. If the proposed Technique enables us to find a QRS-complex in *1000 ms*, that means the interval between two consecutive R-waves is too large. A large R-R wave interval represents irregularity in the heart's functionality. Hence, the entire region of that time interval is presented (displayed) for diagnosis to the physician or cardiologist.

6.5 SIMULATION AND RESULTS

The effectiveness of the biorthogonal *3.1* wavelet transform and adaptive slope predication criterion-based ECG signal detection Technique is verified by evaluating its performance on different ECG signals (ECG signals of different duration, ECG signals of a different physiological condition, etc.). Firstly, the biorthogonal *3.1* wavelet transform is selected based on qualitative and quantitative measures. Then, wavelet decomposition level and wavelet filter bank architecture are selected to denoise the various artifacts present in an ECG. The metrics under consideration are hardware complexity, denoising capabilities, power consumption, and area. After removing the various noises, an adaptive slope prediction criterion is utilized to detect the location of different waves of an ECG signal. Finally, the performance of the proposed technique is compared with the existing literature. For a fair comparison, the performance of the existing ECG signal detection techniques is calculated using a similar environment.

6.5.1 Input ECG Data

Input ECG data from *physionet* [21] and real-time ECG data recorded from iworx® IX-TA-*220* are utilized to test the performance of the proposed technique. *Physionet.org* provided a collection of physiological signals which are free for research. motion artifact contaminated ECG database, MIT-BIH arrhythmia database, and fantasia database from *Physionet.org* are used to evaluate the performance of the proposed technique. Classification of different ECG data from the MIT-BIH arrhythmia database is discussed in Table 6.2. in Table 6.2 'M' indicates the male subject, and 'F' indicates female subjects.

Table 6. 2: Classification of ECG data from the MIT-BIH arrhythmia database

Class of Input Data	Record (MIT-BIH)	Symbolic Representation	Subject and Age	Beat Count
Normal ECG	100, 103, 119, 200, 209, 212, 221	N	(M, 69), (F, 51), (M, 64), (M, 62), (F, 32), (M, 83), (F, 51)	75016
Ventricular premature contraction	119, 200, 221, 233	V	(M, 64), (M, 62), (F, 51), (M, 64),	7130
Atrial premature beat	202, 232	A	(M, 68), (F, 76)	2546
Left bundle branch block	109, 111, 207, 214	L	(F, 64), (F, 47), (F, 84), (M, 53)	8075
Right bundle branch block	118, 124, 212, 231	R	(M, 69), (M, 77), (F, 32), (F, 72)	7259
Paced beat	107, 217	P	(M, 63), (M, 65)	7028
Fusion of paced and normal beat	217	F	(M, 65)	982

The segregation above is done to test whether the proposed Technique is capable of distinguishing between normal and arrhythmic ECG signal, low-quality and high-quality ECG signal and normal and paced ECG signal.

6.5.2 ECG Signal Denoising

Fig. 6.5 shows the performance of wavelet transforms using quantitative measures. Based on the quantitative measures, biorthogonal 3.1 wavelet transform is selected for the present work as it has maximum energy, minimum Shannon entropy, highest energy-to-entropy ratio, large mutual information, high relative entropy, and high normalized correlation coefficient. Further, the denoising capabilities of proposed demand-based biorthogonal *3.1* wavelets transform-based ECG denoising technique is evaluated using signal-to-noise ratio (SNR), percent root-mean-square difference (PRD), and mean square error (MSE). Each of these metrics looks for the different qualitative and quantitative facets of the denoised signals with the help of the clean and noisy ECG. Ideally, high SNR value and low PRD/MSE values signify the better denoising capabilities.

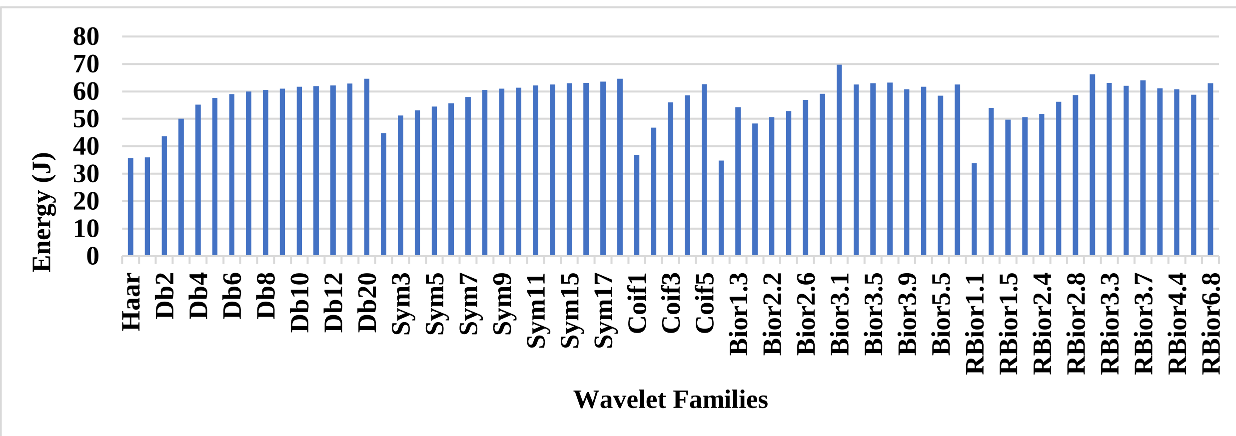

(a)

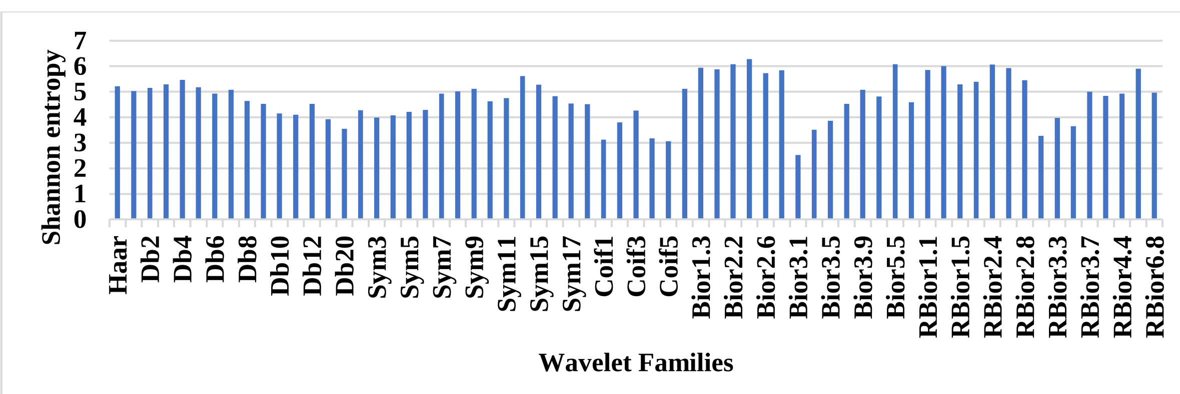

(b)

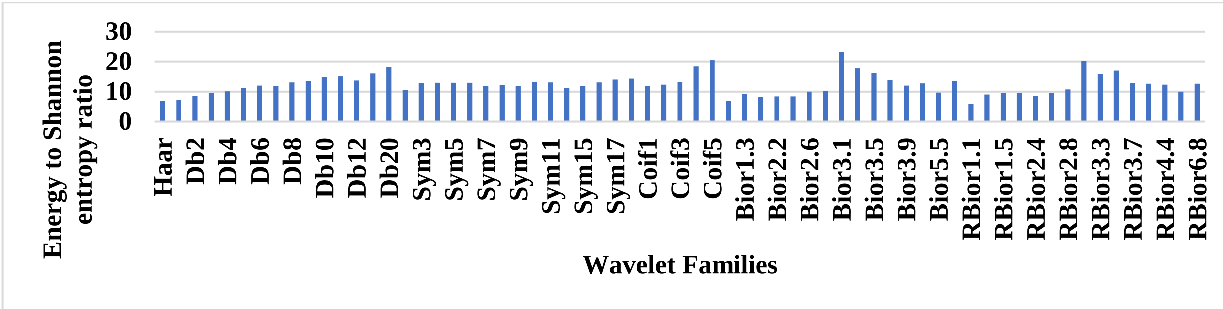

(c)

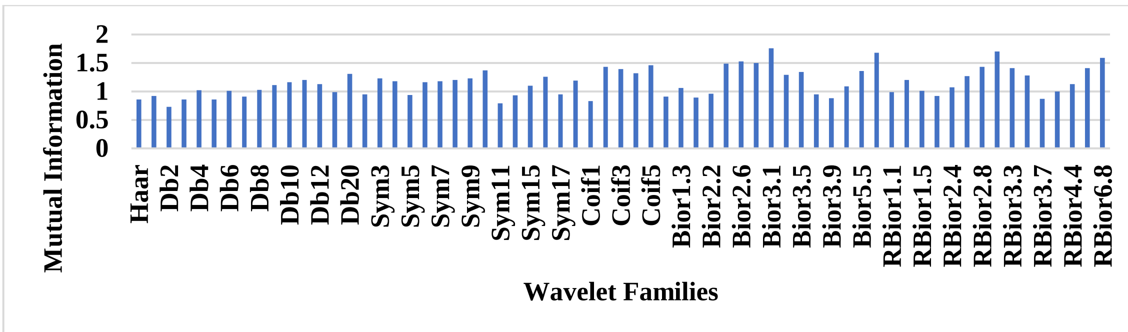

(d)

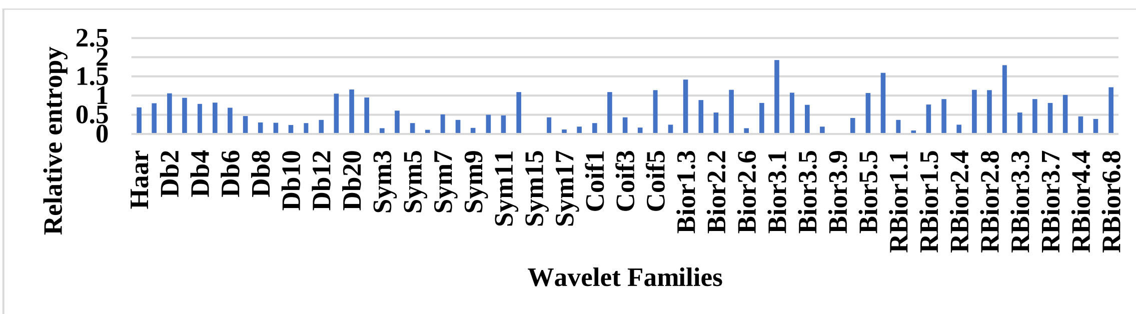

(e)

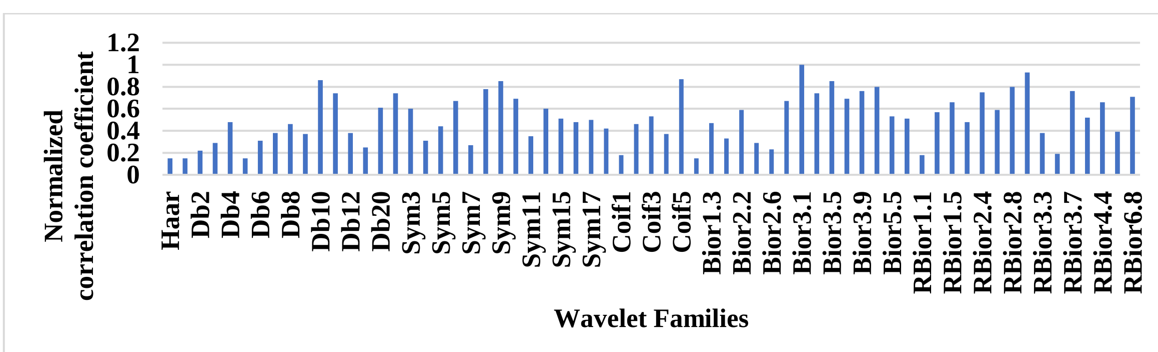

(f)

Fig. 6.5 Performace of different wavelet transform on quantitative measures (a) energy, (b) Shannon entropy, (c) energy to Shannon entropy ratio, (d) mutual information, (e) relative entropy, and (f) normalized correlation coefficient

The results of the proposed method are compared with the four existing wavelet transform based ECG denoising methods [66, 70, 99, 226]. The denoising results of the techniques as mentioned earlier are compared for two separate ECG records from motion artifact contaminated ECG database at four different input SNR noise levels. Through close inspection, it is found that the proposed method generates much smoother denoised results and retains the critical morphology of ECG compared to existing approaches. Denoising performance of the various ECG denoising methods and their comparison with the proposed method for different input SNR is shown in Table 6.3.

Table 6. 3: Comparison of denoising performance of the proposed ECG denoising methods with the existing techniques for different values of input SNR

References		**[27]**	**[28]**	**[35]**	**[36]**	**Proposed**
Input SNR (-10 dB)	Average SNR (dB)	27.702	27.974	28.256	27.942	38.117
	Average PRD (%)	22.19	21.71	24.11	23.85	12.08
	Average MSE	0.120	0.113	0.092	0.102	0.036
Input SNR (-5 dB)	Average SNR (dB)	28.111	29.108	30.280	29.353	40.964
	Average PRD (%)	18.38	19.02	18.09	17.52	11.94
	Average MSE	0.100	0.098	0.089	0.103	0.014
Input SNR (5 dB)	Average SNR (dB)	30.372	31.979	32.120	32.312	47.592
	Average PRD (%)	16.27	15.93	13.99	13.44	11.87
	Average MSE	0.052	0.065	0.048	0.075	0.008
Input SNR (10 dB)	Average SNR (dB)	32.516	33.052	33.989	33.693	54.990
	Average PRD (%)	13.59	13.41	13.04	12.99	11.41
	Average MSE	0.011	0.027	0.021	0.041	0.008

A close inspection of Table 6.3 shows that the proposed method performs better when compared to the other ECG signal denoising methods. The proposed ECG signal denoising Technique achieves the highest SNR of *54.990 dB* and lowest PRD(%)/MSE of *11.41 %* and *0.008*, respectively.

6.5.3 ECG Signal Detection

Detection accuracy (D_{Acc}), sensitivity (Se), detection error (D_{Err}), and time consumption (TC) are the metrics used to evaluate the performance of the adaptive slope predication criterion-based ECG signal detector. Performance of the proposed adaptive slope prediction-based ECG signal detector for different ECG databases is shown in Table 6.4. From Table 6.4, it has been observed that the proposed ECG signal detector achieves the highest average detection accuracy, average sensitivity with a lower average detection error, and time consumption.

Table 6. 4: Detection performance of the proposed adaptive slope prediction criterion-based ECG detector

Class of ECG Data	**Total Beats**	**D_{Acc} (%)**	**Se (%)**	**D_{Err} (%)**	**Average TC (Seconds/ record)**
Normal ECG	75016	99.93	99.95	0.001	1.15
Ventricular premature contraction	7130	99.88	99.91	0.002	1.25
Atrial premature beat	2546	99.89	99.82	0.003	1.18
Left bundle branch block	8075	99.86	99.86	0.002	1.10
Right bundle branch block	7259	99.92	99.92	0.001	1.07
Paced beat	7028	99.93	99.93	0.006	1.28
Fusion of paced and normal beat	982	99.90	99.92	0.004	1.05

Performance comparison between the existing methods and the proposed biorthogonal 3.1 wavelet transform and an adaptive slope predication criterion-based ECG signal detection method is shown in Table 6.5. An inspection of Table 6.5 shows that the proposed ECG signal detector performs better as compared to the existing ECG signal detectors. The proposed ECG signal detector can differentiate between normal ECG, paced ECG, arrhythmic ECG, low-quality ECG, and high-quality ECG with higher detection accuracy ranging from *99.86%* to *99.93%*.

Table 6. 5: Performance comparison between the existing and the proposed ECG detection method

Performance Metrics	**References**				
	[28]	**[32]**	**[35]**	**[36]**	**Proposed**
Average D_{Acc} (%)	99.38	99.86	99.77	99.70	99.90
Average Se (%)	99.89	99.80	99.60	99.31	99.90
Average D_{Err} (%)	0.736	0.34	0.006	0.009	0.002
Average TC (Sec./record)	1.35	1.28	1.21	1.19	1.15

6.6 FPGA IMPLEMENTATION

The proposed ECG signal detector using biorthogonal *3.1* wavelet transform and an adaptive slope prediction technique has four major blocks, namely, wavelet filter bank, thresholding, comparator, and a counter. System Verilog hardware description language and Xilinx® Vivado® design suit are used to implement the proposed technique and complete its functional verification. Area, power, and delay requirements of the proposed technique are calculated by implementing the detector on the Xilinx® Virtex®-7 FPGA. Top-level register-transfer level (RTL) view of the proposed wavelet filter bank architecture and complete ECG detection Technique are shown in Fig. 6.6.

Initially, *16-bit* ECG signal, clock, and reset are applied as an input to the wavelet filter bank. Threshold function is applied as one of the inputs to the comparator circuit is also of *16-bit*. The output of the proposed detector on a real-time ECG data of one-minute is shown in Fig. 6.7. Area, power, and delay are the measures used to compute the computational complexity of the proposed detector. Area requirements of the proposed wavelet filter bank architecture are reduced by using a demand-based wavelet filter bank architecture. Further, LWDF based digital filter structure realization reduces the count of multipliers and delay elements by *75%* and *80%*, respectively.

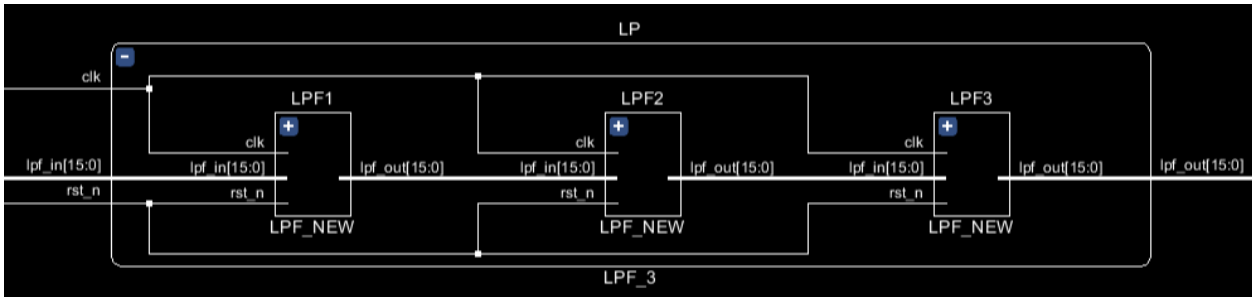

(a)

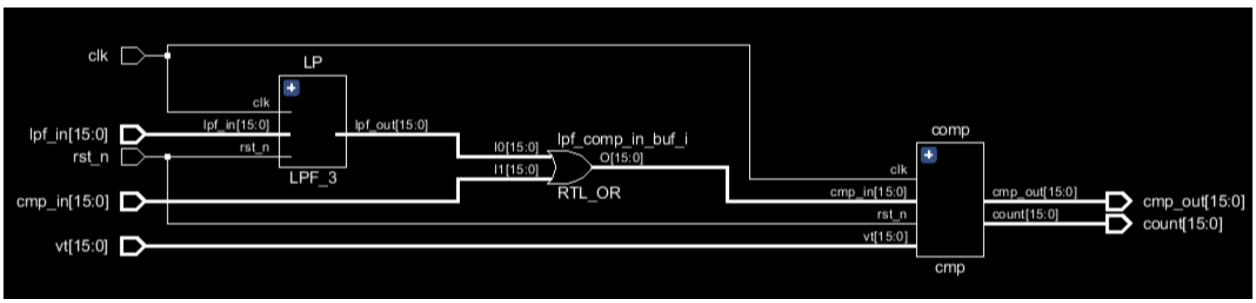

(b)

Fig. 6. 6 RTL top view of proposed ECG detector. (a) wavelet filter bank, (b) complete ECG detection Technique

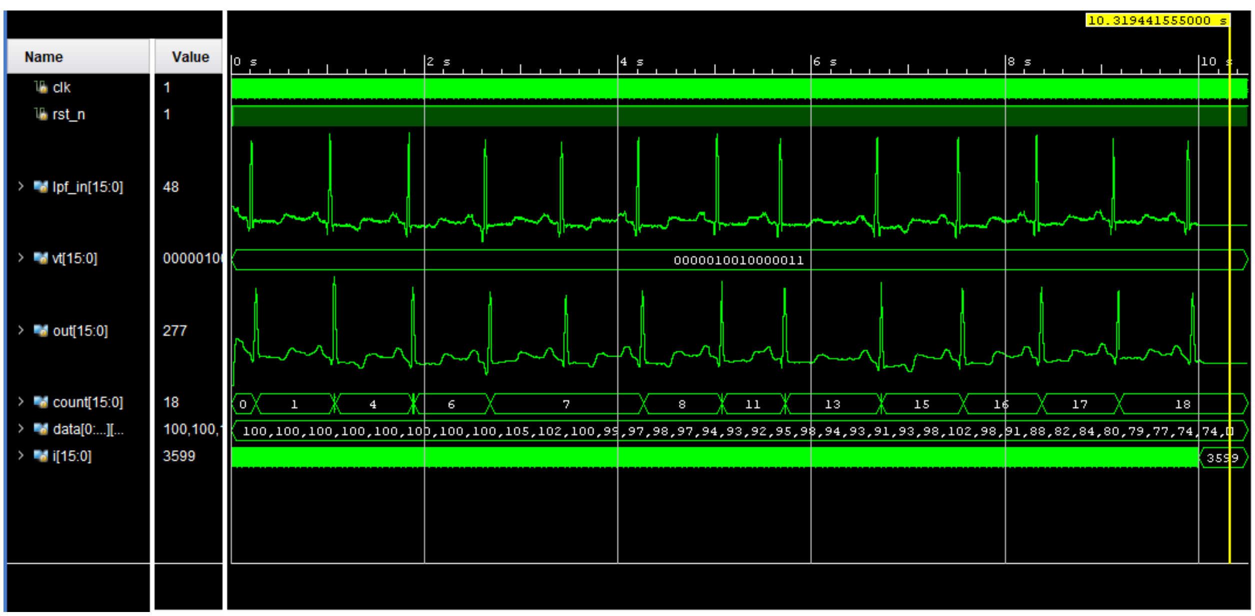

Fig. 6. 7 Output of the proposed ECG detector

Instead of a floating-point algorithm, a fixed-point algorithm is utilized to reduce circuit complexity and power requirements of the proposed design. To maintain symmetry and fair comparison between the proposed ECG signal detector and existing work in the literature, a similar environment as used in the present work to calculate the area, power, and delay requirements. Fig. 6.8 shows the FPGA implementation and test platform of the proposed ECG signal detector.

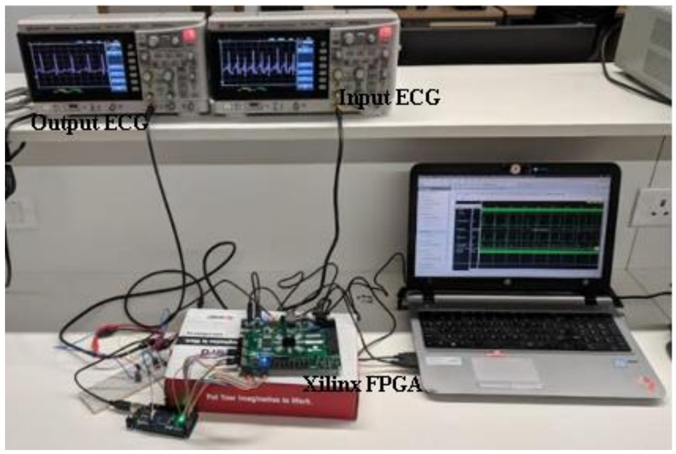

Fig. 6. 8 FPGA implementation and test platform of proposed ECG detector

Area, power, delay of the proposed design is shown in Table 6.6. Table 6.6 brings us to the conclusion that the proposed ECG signal detector has a lower area, power, delay, and switching energy when compared to the existing work.

Table 6. 6: Area, power, and delay comparison of the proposed ECG signal detector with existing literature

References	**[66]**	**[70]**	**[99]**	**[226]**	**Proposed**
Operating frequency (kHz)	1	1	1	1	**1**
V_{DD} (V)	3	3	3	3	**3**
Power consumption (µW)	0.156	16.6	0.560	1.9	**0.099**
Area (mm^2)	1.96	1.36	1.19	6.83	**1.1**
Delay (ns)	42.61	31.03	18.73	26.84	**10**
Switching energy (PDP) (µJ)	6.64	515.098	10.488	50.996	**0.990**

(* for a fair comparison performance of the given references is calculated by generating the similar environment as described in the original paper at 3V V_{DD} and 1 kHz operating frequency).

6.7 SUMMARY

Using biorthogonal *3.1* wavelet transform and an adaptive slope prediction criterion, high detection accuracy, and lowest error has been achieved. Also, using the demand-based wavelet filter bank architecture and lattice wave digital filter realization the lowest power consumption, area, dealay, and switching energy have been achieved. Finally, validation of the proposed design for real-time applications is verified by implementing it on Xilinx® Virtex®-7 FPGA.

CHAPTER 7

CONCLUSION AND FUTURE WORK

In this report, wave detection and lossless data compression of an ECG signal are studied using adaptive slope prediction thresholding and biorthogonal wavelet transform compression. The proposed technique is validated using various ECG signal databases. The biorthogonal *3.1* wavelet transform based filter bank realized using linear phase array structure achieves an SNR of *54.990 dB*. Using the proposed adaptive slope prediction technique, sensitivity, specificity and, overall detection error, respectively, are found to be *99.94 %*, *99.92 %*, and *0.0013*.

Further, using the biorthogonal wavelet transform based lossless data compression technique, a compression ratio of *22.61* is achieved when compared to the existing real-time ECG data compression method. Thus, it can be concluded that the combination of ECG signal detection and lossless ECG data compression not only reduces the false wave detection but also increases the ECG data compression ratio thus facilitating a speedy transmission and efficient bandwidth utilization. The proposed ECG detector is implemented on Xilinx® Virtex®-7 FPGA. Power consumption, area, delay, and switching energy, respectively, of *99 nW*, *1.1* mm^2, *10 ns*, and *0.990 µJ* has been achieved using the proposed technique.

Protecting personal data (information) on the internet seems like becoming a thing of past. Soon, individuals will be struggling to maintain their personal medical information on the internet. The trend shows [227] ECG as one of the most vulnerable data set widely put to use. This increasing use of data on the internet is also exerting necessitating pressure on the worldwide web. To safeguard and protect the data use of watermarks to ECG data is the focus of the future research study. An ECG is the most straightforward test amongst the plethora of heart activity monitoring, which lists the health of the heart. ECG signal helps diagnostic and preventive measures. Such data is generated in large quantities on day to day basis. Hence, data storage with privacy and accuracy is one big challenge for today’s information technology (IT) professionals engaged in the development of medical software applications. Many types of research are being done in the field of making the ECG data more secure. Watermarking combined with new compression methods is gaining importance, and several ways are seen for using such techniques to safeguard ECG data. This proposed methodology can be further extended to analyze various biomedical signals.

Publications From The Thesis

Journal Papers

[1] Kumar, A., Komaragiri, R. and Kumar, M., 2018. From pacemaker to wearable: techniques for ECG detection systems. Journal of Medical Systems, 42(2), p.34. (Impact Factor: 2.098), https://doi.org/10.1007/s10916-017-0886-1

[2] Kumar, A., Kumar, M. and Komaragiri, R., 2018. Design of a Biorthogonal Wavelet Transform Based R-Peak Detection and Data Compression Scheme for Implantable Cardiac Pacemaker Systems. Journal of Medical Systems, 42(6), p.102. (Impact Factor: 2.098), https://doi.org/10.1007/s10916-018-0953-2

[3] Kumar, A., Komaragiri, R. and Kumar, M., 2018. Heart rate monitoring and therapeutic devices: A wavelet transform based approach for the modeling and classification of congestive heart failure. ISA Transactions. (Impact Factor: 4.34), https://doi.org/10.1016/j.isatra.2018.05.003

[4] Kumar, A., Komaragiri, R. and Kumar, M., 2018. Design of wavelet transform based electrocardiogram monitoring system. ISA Transactions. (Impact Factor: 4.34), https://doi.org/10.1016/j.isatra.2018.08.003

[5] Kumar, A., Berwal, D. and Kumar, Y., 2018. Design of high-performance ECG detector for implantable cardiac pacemaker systems using biorthogonal wavelet transform. Circuits, Systems, and Signal Processing, pp.1-20. (Impact Factor: 1.998), https://doi.org/10.1007/s00034-018-0754-3

[6] Berwal, D., Kumar, A. and Kumar, Y., 2018. Design of high performance QRS complex detector for wearable healthcare devices using biorthogonal spline wavelet transform. ISA transactions, 81, pp.222-230. (Impact Factor: 4.34), https://doi.org/10.1016/j.isatra.2018.08.002

[7] Kumar A, Komaragiri R, Kumar M. Design of efficient fractional operator for ECG signal detection in implantable cardiac pacemaker systems. Int J Circ Theor Appl. 2019;1–18. (Impact Factor: 1.54), https://doi.org/10.1002/cta.2667

[8] Kumar, A., Ranganatham, R., Komaragiri, R. and Kumar, M., Efficient QRS complex detection algorithm based on Fast Fourier Transform. Biomedical Engineering Letters, pp.1-7. (SCOPUS Indexed) https://doi.org/10.1007/s13534-018-0087-y

[9] Kumar A, Komaragiri R, Kumar M., 2019. Time–frequency localization using three-tap biorthogonal wavelet filter bank for electrocardiogram compressions. Biomedical Engineering Letters, pp.1-7. (SCOPUS Indexed), https://doi.org/10.1007/s13534-019-00117-9

Under Review

[1] Kumar, A., Komaragiri, R. and Kumar, M. FPGA Implementation of an ECG Detection Scheme for Cardiac Pacemaker. Under Review in IEEE Transaction on Biomedical Circuits and Systems.

Book Chapter

[1] Kumar, A., Komaragiri, R. and Kumar, M., 2018. A Wavelet Transform-Based Filter Bank Architecture for ECG Signal Denoising. In Recent Findings in Intelligent Computing Techniques (pp. 249-255). Springer, Singapore.

Conference Paper

[1] Ashish Kumar, Ramana Ranganatham, Manjeet Kumar, and Rama Komaragiri, Simplified R-peak detection algorithm of an ECG signal using Daubechies-20 wavelet transform, NANOfim-2017

References

[1] Mulpuru, S.K., Madhavan, M., McLeod, C.J., Cha, Y.M. and Friedman, P.A., 2017. Cardiac pacemakers: function, troubleshooting, and management: part 1 of a 2-part series. Journal of the American College of Cardiology, 69(2), pp.189-210.

[2] [Online]. Available: https://www.cnbc.com/2018/03/29/spinal-cord-stimulation-market-grows-as-way-to-treat-chronic-pain.html.

[3] Sanders, R.S. and Lee, M.T., 1996. Implantable pacemakers. Proceedings of the IEEE, 84(3), pp.480-486.

[4] Poon, C.C., Liu, Q., Gao, H., Lin, W.H. and Zhang, Y.T., 2011. Wearable intelligent systems for e-health. Journal of Computing Science and Engineering, 5(3), pp.246-256.

[5] Aging, In World Health Organization. http://www.who.int/topics/ageing/en/,2016.

[6] World Health Statistics 2017, World Health Org., Geneva, Switzerland, 2017.

[7] Banerjee, A. and Gupta, S.K., 2015. Analysis of smart mobile applications for healthcare under dynamic context changes. IEEE Transactions on Mobile Computing, 14(5), pp.904-919.

[8] Zhang, Y., Qiu, M., Tsai, C.W., Hassan, M.M. and Alamri, A., 2017. Health-CPS: Healthcare cyber-physical system assisted by cloud and big data. IEEE Systems Journal, 11(1), pp.88-95.

[9] Zhang, Y., Chen, M., Huang, D., Wu, D. and Li, Y., 2017. iDoctor: Personalized and professionalized medical recommendations based on hybrid matrix factorization. Future Generation Computer Systems, 66, pp.30-35.

[10] Yang, Z., Zhou, Q., Lei, L., Zheng, K. and Xiang, W., 2016. An IoT-cloud based wearable ECG monitoring system for smart healthcare. Journal of medical systems, 40(12), p.286.

[11] Zou, Y., Han, J., Xuan, S., Huang, S., Weng, X., Fang, D. and Zeng, X., 2015. An energy-efficient design for ECG recording and R-peak detection based on wavelet transform. IEEE Transactions on Circuits and Systems II: Express Briefs, 62(2), pp.119-123.

[12] Liu, X., Zheng, Y., Phyu, M.W., Zhao, B., Je, M. and Yuan, X., 2011. Multiple functional ECG signal is processing for wearable applications of long-term cardiac monitoring. IEEE Transactions on Biomedical Engineering, 58(2), pp.380-389.

[13] Buxi, D., Berset, T., Hijdra, M., Tutelaers, M., Geng, D., Hulzink, J., van Noorloos, M., Romero, I., Torfs, T. and van Helleputte, N., 2012, November. Wireless 3-lead ECG system with on-board digital signal processing for ambulatory monitoring. In Biomedical Circuits and Systems Conference (BioCAS), 2012 IEEE (pp. 308-311). IEEE.

[14] Wong, L.S., Hossain, S., Ta, A., Edvinsson, J., Rivas, D.H. and Naas, H., 2004. A very low-power CMOS mixed-signal IC for implantable pacemaker applications. IEEE Journal of solid-state circuits, 39(12), pp.2446-2456.

[15] [Online]. Available: http://www.analog.com/en/analog-dialogue/articles/detecting-and-distinguishing-cardiac-pacing-artifacts.html

[16] Stotts, L.J., Infinger, K.R., Babka, J. and Genzer, D., 1989. An 8-bit microcomputer with analog subsystems for implantable biomedical application. IEEE Journal of Solid-State Circuits, 24(2), pp.292-300.

[17] [Online]. Available:https://brilliantnurse.com/nclex-cardiac-electrical-conduction-system/

[18] [Online]. Available: https://www.alilamedicalmedia.com/

[19] Friesen, G.M., Jannett, T.C., Jadallah, M.A., Yates, S.L., Quint, S.R. and Nagle, H.T., 1990. A comparison of the noise sensitivity of nine QRS detection algorithms. IEEE Transactions on biomedical engineering, 37(1), pp.85-98.

[20] Pan, J. and Tompkins, W.J., 1985. A real-time QRS detection algorithm. IEEE Trans. Biomed. Eng, 32(3), pp.230-236.

[21] [Online]. Available: http://www.physionet.org/physiobank/database/mitdb. [last accessed on 14th December 2017]

[22] Hu, Y.H., Tompkins, W.J., Urrusti, J.L. and Afonso, V.X., 1993. Applications of artificial neural networks for ECG signal detection and classification. Journal of electrocardiology, 26, pp.66-73.

[23] Strintzis, M., Stalidis, G., Magnisalis, X. and Maglaveras, N., 1992. Use of neural networks for electrocardiogram (ECG) feature extraction recognition and classification. Neural Network World, 3(4), pp.313-328.

[24] Lee, H.J., Hwang, S.H., Lee, S.M., Lim, Y.G. and Park, K.S., 2013. Estimation of body postures on bed using unconstrained ECG measurements. IEEE Journal of biomedical and health informatics, 17(6), pp.985-993.

[25] Acharya, U.R., Fujita, H., Lih, O.S., Hagiwara, Y., Tan, J.H. and Adam, M., 2017. Automated detection of arrhythmias using different intervals of tachycardia ECG segments with convolutional neural network. Information sciences, 405, pp.81-90.

[26] Kiranyaz, S., Ince, T. and Gabbouj, M., 2016. Real-time patient-specific ECG classification by 1-D convolutional neural networks. IEEE Transactions on Biomedical Engineering, 63(3), pp.664-675.

[27] Zhou, S., Zhang, Z. and Gu, J., 2011, August. Time-domain ECG signal analysis based on smart-phone. In Engineering in Medicine and Biology Society, EMBC, 2011 Annual International Conference of the IEEE (pp. 2582-2585). IEEE.

[28] Li, C., Zheng, C. and Tai, C., 1995. Detection of ECG characteristic points using wavelet transforms. IEEE Transactions on Biomedical Engineering, 42(1), pp.21-28.

[29] Kadambe, S., Murray, R. and Boudreaux-Bartels, G.F., 1999. Wavelet transform-based QRS complex detector. IEEE Transactions on Biomedical Engineering, 46(7), pp.838-848.

[30] Afonso, V.X., Tompkins, W.J., Nguyen, T.Q. and Luo, S., 1999. ECG beat detection using filter banks. IEEE transactions on biomedical engineering, 46(2), pp.192-202.

[31] Dinh, H.A.N., Kumar, D.K., Pah, N.D. and Burton, P., 2001. Wavelets for QRS detection. Australasian Physics & Engineering Sciences in Medicine, 24(4), p.207.

[32] Kumar, A., Berwal, D. and Kumar, Y., 2018. Design of High-performance ECG detector for implantable cardiac pacemaker systems using biorthogonal wavelet transform. Circuits, Systems, and Signal Processing, pp.1-20.

[33] Sharma, L.N., Tripathy, R.K. and Dandapat, S., 2015. Multiscale energy and eigenspace approach to detection and localization of myocardial infarction. IEEE transactions on biomedical engineering, 62(7), pp.1827-1837.

[34] Sahambi, J.S., Tandon, S.N. and Bhatt, R.K.P., 1997. Using wavelet transforms for ECG characterization. An online digital signal processing system. IEEE Engineering in Medicine and Biology Magazine, 16(1), pp.77-83.

[35] Tripathy, R.K. and Dandapat, S., 2017. Automated detection of heart ailments from 12-lead ECG using complex wavelet sub-band bi-spectrum features. Healthcare technology letters, 4(2), p.57.

[36] Rakshit, M. and Das, S., 2017. An efficient wavelet-based automated R-peaks detection method using Hilbert transform. Biocybernetics and Biomedical Engineering, 37(3), pp.566-577.

[37] Sharma, M., Agarwal, S. and Acharya, U.R., 2018. Application of an optimal class of antisymmetric wavelet filter banks for obstructive sleep apnea diagnosis using ECG signals. Computers in Biology and Medicine.

[38] Milchevski, A. and Gusev, M., 2017. Improved pipelined wavelet implementation for filtering ECG signals. Pattern Recognition Letters, 95, pp.85-90.

[39] Ma, Y., Li, T., Ma, Y. and Zhan, K., 2016. Novel real-time FPGA-based R-wave detection using lifting wavelet. Circuits, Systems, and Signal Processing, 35(1), pp.281-299.

[40] Sharma, L.D. and Sunkaria, R.K., 2018. Inferior myocardial infarction detection using stationary wavelet transform and machine learning approach. Signal, Image and Video Processing, 12(2), pp.199-206.

[41] Sutha, P. and Jayanthi, V.E., 2018. Fetal electrocardiogram extraction and analysis using adaptive noise cancellation and wavelet transformation techniques. Journal of medical systems, 42(1), p.21.

[42] Junior, E.A., de Medeiros Valentim, R.A. and Brandao, G.B., 2016. Real time QRS detection based on redundant discrete wavelet transform. IEEE Latin America Transactions, 14(4), pp.1662-1668.

[43] Tzabazis, A., Eisenried, A., Yeomans, D.C. and Hyatt, M.I., 2018. Wavelet analysis of heartrate variability: Impact of wavelet selection. Biomedical Signal Processing and Control, 40, pp.220-225.

[44] Zidelmal, Z., Amirou, A., Adnane, M. and Belouchrani, A., 2012. QRS detection based on wavelet coefficients. Computer methods and programs in biomedicine, 107(3), pp.490-496.

[45] Azmoudeh, B. and Cvetkovic, D., 2014. Wavelets in Biomedical Signal Processing and Analysis.

[46] Pławiak, P., 2018. Novel genetic ensembles of classifiers applied to myocardium dysfunction recognition based on ECG signals. Swarm and evolutionary computation, 39, pp.192-208.

[47] Vafaie, M.H., Ataei, M. and Koofigar, H.R., 2014. Heart diseases prediction based on ECG signals' classification using a genetic-fuzzy system and dynamical model of ECG signals. Biomedical Signal Processing and Control, 14, pp.291-296.

[48] Pasolli, E. and Melgani, F., 2015. Genetic algorithm-based method for mitigating label noise issue in ECG signal classification. Biomedical Signal Processing and Control, 19, pp.130-136.

[49] Kumaravel, N. and Nithiyanandam, N., 1998. Genetic-algorithm cancellation of sinusoidal powerline interference in electrocardiograms. Medical and Biological Engineering and Computing, 36(2), pp.191-196.

[50] Poli, R., Cagnoni, S. and Valli, G., 1995. Genetic design of optimum linear and nonlinear QRS detectors. IEEE Transactions on Biomedical Engineering, 42(11), pp.1137-1141.

[51] Meyer, C., Gavela, J.F. and Harris, M., 2006. Combining algorithms in automatic detection of QRS complexes in ECG signals. IEEE Transactions on Information Technology in Biomedicine, 10(3), pp.468-475.

[52] Yücelbaş, Ş., Yücelbaş, C., Tezel, G., Özşen, S. and Yosunkaya, Ş., 2018. Automatic sleep staging based on SVD, VMD, HHT and morphological features of single-lead ECG signal. Expert Systems with Applications, 102, pp.193-206.

[53] Vullings, R., De Vries, B. and Bergmans, J.W., 2011. An adaptive Kalman filter for ECG signal enhancement. IEEE transactions on biomedical engineering, 58(4), pp.1094-1103.

[54] Rhyne, V.T., 1969. A digital system for enhancing the fetal electrocardiogram. IEEE Transactions on Biomedical Engineering, (1), pp.80-86.

[55] Martin-Clemente, R., Camargo-Olivares, J.L., Hornillo-Mellado, S., Elena, M. and Roman, I., 2011. Fast technique for noninvasive fetal ECG extraction. IEEE transactions on biomedical engineering, 58(2), pp.227-230.

[56] Martinek, R., Kelnar, M., Koudelka, P., Vanus, J., Bilík, P., Janku, P., Nazeran, H. and Zidek, J., 2015. Enhanced processing and analysis of multi-channel non-invasive abdominal foetal ECG signals during labor and delivery. Electronics Letters, 51(22), pp.1744-1746.

[57] Banerjee, S. and Mitra, M., 2014. Application of cross wavelet transform for ECG pattern analysis and classification. IEEE transactions on instrumentation and measurement, 63(2), pp.326-333.

[58] Barro, S., Fernandez-Delgado, M., Vila-Sobrino, J.A., Regueiro, C.V. and Sanchez, E., 1998. Classifying multichannel ECG patterns with an adaptive neural network. IEEE Engineering in Medicine and Biology Magazine, 17(1), pp.45-55.

[59] Bono, V., Mazomenos, E.B., Chen, T., Rosengarten, J.A., Acharyya, A., Maharatna, K., Morgan, J.M. and Curzen, N., 2014. Development of an automated updated selvester QRS scoring system using SWT-based QRS fractionation detection and classification. IEEE Journal of biomedical and health informatics, 18(1), pp.193-204.

[60] Sannino, G. and De Pietro, G., 2018. A deep learning approach for ECG-based heartbeat classification for arrhythmia detection. Future Generation Computer Systems, 86, pp.446-455.

[61] Satija, U., Ramkumar, B. and Manikandan, M.S., 2018. Automated ECG noise detection and classification system for unsupervised healthcare monitoring. IEEE Journal of biomedical and health informatics, 22(3), pp.722-732.

[62] Zhai, X. and Tin, C., 2018. Automated ECG Classification using Dual Heartbeat Coupling based on Convolutional Neural Network. IEEE Access.

[63] Kohler, B.U., Hennig, C. and Orglmeister, R., 2002. The principles of software QRS detection. IEEE Engineering in Medicine and Biology Magazine, 21(1), pp.42-57.

[64] Elgendi, M., Eskofier, B., Dokos, S. and Abbott, D., 2014. Revisiting QRS detection methodologies for portable, wearable, battery-operated, and wireless ECG systems. PloS one, 9(1), p.e84018.

[65] Kumar, A., Komaragiri, R. and Kumar, M., 2018. From pacemaker to wearable: techniques for ECG detection systems. Journal of medical systems, 42(2), p.34.

[66] Rodrigues, J.N., Olsson, T., Sornmo, L. and Owall, V., 2005. Digital implementation of a wavelet-based event detector for cardiac pacemakers. IEEE Transactions on Circuits and Systems I: Regular Papers, 52(12), pp.2686-2698.

[67] Mallat, S.G., 1989. A theory for multiresolution signal decomposition: the wavelet representation. IEEE transactions on pattern analysis and machine intelligence, 11(7), pp.674-693.

[68] Kay, S.M. and Gabriel, J.R., 2003. An invariance property of the generalized likelihood ratio test. IEEE Signal processing letters, 10(12), pp.352-355.

[69] Martínez, J.P., Almeida, R., Olmos, S., Rocha, A.P. and Laguna, P., 2004. A wavelet-based ECG delineator: evaluation on standard databases. IEEE Transactions on biomedical engineering, 51(4), pp.570-581.

[70] Min, Y.J., Kim, H.K., Kang, Y.R., Kim, G.S., Park, J. and Kim, S.W., 2013. Design of wavelet-based ECG detector for implantable cardiac pacemakers. IEEE transactions on biomedical circuits and systems, 7(4), pp.426-436.

[71] Getreuer, P., 2006. Filter coefficients to popular wavelets. MATLAB Central, May.

[72] Sweldens, W., 1998. The lifting Technique: A construction of second generation wavelets. SIAM journal on mathematical analysis, 29(2), pp.511-546.

[73] Donoho, D.L., 1995. De-noising by soft-thresholding. IEEE transactions on information theory, 41(3), pp.613-627.

[74] Sadler, B.M., Pham, T. and Sadler, L.C., 1998. Optimal and wavelet-based shock wave detection and estimation. The Journal of the Acoustical Society of America, 104(2), pp.955-963.

[75] Kim, K.H. and Kim, S.J., 2003. A wavelet-based method for action potential detection from extracellular neural signal recording with low signal-to-noise ratio. IEEE Transactions on Biomedical Engineering, 50(8), pp.999-1011.

[76] Bhavtosh, Berwal, D. and Kumar, Y., 2015, March. High performance QRS complex detector for wearable ECG systems using Multi Scaled product with booth multiplier and soft threshold algorithm. In Signal Processing and Communication (ICSC), 2015 International Conference on (pp. 204-209). IEEE.

[77] Wang, H.W., Lai, Y. L., Hou, M. C., Lin, S. H., Yen, B. S., Huang, Y. C., Chou, L. C., Hsu, S. Y., Huang, S. C., and Jan, M. Y., 2010, A ±6 ms- accuracy, 0.68 mm^2 and 2.21 μW QRS detection ASIC. In Circuits Systems Symposium, Paris, France, (pp.1372-1375). IEEE.

[78] Chang, M.C., Lin, Z.X., Chang, C.W., Chan, H.L. and Feng, W.S., 2004, December. Design of a system-on-chip for ECG signal processing. In Circuits and Systems, 2004. Proceedings. The 2004 IEEE Asia-Pacific Conference on (Vol. 1, pp. 441-444). IEEE.

[79] Massagram, W., Boric-Lubecke, O., Macchiarulo, L. and Chen, M., 2005. Heartrate variability monitoring and assessment system on chip. In Engineering in Medicine and Biology Society, 2005. IEEE-EMBS 2005. 27th Annual International Conference of the (pp. 7369-7372). IEEE.

[80] Wang, X., Chen, M., Macchiarulo, L. and Boric-Lubecke, O., 2006, August. Fully-integrated heartrate variability monitoring system with an efficient memory. In Engineering in Medicine and Biology Society, 2006. EMBS'06. 28th Annual International Conference of the IEEE (pp. 5064-5067). IEEE.

[81] Phyu, M.W., Zheng, Y., Zhao, B., Xin, L. and Wang, Y.S., 2009, November. A real-time ECG QRS detection ASIC based on wavelet multiscale analysis. In Solid-State Circuits Conference, 2009. A-SSCC 2009. IEEE Asian (pp. 293-296). IEEE.

[82] Massagram, W., Hafner, N., Chen, M., Macchiarulo, L., Lubecke, V.M. and Boric-Lubecke, O., 2010. Digital heart-rate variability parameter monitoring and assessment ASIC. IEEE Transactions on Biomedical Circuits and Systems, 4(1), pp.19-26.

[83] Thakor, N.V., Webster, J.G. and Tompkins, W.J., 1983. Optimal QRS detector. Medical and Biological Engineering and Computing, 21(3), pp.343-350.

[84] Zheng, X., Li, Z., Shen, L. and Ji, Z., 2008, December. Detection of QRS complexes based on biorthogonal spline wavelet. In Information Science and Engineering, 2008. ISISE'08. International Symposium on (Vol. 2, pp. 502-506). IEEE.

[85] Luk, W. and Jones, G., 1987. Systolic arrays for recursive digital filtering. Electronics Letters, 23(22), pp.1174-1175.

[86] Baek, H.J., Chung, G.S., Kim, K.K. and Park, K.S., 2012. A smart health monitoring chair for nonintrusive measurement of biological signals. IEEE Transactions on Information Technology in Biomedicine, 16(1), pp.150-158.

[87] Vuorela, T., Seppä, V.P., Vanhala, J. and Hyttinen, J., 2010. Design and implementation of a portable long-term physiological signal recorder. IEEE Transactions on Information Technology in Biomedicine, 14(3), pp.718-725.

[88] Yang, G., Xie, L., Mäntysalo, M., Chen, J., Tenhunen, H. and Zheng, L.R., 2012. Bio-patch design and implementation based on a low-power system-on-chip and paper-based inkjet printing technology. IEEE transactions on information technology in biomedicine, 16(6), pp.1043-1050.

[89] Tsai, T.H., Hong, J.H., Wang, L.H. and Lee, S.Y., 2012. Low-power analog integrated circuits for wireless ECG acquisition systems. IEEE Transactions on Information Technology in biomedicine, 16(5), pp.907-917.

[90] Yan, L., Bae, J., Lee, S., Roh, T., Song, K. and Yoo, H.J., 2011. A 3.9 mW 25-electrode reconfigured sensor for wearable cardiac monitoring system. IEEE Journal of Solid-State Circuits, 46(1), pp.353-364.

[91] Khayatzadeh, M., Zhang, X., Tan, J., Liew, W. S., and Lian, Y., 2012. A 0.7-V 17.4-μW 3-LeadWireless ECG SoC. IEEE BioCAS-2012, Nov. 2012, pp. 344-47.

[92] Lee, S.Y., Hong, J.H., Hsieh, C.H., Liang, M.C., Chien, S.Y.C. and Lin, K.H., 2015. Low-power wireless ECG acquisition and classification system for body sensor networks. IEEE Journal of biomedical and health informatics, 19(1), pp.236-246.

[93] Kuo, T.H., Chen, K.D. and Chen, J.R., 1999. Automatic coefficients design for high-order sigma-delta modulators. IEEE Transactions on Circuits and Systems II: Analog and Digital Signal Processing, 46(1), pp.6-15.

[94] Kuo, T.H., Chen, K.D. and Chen, J.R., 1999. Automatic coefficients design for high-order sigma-delta modulators. IEEE Transactions on Circuits and Systems II: Analog and Digital Signal Processing, 46(1), pp.6-15.

[95] Hong, J.H., Lee, S.Y., Liang, M.C., Hsieh, C.H. and Chien, S.Y.C., 2013, July. A wireless ECG acquisition and classification system for body sensor networks. In Engineering in Medicine and Biology Society (EMBC), 2013 35th Annual International Conference of the IEEE (pp. 5183-5186). IEEE.

[96] Cocherova, E., Surda, J., Pucik, J. and Stofanik, V., 2009, April. Dependence of the RF field absorption on the human body dimensions. In Radioelektronika, 2009. RADIOELEKTRONIKA'09. 19th International Conference (pp. 327-329). IEEE.

[97] Vetterli, M. and Herley, C., 1992. Wavelets and filter banks: Theory and design. IEEE transactions on signal processing, 40(ARTICLE).

[98] Shyu, L.Y., Wu, Y.H. and Hu, W., 2004. Using wavelet transform and fuzzy neural network for VPC detection from the Holter ECG. IEEE Transactions on Biomedical Engineering, 51(7), pp.1269-1273.

[99] Ieong, C.I., Mak, P.I., Lam, C.P., Dong, C., Vai, M.I., Mak, P.U., Pun, S.H., Wan, F. and Martins, R.P., 2012. A 0.83-QRS detection processor using quadratic spline wavelet transform for wireless ECG acquisition in 0.35-CMOS. IEEE Trans. Biomed. Circuits Syst, 6(6), pp.586-595.

[100] Zou, Y., Han, J., Weng, X. and Zeng, X., 2013. An ultra-low power QRS complex detection algorithm based on down-sampling wavelet transform. IEEE Signal Processing Letters, 20(5), pp.515-518.

[101] Wang, Y., Deepu, C.J. and Lian, Y., 2011, August. A computationally efficient QRS detection algorithm for wearable ECG sensors. In 2011 Annual International Conference of the IEEE Engineering in Medicine and Biology Society (pp. 5641-5644). IEEE.

[102] Chua, E. and Fang, W.C., 2011. Mixed bio-signal lossless data compressor for portable brain-heart monitoring systems. IEEE Transactions on Consumer Electronics, 57(1), pp.267-273.

[103] Chen, S.L. and Wang, J.G., 2013. VLSI implementation of low-power cost-efficient lossless ECG encoder design for wireless healthcare monitoring application. Electronics Letters, 49(2), pp.91-93.

[104] Deepu, C.J. and Lian, Y., 2015. A joint QRS detection and data compression Technique for wearable sensors. IEEE Trans. Biomed. Engineering, 62(1), pp.165-175.

[105] Shyu, L.Y., Wu, Y.H. and Hu, W., 2004. Using wavelet transform and fuzzy neural network for VPC detection from the Holter ECG. IEEE Transactions on Biomedical Engineering, 51(7), pp.1269-1273.

[106] Kyrkos, A., Giakoumakis, E.A. and Carayannis, G., 1988. QRS detection through time recursive prediction techniques. Signal Processing, 15(4), pp.429-436.

[107] Lin, K.P. and Chang, W.H., 1989. QRS feature extraction using linear prediction. IEEE Transactions on Biomedical Engineering, 36(10), pp.1050-1055.

[108] Farhang-Boroujeny, B., 2013. Adaptive filters: theory and applications. John Wiley & Sons.

[109] Der, L. and Razavi, B., 2003. A 2-GHz CMOS image-reject receiver with LMS calibration. IEEE Journal of Solid-State Circuits, 38(2), pp.167-175.

[110] Gutta, S. and Cheng, Q., 2016. Joint feature extraction and classifier design for ECG-based biometric recognition. IEEE Journal of biomedical and health informatics, 20(2), pp.460-468.

[111] Delano, M.K. and Sodini, C.G., 2013, May. A long-term wearable electrocardiogram measurement system. In Body Sensor Networks (BSN), 2013 IEEE International Conference on (pp. 1-6). IEEE.

[112] Junior, E.A., de Medeiros Valentim, R.A. and Brandao, G.B., 2016. Real time QRS detection based on redundant discrete wavelet transform. IEEE Latin America Transactions, 14(4), pp.1662-1668.

[113] Deepu, C.J., Heng, C.H. and Lian, Y., 2017. A hybrid data compression Technique for power reduction in wireless sensors for IoT. IEEE transactions on biomedical circuits and systems, 11(2), pp.245-254.

[114] Huang, P., 2018. Study on a Low-Complexity ECG Compression Technique with Two-Tier Sensors. IEEE Transactions on Very Large-Scale Integration (VLSI) Systems, (99), pp.1-5.

[115] Craven, D., McGinley, B., Kilmartin, L., Glavin, M. and Jones, E., 2017. Adaptive dictionary reconstruction for compressed sensing of ECG signals. IEEE Journal of biomedical and health informatics, 21(3), pp.645-654.

[116] Hooshmand, M., Zordan, D., Del Testa, D., Grisan, E. and Rossi, M., 2017. Boosting the battery life of wearables for health monitoring through the compression of biosignals. IEEE Internet of Things Journal, 4(5), pp.1647-1662.

[117] Berkaya, S.K., Uysal, A.K., Gunal, E.S., Ergin, S., Gunal, S. and Gulmezoglu, M.B., 2018. A survey on ECG analysis. Biomedical Signal Processing and Control, 43, pp.216-235.

[118] American Heart Association, AHA Database, ECRI, 5200 Butler Pike, Plymouth Meeting, PA 19462 USA.

[119] Van Bemmel, J.H. and Willems, J.L., 1990. Standardization and validation of medical decision-support systems: the CSE project. Methods of information in medicine, 29(04), pp.261-262.

[120] Paracha, M.A., Mohammad, S.N., Macfarlane, P.W. and Jenkins, J.M., 2003, September. Implementation of web database for ECG. In Computers in Cardiology, 2003 (pp. 271-274). IEEE.

[121] Moody, G.B. and Mark, R.G., 1996, September. A database to support development and evaluation of intelligent intensive care monitoring. In Computers in Cardiology, 1996 (pp. 657-660). IEEE.

[122] Jager, F., Taddei, A., Moody, G.B., Emdin, M., Antolič, G., Dorn, R., Smrdel, A., Marchesi, C. and Mark, R.G., 2003. Long-term ST database: a reference for the development and evaluation of automated ischaemia detectors and for the study of the dynamics of myocardial ischaemia. Medical and Biological Engineering and Computing, 41(2), pp.172-182.

[123] National Research Council (CNR). European ST-T Database. Institute of Clinical Physiology, Dept. of Bioengineering and Medical Informatics, Pisa, Italy. Available: http://www.ifc.pi.cnr.it/

[124] Laguna, P., Mark, R.G., Goldberg, A. and Moody, G.B., 1997, September. A database for evaluation of algorithms for measurement of QT and other waveform intervals in the ECG. In Computers in Cardiology 1997 (pp. 673-676). IEEE.

[125] Massachusetts General Hospital, Massachusetts General Hospital/ Marquette Foundation Waveform Database, Dr. J. Cooper, MGH, Anesthesia Bioengineering Unit, Fruit Street, Boston, MA.

[126] Mahmoodabadi, S.Z., Ahmadian, A., Abolhasani, M.D., Eslami, M. and Bidgoli, J.H., 2006, January. ECG feature extraction based on multiresolution wavelet transform. In Engineering in Medicine and Biology Society, 2005. IEEE-EMBS 2005. 27th Annual International Conference of the (pp. 3902-3905). IEEE.

[127] Faezipour, M., Saeed, A., Bulusu, S.C., Nourani, M., Minn, H. and Tamil, L., 2010. A patient-adaptive profiling Technique for ECG beat classification. IEEE Transactions on Information Technology in Biomedicine, 14(5), pp.1153-1165.

[128] Goldberger, A.L., Amaral, L.A., Glass, L., Hausdorff, J.M., Ivanov, P.C., Mark, R.G., Mietus, J.E., Moody, G.B., Peng, C.K. and Stanley, H.E., 2000. PhysioBank, PhysioToolkit, and PhysioNet: components of a new research resource for complex physiologic signals. Circulation, 101(23), pp. e215-e220.

[129] Ravanshad, N., Rezaee-Dehsorkh, H., Lotfi, R. and Lian, Y., 2014. A level-crossing based QRS-detection algorithm for wearable ECG sensors. IEEE Journal of biomedical and health informatics, 18(1), pp.183-192.

[130] Suarez, K.V., Silva, J.C., Berthoumieu, Y., Gomis, P. and Najim, M., 2007. ECG beat detection using a geometrical matching approach. IEEE Transactions on Biomedical Engineering, 54(4), pp.641-650.

[131] Chen, S.W., Chen, H.C. and Chan, H.L., 2006. A real-time QRS detection method based on moving-averaging incorporating with wavelet denoising. Computer methods and programs in biomedicine, 82(3), pp.187-195.

[132] Chouhan, V.S. and Mehta, S.S., 2008. Detection of QRS complexes in 12-lead ECG using adaptive quantized threshold. International Journal of Computer Science and Network Security, 8(1), pp.155-163.

[133] Bahoura, M., Hassani, M. and Hubin, M., 1997. DSP implementation of wavelet transform for real time ECG wave forms detection and heartrate analysis. Computer methods and programs in biomedicine, 52(1), pp.35-44.

[134] Ghaffari, A., Golbayani, H. and Ghasemi, M., 2008. A new mathematical based QRS detector using continuous wavelet transform. Computers & Electrical Engineering, 34(2), pp.81-91.

[135] Pan, T., Zhang, L. and Zhou, S., 2010, October. Detection of ECG characteristic points using biorthogonal spline wavelet. In Biomedical Engineering and Informatics (BMEI), 2010 3rd International Conference on (Vol. 2, pp. 858-863). IEEE.

[136] Benmalek, M. and Charef, A., 2009. Digital fractional order operators for R-wave detection in electrocardiogram signal. IET signal processing, 3(5), pp.381-391.

[137] Raj, S. and Ray, K.C., 2017. ECG signal analysis using DCT-based DOST and PSO optimized SVM. IEEE Transactions on Instrumentation and Measurement, 66(3), pp.470-478.

[138] Nayak, C., Saha, S.K., Kar, R. and Mandal, D., 2018. An Efficient QRS Complex Detection Using Optimally Designed Digital Differentiator. Circuits, Systems, and Signal Processing, pp.1-34.

[139] Jain, S., Kumar, A. and Bajaj, V., 2016. Technique for QRS complex detection using particle swarm optimisation. IET Science, Measurement & Technology, 10(6), pp.626-636.

[140] Chiarugi, F., Sakkalis, V., Emmanouilidou, D., Krontiris, T., Varanini, M. and Tollis, I., 2007, September. Adaptive threshold QRS detector with best channel selection based on a noise rating system. In Computers in Cardiology, 2007 (pp. 157-160). IEEE.

[141] Elgendi, M., Mohamed, A. and Ward, R., 2017. Efficient ECG Compression and QRS Detection for E-Health Applications. Scientific reports, 7(1), p.459.

[142] Tang, X., Hu, Q. and Tang, W., 2018. A Real-Time QRS Detection System With PR/RT Interval and ST Segment Measurements for Wearable ECG Sensors Using Parallel Delta Modulators. IEEE Transactions on Biomedical Circuits and Systems, (99), pp.1-11.

[143] Hou, Z., Dong, Y., Xiang, J., Li, X. and Yang, B., 2018. A Real-Time QRS Detection Method Based on Phase Portraits and Box-Scoring Calculation. IEEE Sensors Journal, 18(9), pp.3694-3702.

[144] Adnane, M., Jiang, Z. and Choi, S., 2009. Development of QRS detection algorithm designed for wearable cardiorespiratory system. Computer methods and programs in biomedicine, 93(1), pp.20-31.

[145] Qin, Q., Li, J., Yue, Y. and Liu, C., 2017. An Adaptive and Time-Efficient ECG R-Peak Detection Algorithm. Journal of healthcare engineering, 2017.

[146] Thungtong, A., 2017, July. A robust algorithm for R peak detection based on optimal Discrete Wavelet Transform. In Computer Science and Software Engineering (JCSSE), 2017 14th International Joint Conference on (pp. 1-6). IEEE.

[147] Uthayakumar, J., Vengattaraman, T. and Dhavachelvan, P., 2018. A survey on data compression techniques: From the perspective of data quality, coding Techniques, data type and applications. Journal of King Saud University-Computer and Information Sciences.

[148] Polania, L.F., Carrillo, R.E., Blanco-Velasco, M. and Barner, K.E., 2011, May. Compressed sensing-based method for ECG compression. In Acoustics, Speech and

Signal Processing (ICASSP), 2011 IEEE International Conference on (pp. 761-764). IEEE.

[149] Mamaghanian, H., Khaled, N., Atienza, D. and Vandergheynst, P., 2011. Compressed sensing for real-time energy-efficient ECG compression on wireless body sensor nodes. IEEE Transactions on Biomedical Engineering, 58(9), pp.2456-2466.

[150] Mishra, A., Thakkar, F., Modi, C. and Kher, R., 2012, August. ECG signal compression using Compressive Sensing and wavelet transform. In Engineering in Medicine and Biology Society (EMBC), 2012 Annual International Conference of the IEEE (pp. 3404-3407). IEEE.

[151] Ansari-Ram, F. and Hosseini-Khayat, S., 2012, May. ECG signal compression using compressed sensing with nonuniform binary matrices. In Artificial Intelligence and Signal Processing (AISP), 2012 16th CSI International Symposium on (pp. 305-309). IEEE.

[152] Casson, A.J. and Rodriguez-Villegas, E., 2012, August. Signal agnostic compressive sensing for body area networks: Comparison of signal reconstructions. In Engineering in Medicine and Biology Society (EMBC), 2012 Annual International Conference of the IEEE (pp. 4497-4500). IEEE.

[153] Kumar, R., Kumar, A. and Pandey, R.K., 2013. Beta wavelet-based ECG signal compression using lossless encoding with modified thresholding. Computers & Electrical Engineering, 39(1), pp.130-140.

[154] Chae, D.H., Alem, Y.F., Durrani, S. and Kennedy, R.A., 2013, May. Performance study of compressive sampling for ECG signal compression in noisy and varying sparsity acquisition. In ICASSP (pp. 1306-1309).

[155] Polania, L.F., Carrillo, R.E., Blanco-Velasco, M. and Barner, K.E., 2015. Exploiting prior knowledge in compressed sensing wireless ECG systems. IEEE Journal of Biomedical and Health Informatics, 19(2), pp.508-519.

[156] Manikandan, M.S. and Dandapat, S., 2007, December. Wavelet-based ECG and PCG signals compression technique for mobile telemedicine. In Advanced Computing and Communications, 2007. ADCOM 2007. International Conference on (pp. 164-169). IEEE.

[157] Lin, S.Y., Lin, H.T. and Lin, Y.Y., 2018. Lossless and Lossy Direct Compression Design with Multi-signal Symptom Detection for Low-temperature Wearable Devices. IEEE Sensors Journal.

[158] Chen, S.L., Lee, H.Y., Chen, C.A., Huang, H.Y. and Luo, C.H., 2009. Wireless body sensor network with adaptive low-power design for biometrics and healthcare applications. IEEE Systems Journal, 3(4), pp.398-409.

[159] Deepu, C.J., Zhang, X., Liew, W.S., Wong, D.L.T. and Lian, Y., 2013, November. An ECG-SoC with 535nW/channel lossless data compression for wearable sensors. In Solid-State Circuits Conference (A-SSCC), 2013 IEEE Asian (pp. 145-148). IEEE.

[160] Capurro, I., Lecumberry, F., Martín, A., Ramírez, I., Rovira, E. and Seroussi, G., 2017. Efficient Sequential Compression of multichannel biomedical signals. IEEE Journal of biomedical and health informatics, 21(4), pp.904-916.

[161] Tsai, T.H. and Kuo, W.T., 2018. An Efficient ECG Lossless Compression System for Embedded Platforms with Telemedicine Applications. IEEE Access, 6, pp.42207-42215.

[162] [Online]. Available: https://www.who.int/nmh/publications/ncd-profiles-2018/en/

[163] Dilaveris, P.E., Gialafos, E.J., Sideris, S.K., Theopistou, A.M., Andrikopoulos, G.K., Kyriakidis, M., Gialafos, J.E. and Toutouzas, P.K., 1998. Simple electrocardiographic markers for the prediction of paroxysmal idiopathic atrial fibrillation. American heart journal, 135(5), pp.733-738.

[164] Webster, J.G., 2009. Medical instrumentation application and design. John Wiley & Sons.

[165] [Online]. Available: https://www.datasci.com/solutions/cardiovascular/ecg-research

[166] Elgendi, M., Jonkman, M. and DeBoer, F., 2010. Frequency bands effects on QRS detection. Pan, 5, p.15Hz.

[167] Sivannarayana, N. and Reddy, D.C., 1999. Biorthogonal wavelet transforms for ECG parameters estimation. Medical engineering & physics, 21(3), pp.167-174.

[168] Unser, M.A., 1997, October. Ten good reasons for using spline wavelets. In Wavelet applications in signal and image processing V (Vol. 3169, pp. 422-432). International Society for Optics and Photonics.

[169] Zorzi, M., 2014. A new family of high-resolution multivariate spectral estimators. IEEE Transactions on Automatic Control, 59(4), pp.892-904.

[170] Johnston, J., 1980, April. A filter family designed for use in quadrature mirror filter banks. In Acoustics, Speech, and Signal Processing, IEEE International Conference on ICASSP'80. (Vol. 5, pp. 291-294). IEEE.

[171] Mallat, S., 2008. A wavelet tour of signal processing: the sparse way. Academic Press.

[172] Barsainya, R., Rawat, T.K. and Kumar, M., 2017. Design of minimum multiplier fractional order differentiator based on lattice wave digital filter. ISA Transactions, 66, pp.404-413.

[173] Zhang, X. and Lian, Y., 2014. A 300-mV 220-nW event-driven ADC with real-time QRS detection for wearable ECG sensors. IEEE Transactions on Biomedical Circuits and Systems, 8(6), pp.834-843.

[174] Lin, C.H., 2008. Frequency-domain features for ECG beat discrimination using grey relational analysis-based classifier. Computers & Mathematics with Applications, 55(4), pp.680-690.

[175] Soman, K.P., 2010. Insight into wavelets: From theory to practice. PHI Learning Pvt. Ltd.

[176] Jansen, M., 2012. Noise reduction by wavelet thresholding (Vol. 161). Springer Science & Business Media.

[177] Priya, K.D., Rao, G.S. and Rao, P.S., 2016. Comparative analysis of wavelet thresholding techniques with wavelet-Wiener filter on ECG signal. Procedia Computer Science, 87, pp.178-183.

[178] Kew, H.P. and Jeong, D.U., 2011. Variable threshold method for ECG R-peak detection. Journal of medical systems, 35(5), pp.1085-1094.

[179] Zhang, F. and Lian, Y., 2009. QRS detection based on multiscale mathematical morphology for wearable ECG devices in body area networks. IEEE Transactions on Biomedical Circuits and Systems, 3(4), pp.220-228.

[180] Teo, T.H., Qian, X., Gopalakrishnan, P.K., Hwan, Y.S., Haridas, K., Pang, C.Y., Cha, H.K. and Je, M., 2010. A 700- μW Wireless Sensor Node SoC for Continuous Real-Time Health Monitoring. IEEE Journal of Solid-State Circuits, 45(11), pp.2292-2299.

[181] Singh, A. and Dandapat, S., 2017. Block sparsity-based joint compressed sensing recovery of multi-channel ECG signals. Healthcare technology letters, 4(2), p.50.

[182] Wang, X., Chen, Z., Luo, J., Meng, J. and Xu, Y., 2016. ECG compression based on combining of EMD and wavelet transform. Electronics Letters, 52(19), pp.1588-1590.

[183] Sharma, M., Goyal, D., Achuth, P.V. and Acharya, U.R., 2018. An accurate sleep stages classification system using a new class of optimally time-frequency localized three-band wavelet filter bank. Computers in biology and medicine, 98, pp.58-75.

[184] Bhati, D., Sharma, M., Pachori, R.B., Nair, S.S. and Gadre, V.M., 2016. Design of time–frequency optimal three-band wavelet filter banks with unit sobolev regularity using frequency domain sampling. Circuits, Systems, and Signal Processing, 35(12), pp.4501-4531.

[185] Bhokare, G., Bhardwaj, A.K., Rai, N. and Gadre, V.M., 2008. Digital watermarking with 3-band filter banks. In Proceedings of the Fourteenth National Conference on Communications (pp. 466-470).

[186] Zhao, P. and Zhao, C., 2013. Three-channel symmetric tight frame wavelet design method. Information Technology Journal, 12(4), p.623.

[187] Abo-Zahhad, M., Al-Ajlouni, A.F., Ahmed, S.M. and Schilling, R.J., 2013. A new algorithm for the compression of ECG signals based on mother wavelet parameterization and best-threshold levels selection. Digital Signal Processing, 23(3), pp.1002-1011.

[188] Elgendi, M., 2013. Fast QRS detection with an optimized knowledge-based method: Evaluation on 11 standard ECG databases. PloS one, 8(9), p.e73557.

[189] Chang, C.H., Gu, J. and Zhang, M., 2005. A review of 0.18-/spl mu/m full adder performances for tree structured arithmetic circuits. IEEE Transactions on very large scale integration (VLSI) systems, 13(6), pp.686-695.

[190] Van, L.D. and Yang, C.C., 2005. Generalized low-error area-efficient fixed-width multipliers. IEEE Transactions on Circuits and Systems I: Regular Papers, 52(8), pp.1608-1619.

[191] Komaty, A., Boudraa, A.O., Augier, B. and Dare-Emzivat, D., 2014. EMD-based filtering using similarity measure between probability density functions of IMFs. IEEE Transactions on Instrumentation and Measurement, 63(1), pp.27-34.

[192] Chang, K.M., 2010. Arrhythmia ECG noise reduction by ensemble empirical mode decomposition. Sensors, 10(6), pp.6063-6080.

[193] Weng, B., Blanco-Velasco, M. and Barner, K.E., 2006, August. ECG denoising based on the empirical mode decomposition. In Engineering in Medicine and Biology Society, 2006. EMBS'06. 28th Annual International Conference of the IEEE (pp. 1-4). IEEE.

[194] Nguyen, P. and Kim, J.M., 2016. Adaptive ECG denoising using genetic algorithm-based thresholding and ensemble empirical mode decomposition. Information Sciences, 373, pp.499-511.

[195] Tan, X., Chen, X., Hu, X., Ren, R., Zhou, B., Fang, Z. and Xia, S., 2014. EMD-based electrocardiogram delineation for a wearable low-power ECG monitoring device. Canadian Journal of Electrical and Computer Engineering, 37(4), pp.212-221.

[196] Wang, J., Ye, Y., Pan, X., Gao, X. and Zhuang, C., 2014. Fractional zero-phase filtering based on the Riemann–Liouville integral. Signal Processing, 98, pp.150-157.

[197] Gopeka, S.V., Murali, L. and Manigandan, T., 2014, May. VLSI design of ECG QRS complex detection using Multiscale Mathematical Morphology. In Advanced Communication Control and Computing Technologies (ICACCCT), 2014 International Conference on (pp. 478-482). IEEE.

[198] Elgendi, M., Al-Ali, A., Mohamed, A. and Ward, R., 2018. Improving Remote Health Monitoring: A Low-Complexity ECG Compression Approach. Diagnostics, 8(1), p.10.

[199] Hamilton, P.S. and Tompkins, W.J., 1986. Quantitative investigation of QRS detection rules using the MIT/BIH arrhythmia database. IEEE transactions on biomedical engineering, (12), pp.1157-1165.

[200] Nallathambi, G. and Principe, J.C., 2014. Integrate and fire pulse train automaton for qrs detection. IEEE Transactions on Biomedical Engineering, 61(2), pp.317-326.

[201] Cvikl, M. and Zemva, A., 2010. FPGA-oriented HW/SW implementation of ECG beat detection and classification algorithm. Digital Signal Processing, 20(1), pp.238-248.

[202] Iliev, I., Krasteva, V. and Tabakov, S., 2007. Real-time detection of pathological cardiac events in the electrocardiogram. Physiological Measurement, 28(3), p.259.

[203] Kumar, V., Saxena, S.C., Giri, V.K. and Singh, D., 2005. Improved modified AZTEC technique for ECG data compression: Effect of length of parabolic filter on reconstructed signal. Computers & Electrical Engineering, 31(4-5), pp.334-344.

[204] Mukhopadhyay, S.K., Mitra, S. and Mitra, M., 2012. An ECG signal compression technique using ASCII character encoding. Measurement, 45(6), pp.1651-1660.

[205] Mukhopadhyay, S.K., Mitra, S. and Mitra, M., 2013. ECG signal compression using ASCII character encoding and transmission via SMS. Biomedical Signal Processing and Control, 8(4), pp.354-363.

[206] Lu, Z., Kim, D.Y. and Pearlman, W.A., 2000. Wavelet compression of ECG signals by the set partitioning in hierarchical trees algorithm. IEEE Transactions on Biomedical Engineering, 47(7), pp.849-856.

[207] Lee, S., Kim, J. and Lee, M., 2011. A real-time ECG data compression and transmission algorithm for an e-health device. IEEE Transactions on Biomedical Engineering, 58(9), pp.2448-2455.

[208] Bilgin, A., Marcellin, M.W. and Altbach, M.I., 2003. Compression of electrocardiogram signals using JPEG2000. IEEE Transactions on Consumer Electronics, 49(4), pp.833-840.

[209] Brajović, M., Orović, I., Daković, M. and Stanković, S., 2017. On the parameterization of Hermite transform with application to the compression of QRS complexes. Signal Processing, 131, pp.113-119.

[210] Kumar, A., Komaragiri, R. and Kumar, M., 2018. Heartrate monitoring and therapeutic devices: A wavelet transform based approach for the modeling and classification of congestive heart failure. ISA Transactions.

[211] Singh, B.N. and Tiwari, A.K., 2006. Optimal selection of wavelet basis function applied to ECG signal denoising. Digital signal processing, 16(3), pp.275-287.

[212] Wang, L.H., Chen, T.Y., Lin, K.H., Fang, Q. and Lee, S.Y., 2015. Implementation of a wireless ECG acquisition SoC for IEEE 802.15. 4 (ZigBee) applications. IEEE Journal of biomedical and health informatics, 19(1), pp.247-255.

[213] Chui, K.T., Tsang, K.F., Chi, H.R., Ling, B.W.K. and Wu, C.K., 2016. An accurate ECG-based transportation safety drowsiness detection Technique. IEEE Transactions on Industrial Informatics, 12(4), pp.1438-1452.

[214] Yang, H., Kan, C., Liu, G. and Chen, Y., 2013. Spatiotemporal differentiation of myocardial infarctions. IEEE Transactions on Automation Science and Engineering, 10(4), pp.938-947.

[215] Liu, W., Zhang, M., Zhang, Y., Liao, Y., Huang, Q., Chang, S., Wang, H. and He, J., 2018. Real-time multilead convolutional neural network for myocardial infarction detection. IEEEJournal of biomedical and health informatics, 22(5), pp.1434-1444.

[216] Kumar, A., Kumar, M. and Komaragiri, R., 2018. Design of a Biorthogonal Wavelet Transform Based R-Peak Detection and Data Compression Technique for Implantable Cardiac Pacemaker Systems. Journal of medical systems, 42(6), p.102.

[217] Kumar, A., Komaragiri, R. and Kumar, M., 2018. Design of wavelet transform based electrocardiogram monitoring system. ISA Transactions, 80, pp.381-398.

[218] Kumar, M.A. and Chari, K.M., 2018. Efficient FPGA-based VLSI architecture for detecting R-peaks in electrocardiogram signal by combining Shannon energy with Hilbert transform. IET Signal Processing.

[219] Cesari, M., Mehlsen, J., Mehlsen, A.B. and Sorensen, H.B.D., 2017. A New Wavelet-Based ECG Delineator for the Evaluation of the Ventricular Innervation. IEEE Journal of translational engineering in health and medicine, 5, pp.1-15.

[220] Tekeste, T., Saleh, H., Mohammad, B., Khandoker, A. and Ismail, M., 2018. A Nano-Watt ECG Feature Extraction Engine in 65-nm Technology. IEEE Transactions on Circuits and Systems II: Express Briefs, 65(8), pp.1099-1103.

[221] Razzaq, N., Sheikh, S.A.A., Salman, M. and Zaidi, T., 2016. An intelligent adaptive filter for elimination of power line interference from high resolution electrocardiogram. IEEE Access, 4, pp.1676-1688.

[222] Salman, M.N., Rao, P.T. and Rahman, M.Z.U., 2018. Novel Logarithmic Reference Free Adaptive Signal Enhancers for ECG Analysis of Wireless Cardiac Care Monitoring Systems. IEEE Access, 6, pp.46382-46395.

[223] Tobón, D.P. and Falk, T.H., 2018. Adaptive spectro-temporal filtering for electrocardiogram signal enhancement. IEEE Journal of biomedical and health informatics, 22(2), pp.421-428.

[224] He, H., Tan, Y. and Wang, Y., 2015. Optimal base wavelet selection for ECG noise reduction using a comprehensive entropy criterion. Entropy, 17(9), pp.6093-6109.

[225] Weeks, M. and Bayoumi, M., 2003. Discrete wavelet transform: architectures, design and performance issues. Journal of VLSI signal processing systems for signal, image and video technology, 35(2), pp.155-178.

[226] Li, P., Zhang, X., Liu, M., Hu, X., Pang, B., Yao, Z., Jiang, H. and Chen, H., 2017. A 410-nW efficient QRS processor for mobile ECG monitoring in 0.18-μm CMOS. IEEE transactions on biomedical circuits and systems, 11(6), pp.1356-1365.

[227] Ibaida, A. and Khalil, I., 2013. Wavelet-based ECG steganography for protecting patient confidential information in point-of-care systems. IEEE Transactions on biomedical engineering, 60(12), pp.3322-3330.